

Sensitivity Analysis for Nonsmooth Mechanical Systems with Simultaneous Impacts and Spatial Friction

M. Bouma (0784690)
Department of Mechanical Engineering
Dynamics and Control group
Eindhoven University of Technology
DC 2019.XXX

Project Supervisor

PROF. DR. IR. N. VAN DE WOUW

Co-Supervisors

DR. IR. A. SACCON

DR. IR. M.W.L.M. RIJNEN

Committee

PROF. DR. IR. N. VAN DE WOUW *

DR. IR. A. SACCON *

DR. IR. M.W.L.M. RIJNEN *

DR. IR. D.J. ANTUNES †

* Eindhoven University of Technology (Dynamics and Control)

† Eindhoven University of Technology (Control Systems Technology)

December 25, 2018

Abstract

Acknowledgments

Contents

Abstract	i
Acknowledgments	iii
Nomenclature	vii
1 Introduction	1
1.1 High performance physical interaction in robotics	1
1.2 Nonsmooth modeling frameworks	2
1.3 Tracking control for nonsmooth systems	3
1.4 Reference spreading control	4
1.5 Research objectives and contribution	6
1.6 Report outline	7
2 Mechanical Systems with Unilateral Constraints and Spatial Friction	9
2.1 General system definition	9
2.2 Model formulation including set-valued force laws	11
2.3 Hybrid system formulation	15
2.4 Summary	21
3 Sensitivity Analysis with Isolated State-and-Input-Triggered Events	23
3.1 Trajectories with state-and-input-triggered jumps	23
3.2 Approximating perturbed trajectories with isolated guard-activations	27
3.3 Summary	32
4 Sensitivity Analysis with Simultaneous State-and-Input-Triggered Events	35
4.1 Simultaneous guard-activation	35
4.2 Approximating perturbed trajectories with simultaneous guard-activations	40
4.3 Summary	49
5 Numerical Validation	51

6	Conclusions and Recommendations	53
6.1	Conclusions	53
6.2	Recommendations	54
	Bibliography	55
A	Nonsmooth modeling	61
A.1	Hybrid system formulation for mechanical systems	61
A.2	Proximal Point Formulation	66
B	Spatial Friction in Mechanical Systems with Unilateral Constraints	71
B.1	Reference trajectories with impact away from slip-stick border	71
B.2	Reference trajectories with impact at the slip-stick border	72
B.3	Post-impact accelerations in open-to-stick transitions	72
B.4	Slip-stick transition in closed-contact	73
C	Sensitivity Analysis for Input-Dependent Guards	75
C.1	Linearization for single jumps	75
C.2	Linearization for multiple jumps	78
C.3	Stability analysis of LTTHS	81
D	Positive Homogenization for Input-Dependent Guards	83
D.1	Conewise constant jump gain	83
D.2	Positive homogeneity	85
D.3	Stability analysis of PTTHS	86
E	Considered Trajectories	87
E.1	Associativity	87
E.2	Transversality	87
E.3	Superfluous Contacts	87
E.4	Nominal Guard-Activations	87
E.5	Non-impacting contact points can not switch modes	87
E.6	All closed contact points are in the same mode	87
F	Simulation Design	89
F.1	Plank box dynamics	89
F.2	Reference Trajectory Design	93

Nomenclature

Abbreviations

LTTHS	Linear Time-Triggered Hybrid System
NCP	Nonlinear Complementarity Problem
NSITHS	Nonlinear State-and-Input-Triggered Hybrid System
NSTHS	Nonlinear State-Triggered Hybrid System
PTTHS	Positively homogeneous Time-Triggered Hybrid System
RS	Reference Spreading

Greek symbols

α	The nominal reference trajectory
Γ	An impulsive guard function
γ	A flow guard function
Δ	The linearization of the perturbed event time around zero perturbation
ϵ	The scalar perturbation parameter
η	The set of indexes of inactive guards
ι	The contact point counter
κ	Historical notation counter
κ_ι	Magnitude of the tangential velocity of contact point ι
$\Lambda_{n,\iota}$	The normal impulsive reaction force of contact point ι
$\lambda_{n,\iota}$	The normal reaction force of contact point ι
$\Lambda_{t,\iota}$	The tangential impulsive reaction force of contact point ι
$\lambda_{t,\iota}$	The tangential reaction force of contact point ι
μ_ι	The friction coefficient of contact point ι
μ	The nominal reference input
ν	The generalized coordinates defined on the continuous segments of a trajectory
σ_j	The system-mode descriptor of event j
τ	The nominal event time

Roman symbols

A	Linear state matrix
-----	---------------------

B	Linear input matrix
C	The column containing centripetal, Coriolis and gravitational effects
c	The number of contact points
c_i	The event-character of macro event i
D	Delassus matrix
\mathcal{D}_j	The discrete event set of event j
$D_i(\cdot)$	The derivative with respect to the i th term
$e_{n,\iota}$	The normal restitution coefficient of contact point ι
$e_{t,\iota}$	The tangential restitution coefficient of contact point ι
f	A nonlinear continuous function
G	Positively homogeneous jump gain for the perturbed state direction
g	A jump map
H	The positively homogeneous jump gain
$\mathbf{h}_{t,\iota}$	Tangential contact distance of contact point ι
$\mathbf{h}_{n,\iota}$	Normal contact distance of contact point ι
\mathcal{I}	A set of contact points
I	Domain of a segment
i	The macro event counter
J	Positively homogeneous jump gain for the perturbed input direction
j	Event counter and hybrid time
k	The micro event counter
l_κ	The number of simultaneous activations of macro event κ
M	The mass matrix
N	The number of events
$o(\cdot)$	Landau's symbol little-o
q	The generalized coordinates
\mathcal{S}	The set of mode descriptors related to all possible post-event modes
S	The matrix containing generalized directions of the actuator forces
S_i^k	The historical notation of macro event i from micro event 0 up to k
s_i^k	The event-mode descriptor of macro event i and micro event k
t	Regular time
t_i^k	The perturbed event time of micro event k in macro event i
u	The input
v	The input perturbation
$v_{n,\iota}$	Normal velocity of contact point ι

$\mathbf{v}_{t,\iota}$	Tangential velocity of contact point ι
$\mathbf{w}_{n,\iota}^T$	The normal Jacobian of contact point ι
$\mathbf{W}_{t,\iota}^T$	The tangential Jacobian of contact point ι
\mathbf{x}	The state coordinates
\mathbf{z}	The state perturbation

Sub- and superscripts

$(\cdot)_0$	Initial condition
$\dot{(\cdot)}$	First time derivative
$\ddot{(\cdot)}$	Second time derivative
$(\cdot)^-$	The left limit
$(\cdot)^+$	The right limit
$(\cdot)_\alpha$	Related to reference trajectory α
$(\cdot)^\epsilon$	A variable dependent on the initial perturbation
$(\cdot)_\iota$	Related to reference trajectory ι
$(\cdot)_{\text{cl}}$	The closed-contact mode sub/superscript
$(\cdot)_i$	Related to macro-event or segment i
$(\cdot)_j$	Related to event or segment j
$(\cdot)_k$	Related to micro-event or segment k
$(\cdot)_n$	Scalar or vector in normal direction
$(\cdot)_{\text{op}}$	The open-contact mode sub/superscript
$(\cdot)_{\text{sl}}$	The slip-contact mode sub/superscript
$(\cdot)_{\text{st}}$	The stick-contact mode sub/superscript
$(\cdot)_t$	Scalar or vector in tangential direction
$(\cdot)_\mathbf{x}$	Related to reference trajectory \mathbf{x}

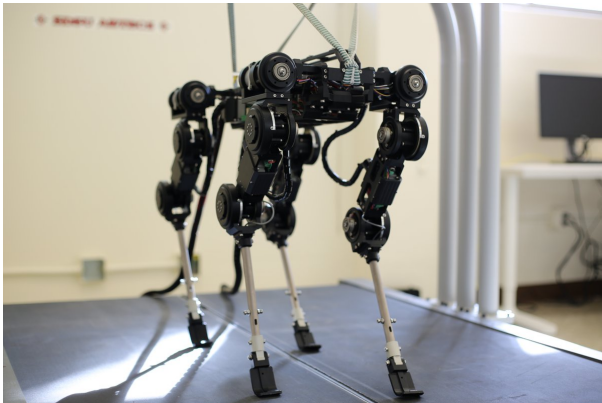
Chapter 1

Introduction

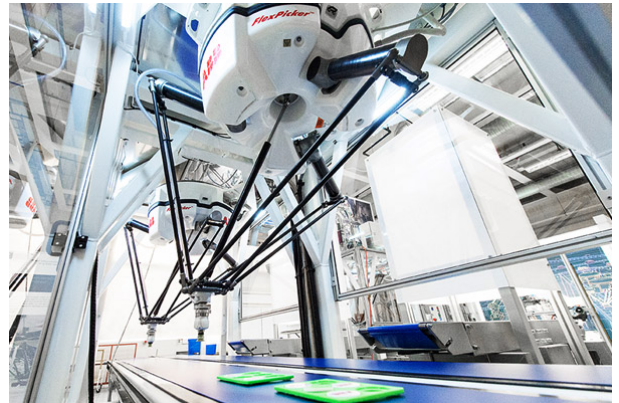
1.1 High performance physical interaction in robotics

In many applications of mechanical systems physical interaction with the environment is necessary to function, particularly in robotics. Humanoid robots, quadrupeds, and industrial robots are some examples of robots that repeatedly interact with their environment. Common control strategies that are available for these applications are limiting in performance. To avoid complexity of the controller, they often assume contact with their environment to happen at zero relative speed. This makes the robots less suitable for situations where speed is of significance, e.g., an industrial robot aiming to reach a certain throughput or a quadruped performing a trotting motion. Examples of such robots the SimLab quadruped [1] and the ABB IRB 360 flexpicker [2], which are depicted in Figure 1.1. High performance is desirable in such cases, and zero velocity contact limits this performance. Therefore it is clear that the field of robotics can benefit from control strategies that are capable of handling non-zero relative velocity. Such controllers, however, are more complex than the controllers that require zero velocity contact situations.

When two bodies make physical contact at non-zero velocity, impact occurs. Impact is a complex physical event, that is characterized by dynamics at short timescales, high force levels, high energy dissipation rates, and large accelerations and decelerations. Due to the small time scale at which



(a) *SimLab quadruped used at Virginia Tech [1].*



(b) *The ABB IRB 360 FlexPicker [2].*

Figure 1.1: *Two examples of robots with physical interaction that can benefit from high performance control strategies.*

impacts happen, their effect is often modeled as instantaneous. In such a modeling setting, the contact forces are impulsive and the velocity experiences jumps during an impact. Such a modeling approach is pursued within *nonsmooth mechanics*. Nonsmooth mechanical systems with impact are systems that have discontinuities in their state-evolution. In nonsmooth mechanics, a unilateral constraint is a constraint that prevents two bodies from penetrating. Mechanical systems with unilateral constraints are an example of systems that can exhibit nonsmooth behavior, as they experience velocity jumps when their unilateral constraints are closed at non-zero velocities. Control strategies for such systems are necessary to achieve higher performance.

1.2 Nonsmooth modeling frameworks

Nonsmooth systems can be described by several mathematical frameworks, e.g., singularly perturbed systems, hybrid systems, complementarity systems, and (measure-)differential inclusions [3]. The singular perturbation framework approximates the nonsmooth behaviour using a singularly perturbed smooth system. In this way, the singularly perturbed system can be evaluated numerically using a single smooth differential equation. However, due to the smooth approximation the system becomes very stiff and needs extremely small time-steps in numerical simulation.

More suitable for numerical evaluation are differential inclusions, which are applicable to systems with a discontinuous right-hand side but a time-continuous state-evolution (also called Filippov-systems [4]). A common example of Filippov-systems are systems experiencing dry friction. The differential inclusion gives a description of the nonsmooth dynamics in a single inclusion. However, mechanical systems with unilateral constraints and impact do not satisfy the requirement of having a time-continuous state-evolution. A measure-differential inclusion describes the continuous as well as the impulsive dynamics of a nonsmooth system [5]. In this way, measure-differential inclusions are suitable for systems with time-discontinuities in their state-evolution [6,7]. Using this approach, the dynamics can be accurately integrated using the timestepping method [8].

From a control point-of-view the complementarity framework is often considered. This framework describes nonsmoothness through a combination of differential equations and inequalities [9,10]. In [11], the complementarity problem is used to describe mechanical systems with unilateral constraints. It plays a key role in mathematical programming, and several solutions for trajectory tracking using complementarity systems exist [12,13].

In recent years, the hybrid systems framework has drawn more interest for solving the trajectory tracking problem of nonsmooth systems [14,15]. A hybrid system is a dynamical system that exhibits both continuous and discrete dynamics behaviour, where it reinitializes the state and switches (discrete behaviour) between several differential equations (continuous behaviour) [16]. According to [17], the hybrid systems framework is suitable for the modeling of mechanical systems with unilateral constraints as well as robotics. In a hybrid dynamical model guard sets are defined, which when entered by the state of the system, will cause the dynamics to switch from one differential equation to another and possibly reinitialize the state. This makes it a very intuitive approach to the modeling of nonsmoothness.

A known difficulty with the hybrid system framework however, is a phenomenon called Zeno-behaviour. One speaks of Zeno-behaviour when an infinite amount of guard activations happen in a finite time. A classic example is the bouncing ball. Measure-differential inclusions with a timestepping scheme would be more suitable in such a situation, since the combined effect of several state resets is captured in a single time step. An advantage of using the hybrid systems framework, is that it is a more intuitive description of the dynamics whereas measure-differential inclusions are more abstract. The stability analyses for these frameworks are well-developed, i.e., [16,18,19] for

hybrid systems, [20–22] for measure differential inclusions, and [7, 23, 24] for linear complementarity problems.

1.3 Tracking control for nonsmooth systems

Legged robotic systems account for a substantial part of the research done into the trajectory tracking control of mechanical systems with unilateral constraints. Many results in this area deal with the stability of periodic orbits of systems with impacts. In [25], a first big step has been made into modeling and controlling a one-legged hopping robot. In this research, the energy-loss during impact is modeled through damping and coupling effects are modeled as perturbations. Other pioneering works can be found in [26–28].

In [15, 29], the hybrid framework is adopted to find stable walking gaits for biped robots. Using Poincaré maps, the stability of periodic orbits with discontinuities of under-actuated systems are analyzed. Phases can be distinguished where the system is fully actuated and where the system is under-actuated. The fully actuated phase can then be used to stabilize the periodic trajectory despite the under-actuated phase. The work is continued in [30], generating control laws using data of walking humans and in [31] the energy-efficiency of generated walking gaits has been the focus. An example of a humanoid robot on which such controllers have been implemented is Agility Robotics’ Cassie [32], which is depicted in Figure 1.2. An extensive survey in the field of bipedal robotic walking can be found in [33]. The analysis of stable walking gaits is applied to the MIT Cheetah in [14], where a stability analysis and controller design is presented for the trot-running of a quadrupedal robot.

Considerable progress has been made in the field of walking robots and billiards, but it is easy to think of an example where nonperiodic trajectories are of interest. Under the assumption that the state trajectory jumps at the exact same time as the reference trajectory, the trajectory tracking problem for nonsmooth systems has been solved for several types of systems. The tracking problem for Lur’e type systems has been analyzed in [34, 35], using MDI’s to describe nonsmooth and impulsive dynamics. The work uses the convergence property to provide a solution to the tracking problem, where the solution may be time-varying and exhibit state-jumps. In [12], a passivity-based approach is used to solve the tracking control problem of complementarity Lagrangian systems.



Figure 1.2: *The bipedal robot Cassie developed by Agility Robotics [32].*

Asymptotic stability is achieved for Lagrangian systems with unilateral constraints. The same approach has been applied to the hybrid system framework in [36], which results in a control law that can guarantee stability of a trajectory with multiple impacts. By embedding the reference trajectory with discontinuities into a set, Lyapunov tools can be used to analyze stability as in [37,38]. In [39] a stability analysis of systems with impacts and friction has been presented. The results are obtained using the measure-differential inclusion framework, resulting in a smooth control law. The planning and control of non-periodic bipedal locomotion with impacts and friction is discussed in [40].

In the prior discussed work, the tracking problem has been solved under the assumption that the jump of the state trajectory occurs at the same time-instant as the jump of the reference trajectory, i.e., in [36,38,39]. In reality, especially in high velocity conditions, the time instant of the state jump and that of the reference trajectory jump are noncoincident more often than not. In this case a phenomenon called *peaking* occurs [41]. Spikes in the tracking error will arise around the jump times, which generate large actuation forces and contradict stability.

Solutions to peaking of the tracking error exist for periodic orbits in [42,43], where the results are compatible with a mismatch in reference jump-time and state jump-time for infinite time periodic trajectories with infinitely many state-jumps. Such trajectories are often found in so-called *Birkhoff Billiards* where the coefficient of restitution is 1. [44] also presents results for billiards, applicable to a large class of trajectories than [42,43]. In [41,45], a novel definition of the tracking error is introduced, using a distance function which is not sensitive to jumps of the state and the reference trajectory. Lyapunov-based conditions for the global asymptotic stability of non-smooth trajectories have been derived. Another solution for the problem of a jump-time mismatch is proposed in [46] in the form of a distance function similar to [41,45] based on a quotient metric. When a state jump happens at a different time than the reference jump, this approach applies the jump map to the reference to be able to compare the state to the reference. In [47], a novel controller design using gluing functions is introduced to connect the start and end point of a jump in the state space. After gluing, the system can be considered a continuous or piecewise continuous function without state jumps. In [48], a tracking error is defined by taking the smallest of two values: the ante-impact tracking error and post-impact tracking error.

The solutions to the peaking behavior mentioned in the section above, do not always appear to be the best choice. It is beneficial to have some control over how the tracking error is defined, and particularly what the reference trajectory is, around the jump times. For this reason, a more intuitive and controllable solution to the peaking behavior is introduced.

1.4 Reference spreading control

In [49,50] a novel notion of error is introduced for systems with state jumps, by extending the reference trajectory segments, and considering the error between the reference trajectory and state trajectory that have encountered the same number of jumps. This way, an ante-event state trajectory can always be compared to an ante-event reference trajectory and a post-event state trajectory can always be compared to a post-event reference trajectory, even when the event times do not coincide. The extensions are defined by integrating the vector field, forwards and backwards, past the event times. This way, the input during the extension can be chosen in a particular way, to find a desired extension of the reference trajectory. These extensions will, comparable to the solutions presented in previous section, avoid peaking of the tracking error. The authors of [49,50] then use that notion of error as the basis for extending the sensitivity analysis introduced in [51] to the hybrid system framework. These results are then used to obtain a local approximation of the perturbed state dynamics. This analysis gives insight in how the system behaves under the presence

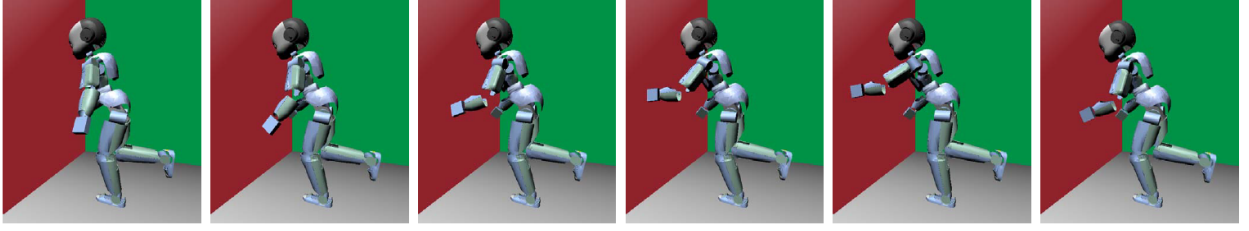


Figure 1.3: *Snapshots of the motion the iCub robot makes in the simulation done in [56] using reference spreading control.*

of perturbations, which is useful for controller design. Experimental results for this control law are presented in [52], where a 1-DOF robot arm performs an impacting trajectory using the control law proposed in [49]. In [53], a control strategy for hybrid systems with state triggered jumps is used on a hopping robotic leg model from [54]. The control strategy is named *reference spreading control* in [55], due to the extensions made on the reference trajectories in the notion of error. In [56], the reference spreading control law is used in simulations with an iCub robot. The iCub robot balances on one foot and keeps himself standing upright by making and breaking contact with a wall using one of its arms. Some snapshots of the motion are depicted in Figure 1.3. As mentioned earlier, many works in literature assume that the exact impact time is known. This is extremely limiting during implementation of the control law. Using the reference spreading approach, the impact time of the state is allowed to deviate from that of the reference, making implementation of the control law in practical applications more viable while still allowing for state-jumps.

As is the case in the simulations with the iCub in Figure 1.3, impacts are often modeled using a one-point contact between two bodies. However, in practice, more complex geometries can make contact with each other. The feet of Cassie in Figure 1.2 for example, have a clear resemblance to human feet, which often results in distinct heel and toe strikes during walking motions. A more realistic contact geometry is used in [57], in which the foot strike of a humanoid bipedal robot is modeled using multiple impacts. One strike is modeled by a heel impact, a toe impact, a heel release, and finally a toe release, resulting in a more realistic model of the walking gait of the bipedal robot. In such a movement, the order of impacts is known.

When considering a trajectory with multiple contacts closing at one time-instant, the problem becomes more complex. Imagine for example the iCub in [56] having a physically realistic geometry at the end of its arm. Consider Figure 1.4. The arm can first make a point contact, then a line contact, and finally a surface contact to make full contact with the wall. It can also track a trajectory where the surface of the arm makes a surface contact with the wall at one time-instant. Such events can be considered as multiple impacts happening at the same time-instant and are called *simultaneous impacts*. One can imagine that a small perturbation can significantly change the behavior of a simultaneous impact. Instead of the expected single jump in the state, a perturbation can cause the state to have multiple jumps. Also the order of impacts of the several parts of the arm is not known beforehand. In Figure 1.4 a 2-dimensional representation of the wrist of the iCub robot is illustrated. This image clearly visualizes the effect a perturbation has on a trajectory with simultaneous impacts. The approach used in [57] is not suitable for these situations.

The phenomenon of simultaneous impacts is first introduced in [58], where the first step is taken into solving the trajectory tracking problem for such impacts. A hybrid system framework is used to model the impacts, where multiple guards can be activated at once. The reference spreading control in [53,55] and the sensitivity analysis to approximate a system's behavior around trajectories with single guard activation, introduced in [49], are extended to be suitable for simultaneous guard



Figure 1.4: A 2-dimensional illustration of the end effector of the wrist of the iCub robot. On the left: a nominal trajectory is illustrated (from top to bottom), where a simultaneous impact happens at the points indicated by black dots. The wrist immediately makes a line-contact with the surface. On the right: the trajectory is perturbed, which results in two subsequent impacts instead of one simultaneous impact.

activation. The results of the sensitivity analyses are used to find a first-order approximation of the perturbed trajectory, which can be used to find suitable feedback gains. In addition to an impulse perpendicular to the impact-surface, taking friction into account will result in a tangential impulse. Also the release phase is not considered in [58]. During the release phase, no discontinuity in the state-evolution is seen, only a change in the number of active constraints on the system occurs. The aim of this research is to apply the reference spreading control strategy and sensitivity analysis to systems experiencing both impacts including friction and releasing motions.

1.5 Research objectives and contribution

The research objective of this work is to extend the work presented in [67] in two ways: extending the sensitivity analysis to friction cases and release cases.

Simultaneous impacts with friction

Friction elements are often disregarded when analyzing impacts. However, to set up a unifying theory, friction elements should not be ignored. Tangential impulses can have a considerable effect on a system's dynamics. Particularly for walking motions the frictional element of an impact is of importance. The impact laws used in the work of [58] can be extended using one of the several available friction laws [22]. When impact laws are supplemented with a tangential element, this is often done using a Coulomb friction law [60]. Besides the tangential impulse, also a Filippov-like discontinuity will be present due to Coulomb friction. Also in this work a Coulomb friction law will be used, which can lead to more accurate models and controllers for mechanical systems with unilateral constraints.

Research Objective:

Find a model suitable to describe mechanical systems with unilateral constraints and spatial friction. The sensitivity analysis and mathematical notation presented in [67] shall be extended to be

compatible with such models.

Simultaneous releases

The release of two bodies is based on a force equilibrium. For this reason, the conditions that determine whether release happens is not only state dependent, but also input dependent. In [53] and [61], tracking of trajectories with events experiencing input-based triggers has been extensively researched. However, these results only include subsequent events. The release phase for simultaneous events is not yet investigated. In [58], only the establishment of contact is simulated and release is not included. Extending the sensitivity analysis in [58] to be suitable for simultaneous releases would make it possible to simulate and control one trajectory with several simultaneous impacts and releases.

Research Objective:

Extending the sensitivity analysis presented in [67] such that it is suitable for input-triggered events.

1.6 Report outline

The modeling of mechanical systems with unilateral constraints and spatial friction is discussed in Chapter 2. The generic dynamics of a mechanical system including contact and friction laws are derived, eventually resulting in a hybrid system with impulsive effects. Then, in Chapter 3, a tracking control strategy for hybrid systems with ordered state-input-triggered events is presented. In Chapter 4, this tracking control strategy is extended to trajectories involving simultaneous impacts. An example of a mechanical system with unilateral constraints and spatial friction is given in Chapter 5, which is used for a numerical validation of the presented control strategy. Finally, in Chapter 6, conclusions are drawn and recommendations for future research are provided.

Chapter 2

Mechanical Systems with Unilateral Constraints and Spatial Friction

In this chapter, several modeling approaches for mechanical systems with unilateral constraints and spatial friction are presented. We start by presenting a general representation of mechanical systems. Then, several formulations of contact and friction laws are introduced in the form of complementarity conditions. The complementarity problem formulation is a complete and often used formulation for mechanical systems with unilateral constraints. This complementarity formulation is then transformed into a hybrid system formulation, that will be used in this work to analyze the tracking of trajectories of mechanical systems with unilateral constraints and spatial friction. While the hybrid system formulation is restrictive in modeling, it is a powerful tool for the control of systems with a special class of trajectories. Since the analysis that will be presented in this work is done with controller design in mind, the analysis will be presented in the hybrid system framework.

2.1 General system definition

When a unilateral constraint is activated, the differential equation that describes the dynamics of the system can change. The state even goes through a reinitialization when the constraint is activated with non-zero velocity. Two bodies already in contact can also experience changes in their dynamics, as a result from the friction between these bodies. This behavior can be described by dynamics consisting of a continuous part and a discrete part; the continuous part describes the flow of the state, and the discrete part describes the reinitialization of the state. The occurrence of a change in differential equation and a possible state reinitialization are referred to as *events*. To be able to detect when the system goes through a such an event, contact points are defined on the bodies. These contact points can activate and deactivate unilateral constraints, which corresponds with opening and closing contact with another body. A contact point that has activated a unilateral constraint can transition between stick and slip. A contact point in stick has a tangential relative velocity of zero, whereas a contact point in slip has a nonzero tangential relative velocity. The *mode* of the contact point is defined. The mode determines if a contact point is in contact or not, and if it is in stick or slip when the contact point is in contact. Using these contact points, a method is presented to model mechanical systems with unilateral constraints and spatial friction.

Let us now consider a mechanical system whose current configuration is described by the generalized coordinates $\mathbf{q} \in \mathbb{R}^n$ and whose generalized velocity is denoted $\boldsymbol{\nu} \in \mathbb{R}^n$ with $\boldsymbol{\nu} = \dot{\mathbf{q}}$ almost everywhere. The configuration space of the system is restricted using c unilateral constraints for

modeling contact, using the set of contact points $\mathcal{I} = \{\iota_1, \iota_2, \dots, \iota_c\}$. The set \mathcal{I}_{cl} is defined as the set of c_{cl} closed contact points, i.e., for a contact $\iota \in \mathcal{I}_{cl}$ the corresponding unilateral constraint is active. The set of potential contact points for which this geometric constraint is inactive, or open contact points, we define as $\mathcal{I}_{op} := \{\iota \mid \iota \notin \mathcal{I}_{cl}\}$. Note that in a physics-based engine the set \mathcal{I}_{op} is often undefined, because not all contact points are tracked. Only the contact points generating reaction forces are tracked. The set \mathcal{I}_{op} is only defined for convenience when the mode of the system is discussed. When a unilateral constraint is activated at a nonzero relative velocity, impact happens. For the unilateral constraint not to be violated, a jump in the velocity has to occur. These impact-times are denoted τ_j , where $j \in \{1, 2, \dots, N\}$ is a counter for unilateral constraint activations, with N the number of jumps in a trajectory.

Consider Figure 2.1 showing two bodies. A contact point ι is defined on one of the bodies, at which a plane tangent to the surface of the body is spanned. In the direction normal to this plane, the contact distance $h_{n,\iota}(\mathbf{q})$ is defined. The contact distance is the minimal distance between the contact point and the surface that it can make contact with. For the relative normal velocity $\mathbf{v}_{n,\iota} \in \mathbb{R}$ of contact point ι follows that

$$\mathbf{v}_{n,\iota} = \frac{\partial h_{n,\iota}}{\partial \mathbf{q}} \frac{d\mathbf{q}}{dt} = \mathbf{w}_{n,\iota}^T \dot{\mathbf{q}}, \quad (2.1)$$

with $\mathbf{w}_{n,\iota}^T \in \mathbb{R}^n$ representing the Jacobian of the normal velocity $\mathbf{v}_{n,\iota}$. The relative tangential velocity $\mathbf{v}_{t,\iota} \in \mathbb{R}^2$ is defined in the tangent plane of contact point ι . Similar to the normal direction, $\mathbf{h}_{t,\iota} = [\mathbf{h}_{t_1,\iota} \quad \mathbf{h}_{t_2,\iota}]^T$, where $\mathbf{h}_{t_1,\iota}$ and $\mathbf{h}_{t_2,\iota}$ are the contact distances in t_1 direction and t_2 direction, respectively. It then follows that the relative tangential velocity is given by

$$\mathbf{v}_{t,\iota} = \frac{\partial \mathbf{h}_{t,\iota}^T}{\partial \mathbf{q}} \frac{d\mathbf{q}}{dt} = \mathbf{W}_{t,\iota}^T \dot{\mathbf{q}}, \quad (2.2)$$

with $\mathbf{W}_{t,\iota}^T \in \mathbb{R}^{n \times 2}$ representing the Jacobian of the tangential relative velocity $\mathbf{v}_{t,\iota}$.

Then, the continuous dynamics of a mechanical system with unilateral constraints and spatial friction are of the form

$$\mathbf{M}(\mathbf{q})\dot{\boldsymbol{\nu}} + \mathbf{C}(\mathbf{q}, \boldsymbol{\nu}) = \mathbf{S}(\mathbf{q})\mathbf{u} + \sum_{\iota \in \mathcal{I}_{cl}} \mathbf{w}_{n,\iota}(\mathbf{q})\lambda_{n,\iota} + \mathbf{W}_{t,\iota}(\mathbf{q})\boldsymbol{\lambda}_{t,\iota}, \quad (2.3)$$

(Contact Law),

(Friction Law),

with $\mathbf{q}, \boldsymbol{\nu} \in \mathbb{R}^n$ and $\mathbf{u} \in \mathbb{R}^m$. In (2.3), $\mathbf{M}(\mathbf{q}) \in \mathbb{R}^{n \times n}$ is the mass matrix of the system, $\mathbf{C}(\mathbf{q}, \boldsymbol{\nu}) \in \mathbb{R}^n$ contains the centripetal, Coriolis, stiffness and damping related forces, and gravitational forces in the system and $\mathbf{S}(\mathbf{q}) \in \mathbb{R}^{n \times m}$ represents the generalized directions of the input forces \mathbf{u} . $\lambda_{n,\iota} \in \mathbb{R}$ and $\boldsymbol{\lambda}_{t,\iota} \in \mathbb{R}^2$ are the normal and tangential reaction forces, respectively, of contact point ι with $\mathbf{w}_{n,\iota} \in \mathbb{R}^n$ and $\mathbf{W}_{t,\iota} \in \mathbb{R}^{n \times 2}$ the transposed corresponding Jacobians. To make the system description in (2.3) complete, a contact law and friction law is required. These laws will be discussed in Section 2.2.

As mentioned above, when a unilateral constraint is activated, impulsive dynamics can cause a jump in the generalized velocity of the system. The impulsive dynamics, derived in [22, Section 5.4], are of the form

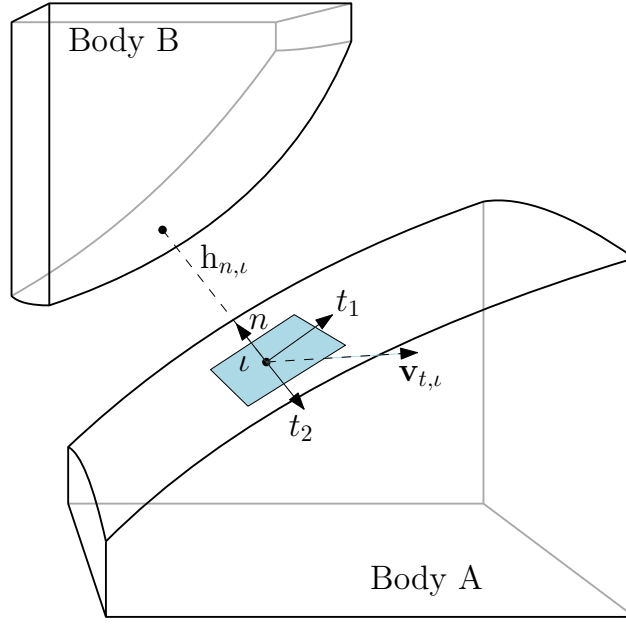


Figure 2.1: An illustration of two bodies about to make contact. The contact distance $h_{n,\iota}$ and the relative tangential velocity $\mathbf{v}_{t,\iota}$ for contact point ι are illustrated, which are defined on the surface of Body A.

$$\mathbf{M}(\mathbf{q})(\boldsymbol{\nu}^+ - \boldsymbol{\nu}^-) = \sum_{\iota \in \mathcal{I}_{cl}} \mathbf{w}_{n,\iota}(\mathbf{q}) \boldsymbol{\Lambda}_{n,\iota} + \mathbf{W}_{t,\iota}(\mathbf{q}) \boldsymbol{\Lambda}_{t,\iota}, \quad (2.4)$$

(Impulsive Contact Law),

(Impulsive Friction Law),

with $\boldsymbol{\Lambda}_{n,\iota}$ and $\boldsymbol{\Lambda}_{t,\iota}$ the normal and tangential impulsive reaction forces, respectively, of contact point ι . These dynamics are impulsive, and happen at one instance in time. In (2.4), $\boldsymbol{\nu}^-$ and $\boldsymbol{\nu}^+$ denote the left, respectively the right limit of the generalized velocity $\boldsymbol{\nu}$ at the time of impact τ_j . The expression moreover states that, similarly to the continuous dynamics (2.3), constitutive laws for contact and friction are required. These will be discussed in the following. First a complementarity problem formulation of mechanical systems with unilateral constraints is given, from which later a proximal point formulation and a hybrid system formulation are derived. For more information on modeling of multibody systems, the reader is referred to [22] and [62].

2.2 Model formulation including set-valued force laws

Mechanical systems with unilateral constraints can conveniently be described using so-called complementarity constraints or set-valued force laws. Particularly impacts and frictional effects are often described using these complementarity constraints, introducing a nonsmoothness into the mechanical system. In this section, the contact and friction laws required to describe a mechanical system with unilateral constraints and spatial friction are presented in a complementarity fashion. First, the contact case is handled in Section 2.2.1, where the complementarity constraints describing contact behavior for both flow and impulsive situations are presented. In Section 2.2.2, the complementarity constraints for frictional effects are presented, similar to the contact case, for both flow

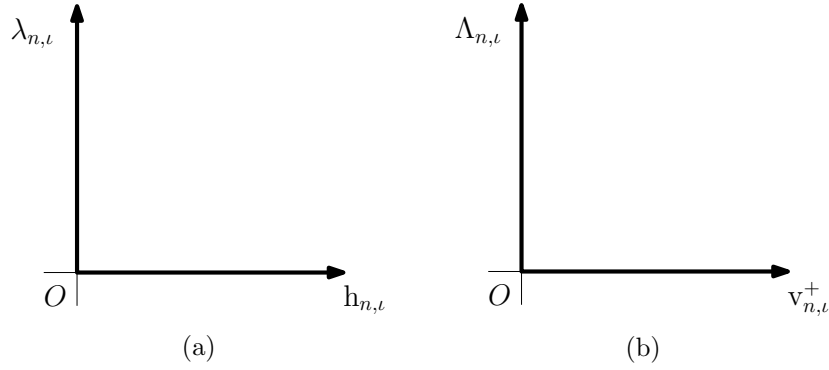


Figure 2.2: In (a) *Signorini's contact law* and in (b) *Newton's impact law without restitution*.

and impulsive situations. Finally, a complete complementarity description of mechanical system with unilateral constraints and spatial friction is presented in Section 2.2.3.

2.2.1 Signorini's contact law and Newton's impact law

To describe the contact interaction between rigid bodies, Signorini's contact law is used. Since we assume that the bodies composing the system are rigid and therefore impenetrable, and that the reaction forces caused by contact cannot prevent two or more bodies from separating, both the contact distance $h_{n,\ell}$ and reaction force $\lambda_{n,\ell}$ cannot become negative. For a contact point $\ell \in \mathcal{I}$, two situations are then possible, i.e.,

1. $h_{n,\ell} = 0 \wedge \lambda_{n,\ell} \geq 0$ (closed-contact)
2. $h_{n,\ell} > 0 \wedge \lambda_{n,\ell} = 0$ (open-contact)

These situations are illustrated in Figure 2.2a, from which can be seen that the two situations are orthogonal. This behavior can be summarized in the complementarity condition, as presented in [22, Section 5.3.1],

$$0 \leq h_{n,\ell} \perp \lambda_{n,\ell} \geq 0, \quad (2.5)$$

where the symbol \perp is used to express the orthogonality between the constraints on $h_{n,\ell}$ and $\lambda_{n,\ell}$. The complementarity condition (2.5) is called Signorini's contact law. A separate model is required for describing the contact dynamics during an impact event. As mentioned above, when contact is established at nonzero velocity, a jump in the velocity is generally seen. To describe this impact effect, Newton's impact law is used. Newton's impact law relates the normal velocities at the contact points after impact to the normal velocities just before the impact using a so-called coefficient of restitution e . Mathematically, Newton's impact law can be expressed as

$$v_{n,\ell}^+ = -e_{n,\ell} v_{n,\ell}^-, \text{ when } h_{n,\ell} = 0, \dot{h}_{n,\ell} < 0. \quad (2.6)$$

In this work, the coefficient of restitution $e_{n,\ell}$ is assumed to be 0 for all ℓ , corresponding to a completely inelastic impact. For closed contacts, an impact law can be defined that relates the impulsive contact force $\Lambda_{n,\ell}$ to the post-impact normal velocity $v_{n,\ell}^+$. Considering multi-contact systems, two situations can occur when a contact is closed:

1. $\Lambda_{n,\iota} > 0 \wedge \mathbf{v}_{n,\iota}^+ = 0$ (ι participating in impact)
2. $\Lambda_{n,\iota} = 0 \wedge \mathbf{v}_{n,\iota}^+ \geq 0$ (ι not participating in impact)

The situations described above are illustrated in Figure 2.2b, where again the orthogonality can be observed. The behavior can be summarized in the complementarity condition

$$0 \leq \mathbf{v}_{n,\iota}^+ \perp \Lambda_{n,\iota} \geq 0, \quad \forall \iota \in \mathcal{I}_{\text{cl}}, \quad (2.7)$$

with \mathcal{I}_{cl} the set of closed contacts. The complementarity condition (2.7) is called Newton's impact law. Note that the impact law is defined on velocity level, whereas the contact law is defined on position level.

2.2.2 Coulomb's friction law

Coulomb's friction law is often used to model dry friction in mechanical systems. When considering isotropic friction in 3-dimensional environments, Coulomb's friction law states that the tangential reaction force vector at contact point ι satisfies the inclusion

$$-\boldsymbol{\lambda}_{t,\iota} \in \begin{cases} \|\mathbf{v}_{t,\iota}\| = 0 & \Rightarrow \|\boldsymbol{\lambda}_{t,\iota}\| \leq \mu_\iota \lambda_{n,\iota} \\ \|\mathbf{v}_{t,\iota}\| > 0 & \Rightarrow \boldsymbol{\lambda}_{t,\iota} = \mu_\iota \lambda_{n,\iota} \frac{\mathbf{v}_{t,\iota}}{\|\mathbf{v}_{t,\iota}\|} \end{cases}, \quad (2.8)$$

with μ_ι the friction coefficient at contact point ι . The behavior described in (2.8) can conveniently be described using the normal cone formulation [22, Section 5.3.2]. The set of admissible friction forces $C_{t,\iota} \subset \mathbb{R}^2$, which for isotropic friction is a disk given by

$$C_{t,\iota} = \{-\boldsymbol{\lambda}_{t,\iota} \mid \|\boldsymbol{\lambda}_{t,\iota}\| \leq \mu_\iota \lambda_{n,\iota}\}. \quad (2.9)$$

The spatial Coulomb's friction law can then given be formulated as

$$\mathbf{v}_{t,\iota} \in \mu \lambda_{n,\iota} N_{C_{t,\iota}}(-\boldsymbol{\lambda}_{t,\iota}), \quad (2.10)$$

where $N_{C_{t,\iota}}$ is the normal cone set of $C_{t,\iota}$. The normal cone set N_C of a convex set C is given by

$$N_C(\mathbf{x}) := \{\mathbf{y} \mid \mathbf{y}^T(\mathbf{x}^* - \mathbf{x}) \leq 0, \quad \mathbf{x} \in C, \forall \mathbf{x}^* \in C\}. \quad (2.11)$$

The normal cone set $N_C(\mathbf{x}) = 0$, $\forall \mathbf{x} \in C \setminus \partial C$, where ∂C denotes the boundary of C . $N_C(\mathbf{x}) \neq 0$, $\forall \mathbf{x} \in \partial C$. For all \mathbf{x} on the boundary of C , $N_C(\mathbf{x})$ consists of the normal cone to the boundary of C on the point \mathbf{x} . The normal cone set can be explained more intuitively using Figure 2.3. We consider two situations: situation one, where $\|(\boldsymbol{\lambda}_{t,\iota})_1\| < \mu_\iota \lambda_{n,\iota}$, and situation two, where $\|(\boldsymbol{\lambda}_{t,\iota})_2\| = \mu_\iota \lambda_{n,\iota}$. In situation one, $(\boldsymbol{\lambda}_{t,\iota})_1 \in C_{t,\iota} \setminus \partial C_{t,\iota}$, meaning that $(\mathbf{v}_{t,\iota})_1 = 0$ according to (2.10). In situation two, $(\boldsymbol{\lambda}_{t,\iota})_2 \in \partial C_{t,\iota}$, meaning that $(\mathbf{v}_{t,\iota})_2$ is somewhere in the normal cone of $\partial C_{t,\iota}$ at $-\boldsymbol{\lambda}_{t,\iota}$. When the boundary of $\partial C_{t,\iota}$ is smooth at $-\boldsymbol{\lambda}_{t,\iota}$, the normal cone $N_{C_{t,\iota}}(-\boldsymbol{\lambda}_{t,\iota})$ is actually a ray. While the normal cone N_C is also defined for nonsmooth boundaries of C , this situation is not considered as the boundary of the set of admissible friction forces $\partial C_{t,\iota}$ is smooth everywhere. The relative tangential velocity $\mathbf{v}_{t,\iota}$ is therefore somewhere in the direction of $-\boldsymbol{\lambda}_{t,\iota}$, which is equivalent to the desired behavior described in (2.8), i.e.,

$$\mathbf{v}_{t,\iota} \in \mu \lambda_{n,\iota} N_{C_{t,\iota}}(-\boldsymbol{\lambda}_{t,\iota}) \Leftrightarrow -\boldsymbol{\lambda}_{t,\iota} \in \begin{cases} \|\mathbf{v}_{t,\iota}\| = 0 & \Rightarrow \|\boldsymbol{\lambda}_{t,\iota}\| \leq \mu_\iota \lambda_{n,\iota} \\ \|\mathbf{v}_{t,\iota}\| > 0 & \Rightarrow \boldsymbol{\lambda}_{t,\iota} = \mu_\iota \lambda_{n,\iota} \frac{\mathbf{v}_{t,\iota}}{\|\mathbf{v}_{t,\iota}\|} \end{cases}. \quad (2.12)$$

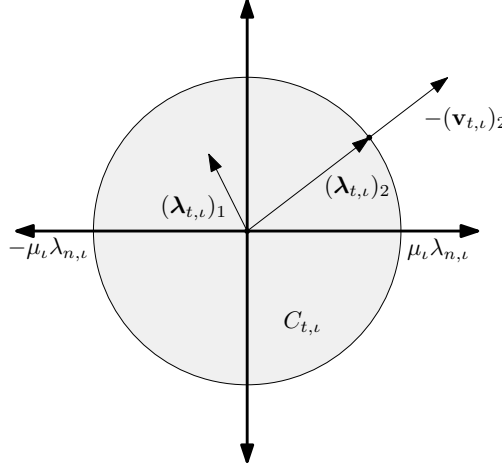


Figure 2.3: The friction disk with two separate friction forces $\lambda_{t,1}$ and $\lambda_{t,2}$. $\lambda_{t,1} = \mu\lambda_{n,1}$, resulting in a tangential velocity $\zeta_{t,i} > 0$. $\lambda_{t,2} < \mu\lambda_{n,2}$, leading to a tangential velocity $\zeta_{t,i} = 0$.

The work in [63] shows a complementarity formulation that is algebraically equivalent to (2.10). This formulation is given by

$$\mathbf{v}_{t,\epsilon} ||\lambda_{t,\epsilon}|| = -\kappa_\epsilon \lambda_{t,\epsilon}, \quad (2.13)$$

$$0 \leq \mu_\epsilon \lambda_{n,\epsilon} - ||\lambda_{t,\epsilon}|| \perp \kappa_\epsilon \geq 0, \quad (2.14)$$

where κ_ϵ is a variable that determines the length of the velocity vector $\mathbf{v}_{t,\epsilon}$. Equations (2.13)-(2.14) will be used in this work to model spatial coulomb friction. We employ again Newton's impact law for modeling the impact behavior where now the tangential contact velocities before and after impact are related to each other using

$$\mathbf{v}_{t,\epsilon}^+ = -e_{t,\epsilon} \mathbf{v}_{t,\epsilon}^-, \quad (2.15)$$

where $e_{t,\epsilon}$ is the tangential coefficient of restitution that we consider to be zero in this work. Then, similarly to the non-impulsive case, the impulsive Coulomb's friction law can be expressed as

$$\mathbf{v}_{t,\epsilon}^+ ||\Lambda_{t,\epsilon}|| = \kappa_\epsilon \Lambda_{t,\epsilon}, \quad \forall \epsilon \in \mathcal{I}_{cl}, \quad (2.16)$$

$$0 \leq \mu \Lambda_{n,\epsilon} - ||\Lambda_{t,\epsilon}|| \perp \kappa_\epsilon \geq 0. \quad \forall \epsilon \in \mathcal{I}_{cl}. \quad (2.17)$$

Note that, just as the impulsive dynamics in the normal direction, the impulsive friction law only applies to closed contacts.

2.2.3 System dynamics with contact and friction law

When the contact and friction laws (2.5), (2.13) and (2.14) introduced in Sections 2.2.1 and 2.2.2 are incorporated in the flow dynamics (2.3) of the system, a complete model for the continuous dynamics is found, i.e.,

$$\mathbf{M}(\mathbf{q})\dot{\boldsymbol{\nu}} + \mathbf{C}(\mathbf{q}, \boldsymbol{\nu}) = \mathbf{S}(\mathbf{q})\mathbf{u} + \sum_{\epsilon \in \mathcal{I}_{cl}} \mathbf{w}_{n,\epsilon}(\mathbf{q})\lambda_{n,\epsilon} + \mathbf{W}_{t,\epsilon}(\mathbf{q})\lambda_{t,\epsilon}, \quad (2.18)$$

$$0 \leq h_{n,\epsilon} \perp \lambda_{n,\epsilon} \geq 0, \quad (2.19)$$

$$\mathbf{v}_{t,\epsilon} ||\lambda_{t,\epsilon}|| = -\kappa_\epsilon \lambda_{t,\epsilon}, \quad (2.20)$$

$$0 \leq \mu \lambda_{n,\epsilon} - ||\lambda_{t,\epsilon}|| \perp \kappa_\epsilon \geq 0, \quad (2.21)$$

with

$$h_{n,\ell} := h_{n,\ell}(\mathbf{q}), \quad (2.22)$$

$$\mathbf{v}_{n,\ell}(\mathbf{q}) := \mathbf{w}_{n,\ell}^T(\mathbf{q})\boldsymbol{\nu}, \quad (2.23)$$

$$\mathbf{v}_{t,\ell}(\mathbf{q}) := \mathbf{W}_{t,\ell}^T(\mathbf{q})\boldsymbol{\nu}. \quad (2.24)$$

Similarly, incorporating the impulsive contact and friction laws (2.7), (2.16), and (2.16) in the impact/discrete dynamics (2.4) gives a complete model for the impact behavior of the system. It follows that the discrete dynamics that are triggered by the occurrence of an impact event are given by

$$\mathbf{M}(\mathbf{q})(\boldsymbol{\nu}^+ - \boldsymbol{\nu}^-) = \sum_{\ell \in \mathcal{I}_{\text{cl}}} \mathbf{w}_{n,\ell}(\mathbf{q})\Lambda_{n,\ell} + \mathbf{W}_{t,\ell}(\mathbf{q})\boldsymbol{\Lambda}_{t,\ell}, \quad (2.25)$$

$$0 \leq \mathbf{v}_{n,\ell}^+ \perp \Lambda_{n,\ell} \geq 0, \quad \forall \ell \in \mathcal{I}_{\text{cl}}, \quad (2.26)$$

$$\mathbf{v}_{t,\ell}^+ \|\boldsymbol{\Lambda}_{t,\ell}\| = \kappa_\ell \boldsymbol{\Lambda}_{t,\ell}, \quad \forall \ell \in \mathcal{I}_{\text{cl}}, \quad (2.27)$$

$$0 \leq \mu \Lambda_{n,\ell} - \|\boldsymbol{\Lambda}_{t,\ell}\| \perp \kappa_\ell \geq 0. \quad \forall \ell \in \mathcal{I}_{\text{cl}}, \quad (2.28)$$

with

$$\mathbf{v}_{n,\ell}^+(\mathbf{q}) := \mathbf{w}_{n,\ell}^T(\mathbf{q})\boldsymbol{\nu}^+, \quad (2.29)$$

$$\mathbf{v}_{t,\ell}^+(\mathbf{q}) := \mathbf{W}_{t,\ell}^T(\mathbf{q})\boldsymbol{\nu}^+. \quad (2.30)$$

2.3 Hybrid system formulation

In this section, the dynamics of the complementarity system defined in Section 2.2 is written to a hybrid formulation, resulting in a hybrid framework for mechanical systems with unilateral constraints and spatial friction. In [64, p. 222], event driven numerical methods are presented for mechanical systems with spatial friction. The model presented in this section is suitable for the simulation methods presented in [64].

2.3.1 Hybrid systems with impulsive effects

According to [65], an impulsive dynamical system can be described by a hybrid system with impulsive effects. This makes it a valid framework for mechanical systems with unilateral constraints and spatial friction. A hybrid system with impulsive effects consists of three elements:

1. Continuous dynamics, a continuous-time differential equation which defines the behavior of the system in between events
2. Discrete dynamics, a discrete map which defines the way the state of the system is reset during events
3. A criterion to decide when the state of the system is to be reset

The continuous dynamics of the hybrid system with impulsive effects are given by

$$\dot{\mathbf{x}}_j = \mathbf{f}_j(\mathbf{x}_j, \mathbf{u}_j, t), \quad \mathbf{x}_j, \mathbf{u}_j \in \mathcal{C}_j, \quad (2.31)$$

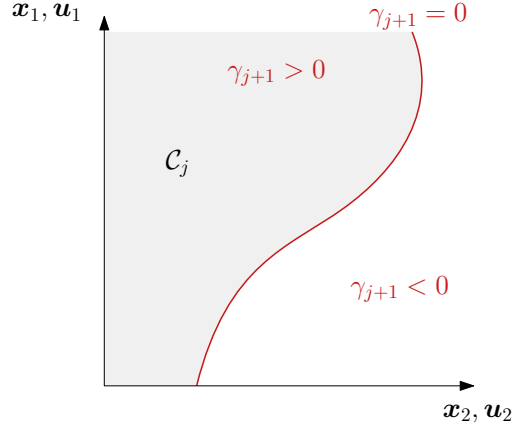


Figure 2.4: A guard function defining the flow set \mathcal{C}_j for a 2-dimensional system is illustrated in this figure.

with the state $\mathbf{x}_j = \mathbf{x}(t, j) \in \mathbb{R}^{n(j)}$ and the input $\mathbf{u}_j = \mathbf{u}(t, j) \in \mathbb{R}^{m(j)}$. The nonlinear function $\mathbf{f}_j : \mathbb{R}^{n(j)} \times \mathbb{R}^{m(j)} \times \mathbb{R} \rightarrow \mathbb{R}^{n(j)}$ is a vector field which describes the flow of segment j . Here $j \in \{0, 1, \dots, N\}$ is a counter that defines the flow set \mathcal{C}_j in which the system resides, where N is the number of segments in a trajectory. When j is increased, and another flow set is entered, the vector field that defines the behavior of the system can change. We refer to (t, j) as the *hybrid time*. Note that the state dimension $n(j)$ and the input dimension $m(j)$ can vary in different segments j .

The discrete dynamics of the hybrid system with impulsive effects are given by

$$\mathbf{x}_{j+1} = \mathbf{g}_j(\mathbf{x}_j, \mathbf{u}_j, t), \quad \mathbf{x}_j, \mathbf{u}_j \in \mathcal{D}_{j+1} \quad (2.32)$$

The discrete dynamics $\mathbf{g}_j : \mathbb{R}^{n(j-1)} \times \mathbb{R}^{m(j-1)} \times \mathbb{R} \rightarrow \mathbb{R}^{n(j)}$ is a mapping function, which maps the ante-event state to the post-event state. This map is evaluated when the system enters the set $\mathcal{D}_{j+1}(t) \subseteq \partial\mathcal{C}_j := \{\mathbf{x}(t, j) \in \mathbb{R}^{n(j)}, \mathbf{u}(t, j) \in \mathbb{R}^{m(j)} \mid \gamma_{j+1}(\mathbf{x}^\wedge, \mathbf{u}^\wedge, t) = 0\}$, indicating that an event should occur. The set \mathcal{D}_{j+1} is defined using some virtual state and input $\mathbf{x}^\wedge, \mathbf{u}^\wedge$ that are not necessarily physically realistic, and a *guard function* γ_{j+1} . A guard function is a state-and-input dependent differentiable function with the properties

$$\gamma_{j+1}(\mathbf{x}, \mathbf{u}, t) > 0, \quad (\mathbf{x}, \mathbf{u}, t) \in \mathcal{C}_j \setminus \partial\mathcal{C}_j, \quad (2.33)$$

$$\gamma_{j+1}(\mathbf{x}, \mathbf{u}, t) = 0, \quad (\mathbf{x}, \mathbf{u}, t) \in \mathcal{D}_{j+1} = \partial\mathcal{C}_j, \quad (2.34)$$

$$\gamma_{j+1}(\mathbf{x}, \mathbf{u}, t) < 0, \quad (\mathbf{x}, \mathbf{u}, t) \in (\mathbb{R}^n \times \mathbb{R}^m \times \mathbb{R}) \setminus \mathcal{C}_j, \quad (2.35)$$

where $\partial\mathcal{C}_j$ is the boundary of flow set \mathcal{C}_j . Using a guard function, \mathcal{C}_j and \mathcal{D}_{j+1} can conveniently be described. This is illustrated in Figure 2.4. While the guard function is greater than zero, the continuous dynamics (2.31) should be evaluated, since the system is in the interior of flow set \mathcal{C}_j . When the guard function is activated, i.e., $\gamma_{j+1} = 0$, the ante-event state $\mathbf{x}_j(t_{j+1})$ is mapped to the post-event state $\mathbf{x}_{j+1}(t_{j+1})$ using the discrete dynamics (2.32). Here t_{j+1} denotes the time-instant where γ_{j+1} is activated. After this event, the system will continue flowing in \mathcal{C}_{j+1} according to the vector field \mathbf{f}_{j+1} .

The hybrid dynamics (2.31), (2.32) will form the starting point in formulating the tracking problem for mechanical systems with unilateral constraints and spatial friction. In this, consider a nominal state-and-input trajectory $(\boldsymbol{\alpha}(t, j), \boldsymbol{\mu}(t, j))$ that is a solution to (2.31), (2.32) for initial condition $\boldsymbol{\alpha}(t_0, 0) = \boldsymbol{\alpha}_0 \in \mathcal{C}_0$ and consists of $N + 1$ absolutely continuous segments discriminated by the event counter $j \in \{0, 1, \dots, N\}$. The nominal event time of event j is denoted τ_j and regular time is denoted t . An example of a reference trajectory is illustrated in Figure 2.5.

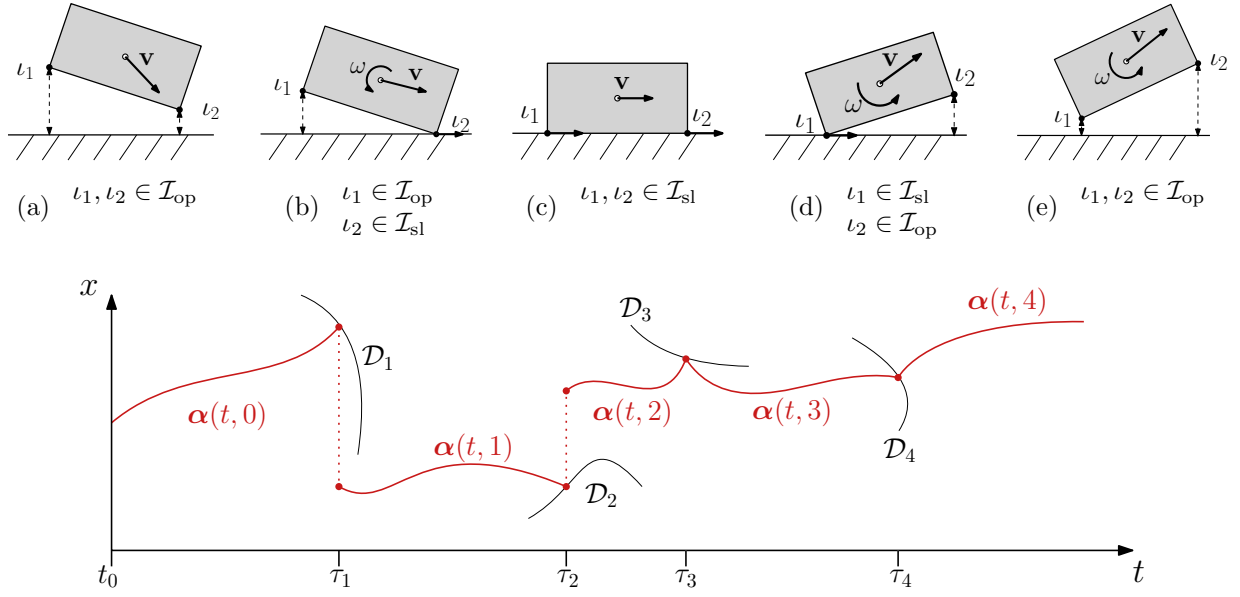


Figure 2.5: An example trajectory, which satisfies the dynamics (2.31)-(2.32), of a block pushing towards and withdrawing from a surface with velocity \mathbf{v} . Note that the sets \mathcal{D} besides being dependent on \mathbf{x} , are also dependent on \mathbf{u} . Also, although not depicted in this image, the state space of the system varies with every event.

The figure shows a block that impacts the ground, slides over the ground, and is subsequently lifted from the ground. The block has two contact points on its edges ι_1 and ι_2 . The motion starts with both contact points open as can be seen in Figure 2.5a. The flow is described by $\dot{\alpha}(t, 0) = \mathbf{f}_0(\alpha(t, 0), \mu(t, 0), t)$ for $t \in [t_0, \tau_1]$. Then, contact is established at contact point ι_2 at the time τ_1 , causing a jump in the state and a change in continuous dynamics to the vector field $\mathbf{f}_1(\alpha(t, 1), \mu(t, 1), t)$ for $t \in [\tau_1, \tau_2]$. This is illustrated in Figure 2.5b, where ι_2 is closed and slipping over the contact surface. At the time τ_2 , another corner of the rectangle, i.e. contact point ι_1 , impacts the ground as well causing another jump and another change in continuous dynamics. The block now has both contact points slipping over the contact surface. After this, both contact points release contact one by one. Since there are no impulsive forces present in this transition, the state does not jump when a contact point releases. However, due to frictional effects, a jump in the time-derivate of the state is possible, which makes these transitions continuous but nonsmooth.

Next, in Sections 2.3.3-2.3.4, the complementarity system defined in Section 2.2 will be fitted into the hybrid system (2.31),(2.32). In Section 2.3.2, the continuous dynamics \mathbf{f}_j will be derived for mechanical systems with unilateral constraints and spatial friction. Then, in Section 2.3.3 the reset set \mathcal{D}_j will be defined. Finally, in Section 2.3.4 the discrete dynamics \mathbf{g}_j will be derived. This will fully define the hybrid system with impulsive effects for mechanical systems with unilateral constraints and spatial friction.

2.3.2 Continuous dynamics

Let us start by considering the state \mathbf{x} to be composed as

$$\mathbf{x} = \begin{bmatrix} \mathbf{q} \\ \dot{\mathbf{q}} \end{bmatrix}. \quad (2.36)$$

As described in Section 2.2, for mechanical systems a set of contact points $\mathcal{I} = \{\iota_1, \iota_2, \dots, \iota_c\}$ is defined, with c is the number of considered contact points. A set \mathcal{I}_{cl} is defined as the set of closed contact points, such that a contact $\iota \in \mathcal{I}_{\text{cl}}$ has closed a unilateral constraint. The set of contact points in open contact is defined as $\mathcal{I}_{\text{op}} := \{\iota \mid \iota \notin \mathcal{I}_{\text{cl}}\}$. The set \mathcal{I}_{cl} is divided in the subsets \mathcal{I}_{sl} and \mathcal{I}_{st} , where \mathcal{I}_{sl} is the set of closed contact points in slip and \mathcal{I}_{st} the set of closed contact points in stick. The division implies that $\mathcal{I}_{\text{cl}} = \mathcal{I}_{\text{sl}} \cup \mathcal{I}_{\text{st}}$ and that $\mathcal{I}_{\text{sl}} \cap \mathcal{I}_{\text{st}} = \emptyset$.

The equations of motion, given in (2.3), can be rewritten to

$$\dot{\nu} = M^{-1}(q) [S(q)u - C(q, \nu) + W_n(q)\lambda_n + W_t(q)\lambda_t], \quad (2.37)$$

with

$$\begin{aligned} W_n &= [w_{n,i_1}, w_{n,i_2}, \dots, w_{n,\iota}] \in \mathbb{R}^{n \times c}, \\ W_t &= [W_{t,i_1}, W_{t,i_2}, \dots, W_{t,\iota}] \in \mathbb{R}^{n \times 2c}, \\ \lambda_n &= [\lambda_{n,\iota_1}; \lambda_{n,\iota_2}; \dots; \lambda_{n,\iota_c}] \in \mathbb{R}^c, \\ \lambda_t &= [\lambda_{t,\iota_1}; \lambda_{t,\iota_2}; \dots; \lambda_{t,\iota_c}] \in \mathbb{R}^{2c}. \end{aligned}$$

Note that since \mathbf{f}_j is only defined on $\mathbf{x}(t, j), \mathbf{u}(t, j) \notin \mathcal{D}_{j+1}$, it is not necessary to use ν to define the equations of motion as done in (2.3). It follows that \mathbf{f}_j can be written as

$$\dot{\mathbf{x}}_j(t) = \left[M^{-1}(q) [S(q)u - C(q, \dot{q}) + W_n(q)\lambda_n + W_t(q)\lambda_t] \right]. \quad (2.38)$$

The closed contact points in \mathcal{I}_{cl} experience reaction forces $\lambda_{n,\iota}$ and $\lambda_{t,\iota}$, as can be seen in (2.37). Therefore, for all closed contact points $\iota \in \mathcal{I}_{\text{cl}}$, constraints are included which restrict these reaction forces. These constraints are given by

$$w_{n,\iota}^T(q)\ddot{q} + \dot{w}_{n,\iota}^T(q)\dot{q} = 0, \quad \forall \iota \in \mathcal{I}_{\text{cl}}, \quad (2.39)$$

$$\lambda_{t,\iota} ||W_{t,\iota}^T \dot{q}|| + \mu_\iota \lambda_{n,\iota} W_{t,\iota}^T \dot{q} = 0, \quad \forall \iota \in \mathcal{I}_{\text{sl}}, \quad (2.40)$$

$$W_{t,\iota}^T(q)\ddot{q} + \dot{W}_{t,\iota}^T(q)\dot{q} = 0, \quad \forall \iota \in \mathcal{I}_{\text{st}}, \quad (2.41)$$

where again \mathcal{I}_{sl} and \mathcal{I}_{st} are the sets of closed contacts in slip and closed contacts in stick, respectively. With (2.38) and (2.39)-(2.41), the continuous dynamics of the hybrid system are correctly defined. A more thorough derivation of these dynamics can be found in Appendix A.1.

System mode descriptor

A system will have different flow dynamics as the system mode changes, as can be seen in (2.39)-(2.41). Also the jump sets \mathcal{D}_j change with the mode, as will be shown in Section 2.3.3. Therefore it is necessary to keep track of the mode the system is in. The system mode descriptor σ_j is introduced to conveniently describe the current system mode. Each contact point can either be in open-contact, closed-contact slip or closed-contact stick. The system mode descriptor is therefore defined as the ordered set

$$\sigma = (\sigma_1, \sigma_2, \dots, \sigma_\iota), \quad (2.42)$$

where σ_ι is the mode of contact point ι . σ_ι can either have the value ‘op’ for a contact point in open-contact, ‘sl’ for a contact point in closed-contact slip, or ‘st’ for a contact point in closed-contact stick. For example, the system mode descriptor of the mode in Figure 2.5b is $\sigma = (\text{op}, \text{sl})$.

2.3.3 Discrete event sets

When the system state enters an event set \mathcal{D} , an event will take place. The current mode for the different contact points is in that case altered and a corresponding state reset is applied. In this section the sets \mathcal{D} are defined for each mode of a contact point. The derivation of the discrete event sets can be found in Appendix A.1. The discrete event sets are defined using guard functions as presented in Section 2.3.1. Furthermore, in this section the superscript $(\cdot)^{\sigma_i^- \rightarrow \sigma_i^+}$ is introduced to indicate that the guard function $\gamma^{\sigma_i^- \rightarrow \sigma_i^+}$, or event set $\mathcal{D}^{\sigma_i^- \rightarrow \sigma_i^+}$ is related to the transition from ante-event mode σ_i^- to post-event mode σ_i^+ .

Discrete events sets in open contact

For all contact points $\iota \in \mathcal{I}_{\text{op}}$, the discrete event sets are defined as

$$\mathcal{D}_\iota^{\text{op} \rightarrow \text{cl}} = \{\mathbf{x} \mid \gamma_\iota^{\text{op} \rightarrow \text{cl}} = 0\}, \quad (2.43)$$

with

$$\gamma_\iota^{\text{op} \rightarrow \text{cl}} = h_{n,\iota}(\mathbf{q}). \quad (2.44)$$

Discrete events sets in closed contact slip

For all contact points $\iota \in \mathcal{I}_{\text{sl}}$, the discrete event sets are defined as

$$\mathcal{D}_\iota^{\text{sl} \rightarrow \text{st}} = \{\mathbf{q} \mid \gamma_\iota^{\text{sl} \rightarrow \text{st}} = 0\}, \quad (2.45)$$

$$\mathcal{D}_\iota^{\text{cl} \rightarrow \text{op}} = \{\mathbf{q}, \mathbf{u} \mid \gamma_\iota^{\text{cl} \rightarrow \text{op}} = 0\}, \quad (2.46)$$

with

$$\gamma_\iota^{\text{sl} \rightarrow \text{st}} = \sqrt{\mathbf{v}_{t,\iota}^T \mathbf{v}_{t,\iota}}, \quad (2.47)$$

$$\gamma_\iota^{\text{cl} \rightarrow \text{op}} = \lambda_{n,\iota}. \quad (2.48)$$

Discrete events sets in closed contact stick

For all contact points $\iota \in \mathcal{I}_{\text{st}}$, the discrete event sets are defined as

$$\mathcal{D}_\iota^{\text{st} \rightarrow \text{sl}} = \{\mathbf{q}, \mathbf{u} \mid \gamma_\iota^{\text{st} \rightarrow \text{sl}} = 0\}, \quad (2.49)$$

$$\mathcal{D}_\iota^{\text{cl} \rightarrow \text{op}} = \{\mathbf{q}, \mathbf{u} \mid \gamma_\iota^{\text{cl} \rightarrow \text{op}} = 0\}, \quad (2.50)$$

with

$$\gamma_\iota^{\text{st} \rightarrow \text{sl}} = \mu^2 \lambda_{n,\iota}^2 - \boldsymbol{\lambda}_{t,\iota} \boldsymbol{\lambda}_{t,\iota}^T, \quad (2.51)$$

$$\gamma_\iota^{\text{cl} \rightarrow \text{op}} = \lambda_{n,\iota}. \quad (2.52)$$

2.3.4 Discrete dynamics

Whenever the state \mathbf{x} reaches the discrete event set \mathcal{D} , continuous evolution in its current mode is generally not feasible. The system should therefore go through a discrete event, in which the state is reinitialized and the mode is changed. One contact point entering a discrete event set can lead to other contact points experiencing infeasible reaction forces, making it difficult to determine in what mode each contact point should be. The reinitialization of the state and selection of a post-event mode is described by the discrete dynamics in this section. First a *nonlinear complementarity problem* (NCP) is solved to reinitialize the state. The NCP generates a unique feasible solution [66],

which for simple systems can be found by iterating over all possible modes until the feasible solution is found. Then, a mode selection algorithm is presented to find a feasible post-event mode, which defines the continuous dynamics to be integrated after the event.

State reinitialization

From the impulsive dynamics (2.25)-(2.28), the discrete dynamics for an impulsive event which determine the post-event joint velocity $\dot{\mathbf{q}}^+$ can be derived as

$$\dot{\mathbf{q}}^+ = \mathbf{M}^{-1} [\mathbf{W}_n \mathbf{\Lambda}_n + \mathbf{W}_t \mathbf{\Lambda}_t] + \dot{\mathbf{q}}^-, \quad (2.53)$$

$$\mathbf{w}_{n,\ell}^T \dot{\mathbf{q}}^+ = 0, \quad \forall \ell \in \mathcal{I}_{\text{cl}}, \quad (2.54)$$

$$\mathbf{\Lambda}_{t,\ell} \|\mathbf{W}_{t,\ell}^T \dot{\mathbf{q}}^+\| + \mu \mathbf{\Lambda}_{n,\ell} \mathbf{W}_{t,\ell}^T \dot{\mathbf{q}}^+ = 0, \quad \forall \ell \in \mathcal{I}_{\text{sl}}, \quad (2.55)$$

$$\mathbf{W}_{t,\ell}^T \dot{\mathbf{q}}^+ = 0, \quad \forall \ell \in \mathcal{I}_{\text{st}}. \quad (2.56)$$

Here the unknown variables are $\dot{\mathbf{q}}^+ \in \mathbb{R}^n$, $\mathbf{\Lambda}_n \in \mathbb{R}^{c_{\text{cl}}}$ and $\mathbf{\Lambda}_t \in \mathbb{R}^{2c_{\text{cl}}}$, which means that there are $n + 3c_{\text{cl}}$ unknown variables. From (2.53) we get n equations, from (2.54) we get c_{cl} equations and since $\mathcal{I}_{\text{sl}} \cup \mathcal{I}_{\text{st}} = \mathcal{I}_{\text{cl}}$, $\mathbf{\Lambda}_{t,\ell} \in \mathbb{R}^2$, and $\mathbf{W}_{t,\ell}^T \dot{\mathbf{q}}^+ \in \mathbb{R}^2$ we get $2c_{\text{cl}}$ equations from (2.55)-(2.56). Since we have $n + 3c_{\text{cl}}$ unknown variables and $n + 3c_{\text{cl}}$ equations, the system is solvable.

The problem that remains is that it is not straightforward to identify what the correct mode and therewith what the sets \mathcal{I}_{op} , \mathcal{I}_{sl} , and \mathcal{I}_{st} should be after an event. The set of equations that should be solved is the set of equations that corresponds to the system-mode which generates a feasible post-event state. When a contact point enters a discrete event set, and thus generates an infeasible state, it can be concluded that the system will go through an event because in it's current mode the system is infeasible. However, it is not guaranteed that the contact point which entered the event set will change their mode. Actually any contact point, or even several contact points, can change their mode. Therefore the dynamics should be solved for several modes, until a feasible post-event state is found. A feasible post-event state is a post-event state solved for a certain system-mode σ , such that the all corresponding guard functions are inactive, i.e., all $\Gamma_\ell > 0$. As mentioned earlier, there will exist a unique system-mode where the system has a feasible post-impact state. Similar to the non-impulsive guard functions defined in Section 2.3.3, the impulsive guard functions are given by

$$\Gamma_\ell^{\text{cl} \rightarrow \text{op}} = \mathbf{\Lambda}_{n,\ell}, \quad (2.57)$$

$$\Gamma_\ell^{\text{sl} \rightarrow \text{st}} = (\mathbf{v}_{t,\ell}^+)^T \mathbf{v}_{t,\ell}^+, \quad (2.58)$$

$$\Gamma_\ell^{\text{st} \rightarrow \text{sl}} = \mu^2 \mathbf{\Lambda}_{n,\ell}^2 - \mathbf{\Lambda}_{t,\ell} \mathbf{\Lambda}_{t,\ell}^T. \quad (2.59)$$

Note that all guard functions are defined at velocity level during the state reinitialization. The NCP (2.53)-(2.56) is defined at velocity level, meaning that only guard functions on velocity level need to be considered. For example, it is impossible for the state reinitialization to generate an infeasible position because the position of the system is not updated during the state reinitialization. When $\mathbf{\Lambda}_{n,\ell} = 0$ and $\mathbf{\Lambda}_{t,\ell} = 0$ during an event, one speaks of a non-impulsive event. In this case, the state is not reinitialized during the event. However, the system will enter a different mode. For both impulsive and non-impulsive events, the post-event mode is determined during the mode selection, which is described below.

Mode selection

The mode σ of a system is determined by the guard functions defined in Section 2.3.3. All guard functions γ_ℓ should be greater than zero for the system to be in a feasible mode. Because some of these guard functions are defined on acceleration level and the post-event acceleration is not constrained by the NCP, we should first find a post-event mode σ^+ where the accelerations $\ddot{\mathbf{q}}$ and reaction forces $\mathbf{\lambda}_n, \mathbf{\lambda}_t$ are feasible before we know which vector field is suitable to define the next flow

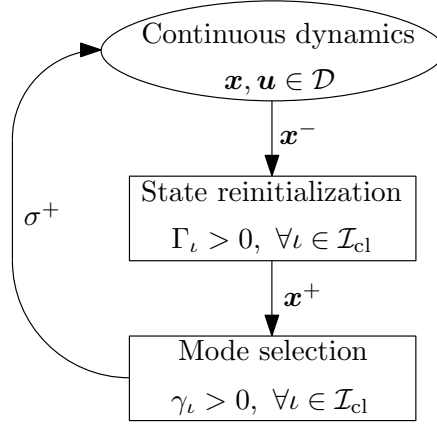


Figure 2.6: The algorithm used to solve a hybrid system with impulsive effects depicted in a flowchart.

phase. From the continuous dynamics (2.18)-(2.21), post-event accelerations and reaction forces can be computed from

$$\ddot{\mathbf{q}}^+ = \mathbf{M}^{-1} [\mathbf{S}\mathbf{u}^+ - \mathbf{C} + \mathbf{W}_n\boldsymbol{\lambda}_n^+ + \mathbf{W}_t\boldsymbol{\lambda}_t^+], \quad (2.60)$$

$$\mathbf{w}_{n,\ell}^T \ddot{\mathbf{q}}^+ + \dot{\mathbf{w}}_{n,\ell}^T \dot{\mathbf{q}}^+ = 0, \quad \forall \ell \in \mathcal{I}_{\text{cl}}, \quad (2.61)$$

$$\boldsymbol{\lambda}_{t,\ell}^+ \|\mathbf{W}_{t,\ell}^T \dot{\mathbf{q}}^+\| + \mu \lambda_{n,\ell}^+ \mathbf{W}_{t,\ell}^T \dot{\mathbf{q}}^+ = 0, \quad \forall \ell \in \mathcal{I}_{\text{sl}}, \quad (2.62)$$

$$\mathbf{W}_{t,\ell}^T \ddot{\mathbf{q}}^+ + \dot{\mathbf{W}}_{t,\ell}^T \dot{\mathbf{q}}^+ = 0, \quad \forall \ell \in \mathcal{I}_{\text{st}}, \quad (2.63)$$

where \mathbf{M} , \mathbf{S} , \mathbf{C} , $\mathbf{w}_{n,\ell}$ and $\mathbf{W}_{t,\ell}$ are evaluated at the post-event joint configuration \mathbf{q}^+ and velocity $\dot{\mathbf{q}}^+$. Because we are interested in whether the accelerations and reaction forces are feasible, the guard functions defined on acceleration level are evaluated. The guard functions that determine the feasibility of a post-event mode are given by

$$\gamma_{\ell}^{\text{cl} \rightarrow \text{op}} = \lambda_{n,\ell}, \quad \forall \ell \in \mathcal{I}_{\text{cl}}, \quad (2.64)$$

$$\gamma_{\ell}^{\text{st} \rightarrow \text{sl}} = \mu_{\ell}^2 \lambda_{n,\ell}^2 - \boldsymbol{\lambda}_{t,\ell} \boldsymbol{\lambda}_{t,\ell}^T, \quad \forall \ell \in \mathcal{I}_{\text{st}}, \quad (2.65)$$

with $\mathcal{I}_{\text{sl}} \cup \mathcal{I}_{\text{st}} = \mathcal{I}_{\text{cl}}$. Note that the guard functions $\gamma_{\ell}^{\text{op} \rightarrow \text{cl}}$ and $\gamma_{\ell}^{\text{sl} \rightarrow \text{st}}$ are not evaluated. This is unnecessary, because open contact points can only trigger guard functions defined at position level. Since the non-impulsive dynamics only update the acceleration, it is impossible for a contact point in open contact to change mode during an impulsive event. This also holds for the guard function from slip to stick, which is defined on velocity level.

The process of solving a hybrid system with impulsive effects is illustrated in Figure 2.6. The system first flows according to a vector field \mathbf{f} . When the event set \mathcal{D} is reached, a jump in the system state \mathbf{x} is applied. This jump is the result of solving an NCP to find the post-event state \mathbf{x}^+ . Finally, the mode selection is performed to find a feasible post-event mode σ^+ for that post-event state \mathbf{x}^+ . The continuous dynamics for the next flow segment is defined by σ^+ with \mathbf{x}^+ as initial condition.

2.4 Summary

The modeling of mechanical systems with unilateral constraints and spatial friction is presented in this chapter. First, a complementarity problem formulation for such systems is presented using Signorini's contact law, Newton's impact law, and Coulomb's friction law. This system fully defines

the dynamics of mechanical systems with unilateral constraints and spatial friction. From the complementarity problem formulation a hybrid system with impulsive effects is derived. This system is constructed with a control point-of-view in mind, and its compatibility with the control strategy that will be presented in the following chapters. The hybrid system is defined in three parts. First the continuous dynamics are presented. Then the discrete event sets are given, which are state-input sets that trigger a discrete event when the state and input enters such a set. Finally, the dynamics of such an event are presented, which consist of a state reinitialization and a mode selection.

Chapter 3

Sensitivity Analysis with Isolated State-and-Input-Triggered Events

In this chapter, the behavior of trajectories tracking a nominal reference trajectory is analyzed. More specifically, an analysis of tracking trajectories with state-and-input-triggered jumps of hybrid systems is presented. We will refer to the considered class of systems as *nonlinear state-and-input-triggered hybrid systems* (NSITHS). In this chapter, isolated events are considered, indicating that guard functions are activated separately, such that there is always flow between the activations. The work in this chapter is an extension on [49, 55, 67], where a sensitivity analysis for *nonlinear state-triggered hybrid systems* (NSTHS) has been presented. In this work, We will analyze the behavior of the system in the neighborhood of a nominal trajectory assuming that atleast locally these isolated events also occur in the same sequence. However, the timing of the events will differ from the nominal event times for nearby trajectories. The mismatch in event time between the nominal trajectory and state trajectory can result in *peaking behavior* of the tracking error [41, 42]. Peaking behavior is known to result in undesirable large actuation forces. First, we introduce a different notion of error to avoid peaking behavior. After that, an approximation of the NSITHS will be presented in the form of a *linear time-triggered hybrid system* (LTTHS), which we expect to be first order. There is no proof yet available that the LTTHS is a first-order approximation of the NSITHS, but it is strongly presumed. This chapter partially extends the work in [55], in the sense that the sensitivity analysis in this chapter is suitable for input-dependent guard functions, which are introduced by frictional effects and releasing motions. In [55] there is also a proof which infers stability properties of an NSTHS about a reference trajectory from its corresponding LTTHS. Our claim is that a similar result will hold for the stability of the LTTHS implying local asymptotic stability of the NSITHS. This proof is however left for future work. Under the presumption that stability of the LTTHS implies local asymptotic stability of the NSITHS, conventional stability analysis tools for LTTHS can be used to asses the local stability of the NSITHS. Finally, a short summary of the findings in this chapter is given.

3.1 Trajectories with state-and-input-triggered jumps

This section presents *reference spreading* (RS) for trajectories with isolated events. Reference spreading is presented for isolated events in [49], which is extended to be suitable for input-dependent guards in this section. When the hybrid system starts from a different initial condition than that of the reference trajectory for example, the resulting state trajectory and reference trajectory will likely have non-coinciding event-times. The notion of error defined in reference spreading eliminates

the peaking behavior that results from the mismatch in event-time. In order to explain this notion of error better, we will first elaborate on the class of systems we consider, on the type of reference trajectories we allow, and we will introduce notation.

3.1.1 Nonlinear state-and-input-triggered hybrid systems

The framework of hybrid systems with impulsive effects is now used to formally define the NSITHS, which is the class of systems that is considered in this work.

Definition 1 (NSITHS). *A nonlinear state-and-input-triggered hybrid system is a system with dynamics of the form*

$$\dot{\mathbf{x}}_j = \mathbf{f}_j(\mathbf{x}_j, \mathbf{u}_j, t), \quad \mathbf{x}_j, \mathbf{u}_j \in \mathcal{C}_j \quad (3.1)$$

$$\mathbf{x}_{j+1} = \mathbf{g}_{j+1}(\mathbf{x}_j, \mathbf{u}_j, t), \quad \mathbf{x}_j, \mathbf{u}_j \in \mathcal{D}_{j+1} \quad (3.2)$$

with the state $\mathbf{x}_j := \mathbf{x}(t, j)$, the input $\mathbf{u}_j := \mathbf{u}(t, j)$, nonlinear vector field \mathbf{f}_j , flow set \mathcal{C}_j after event j , and a jump set $\mathcal{D}_{j+1} \subseteq \partial\mathcal{C}_j$, where when $(\mathbf{x}_j, \mathbf{u}_j) \in \mathcal{D}_{j+1}$ a state reinitialization is triggered according to the jump map \mathbf{g}_{j+1} in (3.2). Note that in \mathbf{x}_j and \mathbf{u}_j , the time-dependency is implicit.

Consider a nominal trajectory of an NSITHS, as illustrated in Figure 3.1 in red. We denote this nominal trajectory $\alpha_j := \alpha(t, j)$ and assume it is the solution to (3.1)-(3.2) for input signal $\mu_j := \mu(t, j)$ starting from initial condition $\alpha(t_0, 0) = \alpha_0 \in \mathcal{C}_0$. The following assumption on the nominal trajectory is imposed, to exclude that nominal jump times accumulate in time. Note that also for α_j and μ_j , the time-dependency is left implicit.

Assumption 1 (t-completeness and non-Zeno behavior of α). *The reference trajectory α is defined for all $t > t_0$. Also, each segment α_j has non-vanishing time-domains $I_j^\alpha = [\tau_j, \tau_{j+1}]$, i.e., $\tau_{j+1} - \tau_j \geq c > 0$, where τ_j is the j^{th} event time and c is a positive constant.*

It can be guaranteed that there is non-zero time between events, if $\mathbf{g}_{j+1}(\alpha_j(\tau_{j+1}), \mu_j(\tau_{j+1})) \notin \mathcal{D}_{j+1}$ for all $j \in \{0, 1, \dots, N\}$.

Consider now a state trajectory \mathbf{x} starting from initial condition $\mathbf{x}(t_0, 0, \epsilon) = \mathbf{x}_0(\epsilon) = \alpha_0 + \epsilon \mathbf{z}_0$ with input $\mathbf{u}_j(\epsilon) = \mu_j + \epsilon \mathbf{v}_j$, where ϵ is an initial state and input perturbation. In this $\mathbf{z}_0 = \partial \mathbf{x}_0 / \partial \epsilon$, $\mu_j = \mu(t, j)$ the feedforward corresponding to α_j , and $\mathbf{v}_j = \mathbf{v}(t, j)$ the feedback. An example of a perturbed trajectory $\mathbf{x}(\epsilon)$ is shown in Figure 3.1.

For the nominal trajectory, the state and input curves are known over the entire time-domain, meaning that the event-times are also known. For the perturbed trajectory this is not the case. Referring to Figure 3.1, there will be a mismatch between the nominal event times τ_1 and τ_2 and the perturbed event times t_1 and t_2 . Taking a closer look at the first event of Figure 3.2, the peaking behavior can be illustrated as the result of a jump mismatch. In Figure 3.2, the state evolution \mathbf{x} of the first event is depicted besides the conventional tracking error $\|\mathbf{x} - \alpha\|$ (assuming that α_j, \mathbf{x}_j and $\alpha_{j+1}, \mathbf{x}_{j+1}$ are of the same dimension), where both trajectories are considered a function of conventional time t alone. One can clearly see that a peak arises in the tracking error when the jump times do not coincide. At time equal to t_1 , the state trajectory jumps, while the reference trajectory does not. At time equal to τ_1 , the reference trajectory jumps as well. This means that in $[t_1, \tau_1]$, a post-event state trajectory is compared to a ante-event reference trajectory, resulting in a large peak in the tracking error. This is undesirable in stability analysis and may for example lead to large and unnecessary actuation forces when considered in feedback control.

In the next section, a different notion of error will be introduced that does not illustrate peaking behavior.

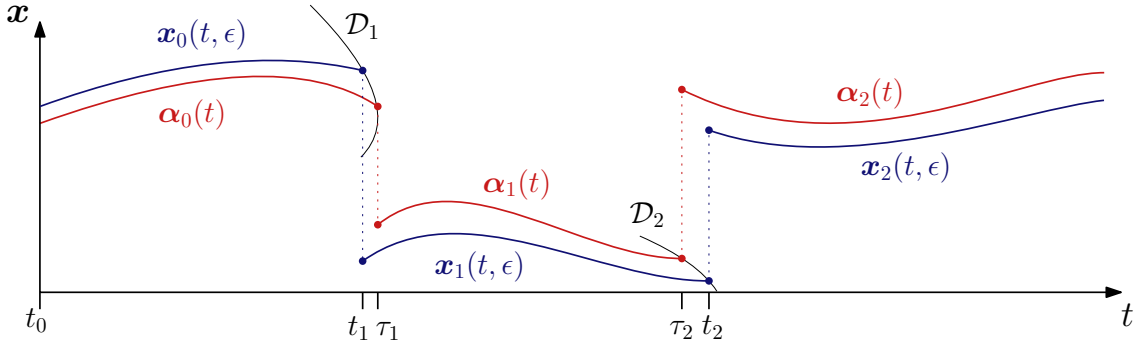


Figure 3.1: A nominal (red) and a perturbed (blue) trajectory of a hybrid system with impulsive effects are depicted in this figure. The nominal and the state trajectory enter the jump sets D at mismatching time instants, as a result from the perturbation in the state trajectory.

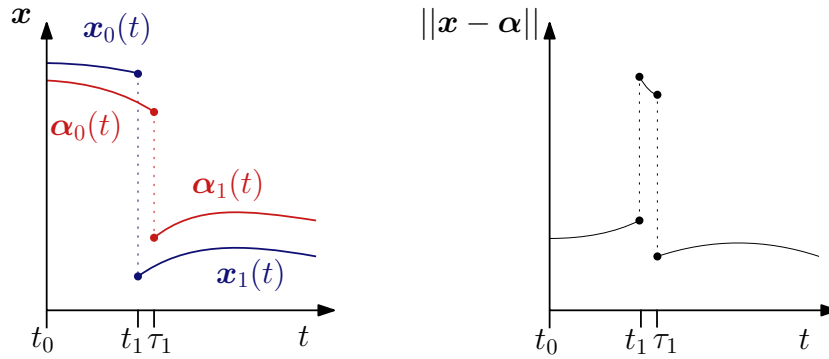


Figure 3.2: A closer look at the first event of the trajectory in Figure 3.1. On the left the state-evolution \mathbf{x} is depicted and on the right the tracking error $\|\mathbf{x} - \boldsymbol{\alpha}\|$. A clear peak can be noticed in the tracking error as a result from the event-time mismatch.

3.1.2 Reference-spreading

To avoid peaking behavior in the tracking error, in [49] a methodology is presented which is named reference spreading in [53]. In reference spreading a novel notion of error is introduced, called the *reference spreading error* (RS error). The methodology uses reference trajectories which are extended beyond event-times, such that an ante-event state trajectory can always be compared to an ante-event reference trajectory and a post-event state trajectory can always be compared to a post-event reference trajectory. This is illustrated in Figure 3.3, where the reference trajectory $\boldsymbol{\alpha}_j$ is extended resulting in $\bar{\boldsymbol{\alpha}}_j$. The extension is made by forward integrating the vector field \mathbf{f}_j beyond τ_{j+1} and backward integrating \mathbf{f}_j before τ_j , for all $j \in \{0, 1, \dots, N\}$. Adopting the notation of [16], the hybrid domain of $\boldsymbol{\alpha}$ is defined by segments $I_j^\alpha = [\tau_j, \tau_{j+1}]$, which together form the entire domain of $\boldsymbol{\alpha}$ as

$$\text{dom } \boldsymbol{\alpha} = \bigcup_{j=0}^N I_j^\alpha \times \{j\}. \quad (3.3)$$

Similarly the state segments \mathbf{x}_j are defined on the time intervals $I_j^x = [t_j, t_{j+1}]$ with the entire domain defined as

$$\text{dom } \mathbf{x} = \bigcup_{j=0}^N I_j^x \times \{j\}. \quad (3.4)$$

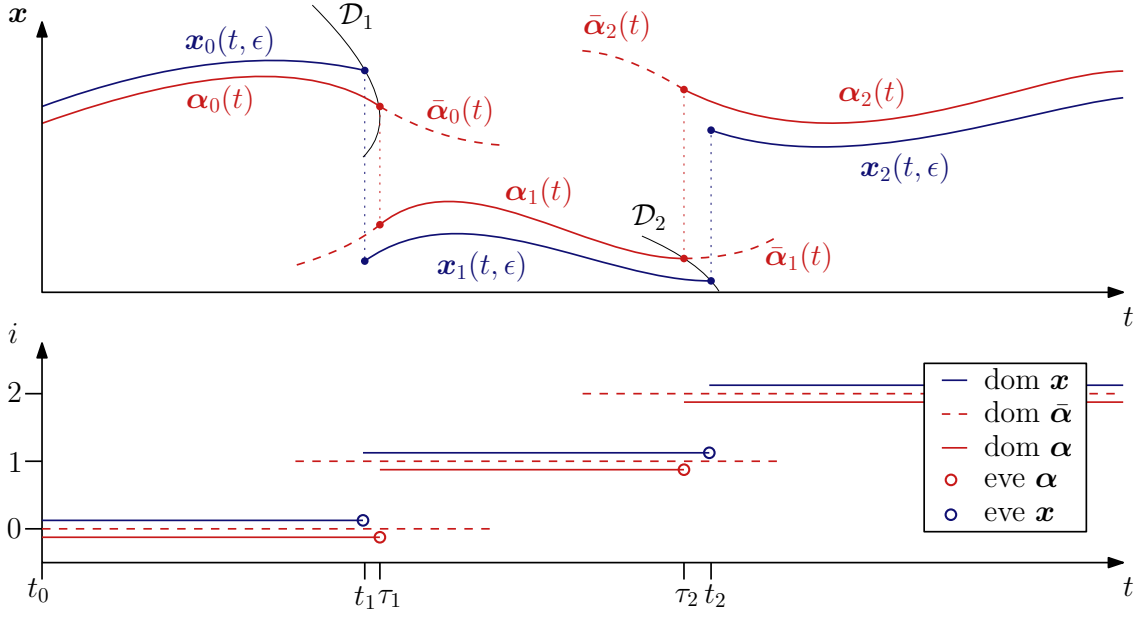


Figure 3.3: An illustration of the nominal reference trajectory (red) and the perturbed trajectory (blue), where the nominal reference trajectory is extended such that $\text{dom } \mathbf{x} \subseteq \text{dom } \bar{\boldsymbol{\alpha}}$.

The domain of the extended reference trajectory segments is extended such that $I_j^{\mathbf{x}} \subseteq I_j^{\bar{\boldsymbol{\alpha}}}$. The set of jump times of $\boldsymbol{\alpha}_j$ and $\mathbf{x}_j(\epsilon)$ are denoted as

$$\text{eve } \boldsymbol{\alpha} = \bigcup_{j=1}^N \{\tau_j\} \times \{j-1\}, \quad (3.5)$$

$$\text{eve } \mathbf{x} = \bigcup_{j=1}^N \{t_j\} \times \{j-1\}, \quad (3.6)$$

respectively.

Let us now pose a continuity based assumption on the vector field \mathbf{f}_j . This assumption (along with other assumptions) is instrumental to making sure that the ante-event state of the perturbed trajectory $\mathbf{x}_j(t_{j+1}, \epsilon)$ lies close to the ante-event state of the nominal trajectory $\boldsymbol{\alpha}_j(\tau_{j+1})$, which is necessary to define an approximation of the perturbed trajectory.

Assumption 2 (Lipschitz continuity of \mathbf{f}_j). *We assume that in a neighborhood of the reference trajectory $\boldsymbol{\alpha}_j$, \mathbf{f}_j is Lipschitz with respect to \mathbf{x} uniformly in t and j . That is, $\exists \epsilon_{\mathbf{f}} > 0$ and $\exists L$, independent of t, j , such that $\forall j, \|\mathbf{f}_j(\mathbf{a}, t) - \mathbf{f}_j(\mathbf{b}, t)\| < L\|\mathbf{a} - \mathbf{b}\|, \forall t \in (\tau_j - \epsilon_{\mathbf{f}}, \tau_{j+1} + \epsilon_{\mathbf{f}})$ and $\forall \mathbf{a}, \mathbf{b} \in B_{\epsilon_{\mathbf{f}}}(\bar{\boldsymbol{\alpha}}_j)$, where $B_{\epsilon_{\mathbf{f}}}(\bar{\boldsymbol{\alpha}}_j)$ is a ball with radius $\epsilon_{\mathbf{f}}$ around $\bar{\boldsymbol{\alpha}}_j$.*

In the lower plot of Figure 3.3, the hybrid time domains of \mathbf{x} , $\boldsymbol{\alpha}$ and $\bar{\boldsymbol{\alpha}}$ are illustrated. Note that for every j , it holds that $I_j^{\mathbf{x}} \subseteq I_j^{\bar{\boldsymbol{\alpha}}}$. This means that the reference spreading error $\|\mathbf{x} - \bar{\boldsymbol{\alpha}}\|$ can be evaluated until $t = t_j$ is reached. The reference spreading error $\|\mathbf{x} - \bar{\boldsymbol{\alpha}}\|$ is therefore continuous for fixed j , even in the case where $t_j \neq \tau_j$, since the state \mathbf{x}_j will be compared to $\boldsymbol{\alpha}_j$ until $t = t_j$ is reached. Once $t = t_j$, the counter j is increased, and \mathbf{x}_{j+1} is compared to $\boldsymbol{\alpha}_{j+1}$. Using this notion of error leaves only one jump at t_j in the tracking error, even under the presence of event-time mismatches. More importantly, the peak in the tracking error is avoided, and an ante-event state trajectory will not be compared to a post-event reference trajectory (and vice versa) anymore.

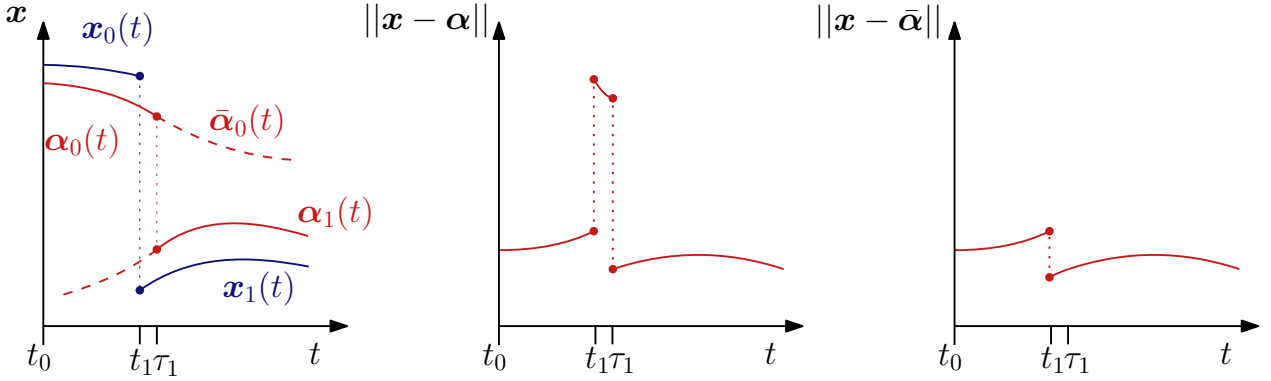


Figure 3.4: A close up of the first event of the reference trajectory, with the conventional error $\|x - \alpha\|$ illustrated in the middle figure, and the reference spreading error $\|x - \bar{\alpha}\|$ in the right figure. Since $\bar{\alpha}$ is evaluated in the same mode as x , i.e., the reference spreading error is $\|x_0 - \bar{\alpha}_0\|$ for $t \leq t_1$ and $\|x_1 - \bar{\alpha}_1\|$ for $t \geq t_1$, the peaking behavior is not observed in the reference spreading error.

This is illustrated in Figure 3.4, where the tracking errors with and without reference spreading are compared. Also, note that α_j and α_{j+1} , for $j \in \{0, 1, \dots, N\}$, do not need to be of the same dimension when the tracking error is defined as $\|x - \bar{\alpha}\|$.

In the next section, the reference spreading error will be used to analyze the behavior of perturbed trajectories with isolated events.

3.2 Approximating perturbed trajectories with isolated guard-activations

In [51] a sensitivity analysis is presented, where so-called sensitivity functions are used to provide first-order approximations of the effects of parameter variations on solutions. These sensitivity functions can also be used to approximate the solution under sufficiently small parameter variations. For the class of systems we consider here, the sensitivity equations describe the response of the system to perturbations in initial condition and input. This perturbation dynamics can be used to formulate an approximation of the perturbed state of the system, which we expect to be first-order. To find an approximation of state reinitializations in nonsmooth trajectories, an extension to this sensitivity analysis is necessary in the form of a linearized jump gain. The linearized jump gain and the linearized perturbation dynamics together define the LTTHS. In [55] stability properties of an NSTHS are associated with the stability the corresponding LTTHS. In this section, the LTTHS is derived for an NSITHS, which we expect can be used to assess the stability of the NSITHS under the presumption that a similar relation between the LTTHS and NSITHS exists. As mentioned in the intro to this chapter, the proof for this relation is left as future work. For a more thorough derivation of the following analysis, Appendix C should be consulted. We will first pose few assumptions on the reference events and jump maps that are required for the sensitivity analysis. First, we assume transversality of the reference events for which we assume the existence of a guard function that locally describes the flow and jump sets about each reference event.

Assumption 3 (Existence of a guard function). *We assume that there exist constants ε_γ , and real valued guard function $\gamma(x, u, t, j)$ which is continuously differentiable with respect to x , u , and t ,*

for each $j \in \{1, 2, \dots, N\}$, where N is potentially infinite, such that

$$\begin{aligned} \gamma_{j+1}(\mathbf{x}_j, \mathbf{u}_j, t) &> 0 & (\mathbf{x}, \mathbf{u}) &\in B_{\varepsilon_\gamma}(\boldsymbol{\alpha}_j(\tau), \boldsymbol{\mu}_j(\tau)) \cap \mathcal{C}_j \setminus \partial\mathcal{C}_j \\ \gamma_{j+1}(\mathbf{x}_j, \mathbf{u}_j, t) &= 0 & (\mathbf{x}, \mathbf{u}) &\in B_{\varepsilon_\gamma}(\boldsymbol{\alpha}_j(\tau), \boldsymbol{\mu}_j(\tau)) \cap \mathcal{D}_{j+1} \\ \gamma_{j+1}(\mathbf{x}_j, \mathbf{u}_j, t) &< 0 & (\mathbf{x}, \mathbf{u}) &\in B_{\varepsilon_\gamma}(\boldsymbol{\alpha}_j(\tau), \boldsymbol{\mu}_j(\tau)) \cap (\mathbb{R}^n \times \mathbb{R}^m \times \mathbb{R}) \setminus \mathcal{C}_j \end{aligned} \quad (3.7)$$

where $B_{\varepsilon_\gamma}(\boldsymbol{\alpha}_j(\tau), \boldsymbol{\mu}_j(\tau))$ is a ball with radius ε_γ around $\boldsymbol{\alpha}_j(\tau), \boldsymbol{\mu}_j(\tau)$ with $\tau = \tau_{j+1}$. The set \mathcal{C}_j is the flow set of a trajectory after event j and $\mathcal{D}_{j+1} \subseteq \partial\mathcal{C}_j$ is the event set which triggers event $j+1$, where $\partial\mathcal{C}_j$ represents the boundary of flow set \mathcal{C}_j . Note that $B_{\varepsilon_\gamma}(\boldsymbol{\alpha}_j(\tau), \boldsymbol{\mu}_j(\tau)) \cap (\mathbb{R}^n \times \mathbb{R}^m \times \mathbb{R}) \setminus \mathcal{C}_j$ only exists if \mathcal{C}_j is not closed.

Assumption 4 (Transversal guard activations). Under Assumption 3, we assume there exists a constant $c > 0$, such that

$$D_1\gamma_j(\boldsymbol{\alpha}_j, \boldsymbol{\mu}_j, t) \cdot \mathbf{f}_j(\boldsymbol{\alpha}_j, \boldsymbol{\mu}_j, t) + D_2\gamma_j(\boldsymbol{\alpha}_j, \boldsymbol{\mu}_j, t) \cdot \mathbf{f}_j(\boldsymbol{\alpha}_j, \boldsymbol{\mu}_j, t) + D_3\gamma_j(\boldsymbol{\alpha}_j, \boldsymbol{\mu}_j, t) \leq -c, \quad (3.8)$$

for every event time $(t, j) \in \text{eve } \boldsymbol{\alpha}$.

Remark. As can be seen in Assumption 4, the time derivative of the guard function at $\gamma_j(\boldsymbol{\alpha}_j, \boldsymbol{\mu}_j, t) = 0$ is needed to check for transversality. For $\gamma^{sl \rightarrow st} = \sqrt{\mathbf{v}_t^T \mathbf{v}_t}$, the time derivative is undefined when $\gamma^{sl \rightarrow st} = 0$. Therefore, a Taylor expansion is used to find the left limit of $\dot{\gamma}^{sl \rightarrow st}$ at $t = \tau_j$, to check whether the guard is activated transversally. More information on this can be found in Appendix A.1.2.

The state, input and time where $\gamma_j(\mathbf{x}_j, \mathbf{u}_j, t) = 0$ represents the set where an event will happen, which together with Assumption 4 guarantees that an event will happen, even under perturbations. If the vector field is continuous with respect to ϵ , Assumption 4 assumes that the vector field pushes the reference trajectory out of the flow set \mathcal{C}_j , and that grazing incidents are avoided. The combination of the existence of a guard function in an area around the nominal ante-event state and the transversal guard activation guarantees that there exists a range of perturbations where the guard is activated as well. Let us now pose an assumption on the jump map \mathbf{g} .

Assumption 5 (Locally differentiability of jump maps). We assume that for all $j \in \{0, 1, 2, \dots, N\}$ the jump map $\mathbf{g}_{j+1}(\mathbf{x}_j, \mathbf{u}_j)$ is locally differentiable, in the sense that $D_1\mathbf{g}_{j+1}(\mathbf{x}_j, \mathbf{u}_j)$ and $D_2\mathbf{g}_{j+1}(\mathbf{x}_j, \mathbf{u}_j)$ exist in the ball $B_{\varepsilon_\gamma}(\boldsymbol{\alpha}_j(\tau), \boldsymbol{\mu}_j(\tau), \tau) \subseteq \mathbb{R}^n \times \mathbb{R}^m \times \mathbb{R}$, where $\tau = \tau_{j+1}$.

The differentiability of the jump map is necessary to construct an approximation of the perturbed state trajectory. This will be explained in more detail in the next section.

3.2.1 Sensitivity analysis

The sensitivity analysis for the continuous segments of a perturbed trajectory gives a set of equations which describe the reaction of the system to an initial state-and-input perturbation. Introducing the initial state-and-input perturbation enables us to analyze the solution of a system under parameter variations. Writing (3.1) in integral form, a perturbed solution $\mathbf{x}_j(t, \epsilon)$ to (3.1) satisfies

$$\mathbf{x}_j(t, \epsilon) = \mathbf{x}_j(t_j, \epsilon) + \int_{t_j}^t \mathbf{f}_j(\mathbf{x}_j(s, \epsilon), \mathbf{u}_j(s, \epsilon), s) ds. \quad (3.9)$$

To find an approximation of the perturbed state, the perturbed state direction $\mathbf{z}(t)$ and the perturbed input direction $\mathbf{v}(t)$ are defined as

$$\mathbf{z}_j := \left. \frac{\partial \mathbf{x}_j(\epsilon)}{\partial \epsilon} \right|_{\epsilon=0}, \text{ and } \mathbf{v}_j := \left. \frac{\partial \mathbf{u}_j(\epsilon)}{\partial \epsilon} \right|_{\epsilon=0}, \quad (3.10)$$

where we use the abbreviations $\mathbf{z}_j = \mathbf{z}(t, j)$, and $\mathbf{v}_j = \mathbf{v}(t, j)$. Conforming to the sensitivity analysis presented in [51], a Taylor expansion is performed on $\mathbf{x}_j(t, \epsilon)$ with respect to ϵ . This results in

$$\mathbf{x}_j(t, \epsilon) = \mathbf{x}_j(t, 0) + \epsilon \left. \frac{\partial \mathbf{x}_j(t, \epsilon)}{\partial \epsilon} \right|_{\epsilon=0} + o(\epsilon). \quad (3.11)$$

Since \mathbf{x}_j evaluated at $\epsilon = 0$ is $\bar{\alpha}_j$, and using (3.10), we find

$$\mathbf{x}_j(t, \epsilon) = \bar{\alpha}_j + \epsilon \bar{\mathbf{z}}_j + o(\epsilon), \quad (3.12)$$

with $o(\epsilon)$ indicating the Landau symbol little-o, which represents higher order terms ϵ . The state perturbation \mathbf{z}_j in (3.12) is also extended, such that the approximation for \mathbf{x}_j can be extended beyond I_j^α . To find an approximation of $\dot{\mathbf{x}}_j(\epsilon)$, an expression for $\dot{\mathbf{z}}_j$ should be found. By first taking the partial derivative of (3.9) with respect to ϵ , and then with respect to t , the perturbation dynamics are found to be

$$\dot{\mathbf{z}}_j = \mathbf{A}_j(t)\mathbf{z}_j + \mathbf{B}_j(t)\mathbf{v}_j, \quad (3.13)$$

with

$$\mathbf{A}_j(t) = D_1 \mathbf{f}_j(\alpha_j, \mu_j, t), \quad (3.14)$$

$$\mathbf{B}_j(t) = D_2 \mathbf{f}_j(\alpha_j, \mu_j, t), \quad (3.15)$$

where D_a represents the partial derivative with respect to the a -th argument. By extending the perturbed input direction \mathbf{v}_j , $\bar{\mathbf{v}}_j$ is obtained. Using $\mathbf{z}_0 = \mathbf{z}(0, \epsilon)$ and $\bar{\mathbf{v}}_j$, $\dot{\mathbf{z}}_j$ can be integrated past the nominal event-time τ_j , which results in the extension of the perturbed state direction $\bar{\mathbf{z}}_j$. With $\bar{\alpha}_j$ and $\bar{\mathbf{z}}_j$, the first-order approximation of the perturbed state dynamics in continuous time can be defined as

$$\dot{\mathbf{x}}_j(\epsilon) = \dot{\bar{\alpha}}_j + \epsilon \dot{\bar{\mathbf{z}}}_j + o(\epsilon). \quad (3.16)$$

Equation (3.16) defines the first-order approximation for the continuous segments of a trajectory. What remains is that the state reinitializations should be linearized as well. The reinitialization of the nominal trajectory satisfies

$$\alpha_j(\tau_j) = \mathbf{g}_j(\alpha_{j-1}(\tau_j), \mu_{j-1}(\tau_j), \tau_j), \quad (3.17)$$

and the reinitialization of the perturbed state is described by

$$\mathbf{x}_j(t_j, \epsilon) = \mathbf{g}_j(\mathbf{x}_{j-1}(t_j, \epsilon), \mathbf{u}_{j-1}(t_j, \epsilon), t_j). \quad (3.18)$$

Similar to the Taylor expansion used in (3.11), the state and input of the next segment evaluated at the perturbed event time t_j can be expanded to

$$\mathbf{x}_j(t_j, \epsilon) = \bar{\alpha}_j(t_j) + \epsilon \bar{\mathbf{z}}_j(t_j) + o(\epsilon), \quad (3.19)$$

$$\mathbf{u}_j(t_j, \epsilon) = \bar{\mu}_j(t_j) + \epsilon \bar{\mathbf{v}}_j(t_j) + o(\epsilon). \quad (3.20)$$

The same can be done for $\alpha_j(t_j)$, $\mu_j(t_j)$, $\mathbf{z}_j(t_j)$, and $\mathbf{v}_j(t_j)$, which also depend on ϵ since they are evaluated at the perturbed event time $t_j(\epsilon)$. Substituting these expansions in (3.19) and (3.20) results in

$$\mathbf{x}_j(t_j, \epsilon) = \alpha_j(\tau_j) + \epsilon \dot{\alpha}_j(\tau_j)\Delta + \epsilon \mathbf{z}_j(\tau_j) + o(\epsilon), \quad (3.21)$$

$$\mathbf{u}_j(t_j, \epsilon) = \mu_j(\tau_j) + \epsilon \dot{\mu}_j(\tau_j)\Delta + \epsilon \mathbf{v}_j(\tau_j) + o(\epsilon), \quad (3.22)$$

with

$$\Delta = \left. \frac{dt_j}{d\epsilon} \right|_{\epsilon=0}. \quad (3.23)$$

To find Δ , we observe that

$$\gamma_j(\mathbf{x}_{j-1}(t_j, \epsilon), \mathbf{u}_{j-1}(t_j, \epsilon), t_j) = 0. \quad (3.24)$$

Note that γ_j is dependent on the input \mathbf{u}_j , whereas in [58] the sensitivity analysis is performed for guard functions which solely depend on state \mathbf{x}_j and time t . From (3.24) the expression for Δ is found to be

$$\Delta = -\frac{D_1\gamma^- \cdot \mathbf{z}^- + D_2\gamma^- \cdot \mathbf{v}^-}{\dot{\gamma}^-}, \quad (3.25)$$

with

$$\begin{aligned} \gamma^- &:= \gamma_j(\boldsymbol{\alpha}_{j-1}(\tau_j), \boldsymbol{\mu}_{j-1}(\tau_j), \tau_j), \\ \dot{\gamma}^- &:= D_1\gamma^- \cdot \dot{\boldsymbol{\alpha}}_{j-1}(\tau_j) + D_2\gamma^- \cdot \dot{\boldsymbol{\mu}}_{j-1}(\tau_j) + D_3\gamma^-, \\ \mathbf{z}^- &:= \mathbf{z}_{j-1}(\tau_j), \\ \mathbf{v}^- &:= \mathbf{v}_{j-1}(\tau_j), \end{aligned}$$

where the $(\cdot)^-$ superscript indicates a left limit of event j . Expanding the right-hand side of (3.18) gives

$$\mathbf{x}^+ = \mathbf{g}^- + \epsilon \left[\frac{\partial \mathbf{g}_j}{\partial \epsilon} \right]_{\epsilon=0} + o(\epsilon), \quad (3.26)$$

$$= \boldsymbol{\alpha}^+ + \epsilon \left[\frac{\partial \mathbf{g}_j}{\partial \mathbf{x}} \left(\frac{\partial \mathbf{x}^-}{\partial \epsilon} + \frac{\partial \mathbf{x}^-}{\partial t} \frac{dt_j}{d\epsilon} \right) + \frac{\partial \mathbf{g}_j}{\partial \mathbf{u}} \left(\frac{\partial \mathbf{u}^-}{\partial \epsilon} + \frac{\partial \mathbf{u}^-}{\partial t} \frac{dt_j}{d\epsilon} \right) + \frac{\partial \mathbf{g}_j}{\partial t} \frac{dt_j}{d\epsilon} \right]_{\epsilon=0} + o(\epsilon), \quad (3.27)$$

$$= \boldsymbol{\alpha}^+ + \epsilon [D_1\mathbf{g}^- \cdot (\mathbf{z}^- + \dot{\boldsymbol{\alpha}}^- \Delta) + D_2\mathbf{g}^- \cdot (\mathbf{v}^- + \dot{\boldsymbol{\mu}}^- \Delta) + D_3\mathbf{g}^- \cdot \Delta] + o(\epsilon), \quad (3.28)$$

with

$$\begin{aligned} \mathbf{x}^- &:= \mathbf{x}_{j-1}(t_j, \epsilon), \\ \mathbf{x}^+ &:= \mathbf{x}_j(t_j, \epsilon), \\ \mathbf{u}^- &:= \mathbf{u}_{j-1}(t_j, \epsilon), \\ \mathbf{g}^- &:= \mathbf{g}_j(\boldsymbol{\alpha}^-, \boldsymbol{\mu}^-, \tau_j), \\ \mathbf{g}_j &:= \mathbf{g}_j(\mathbf{x}^-, \mathbf{u}^-, t_j), \\ \boldsymbol{\alpha}^- &:= \boldsymbol{\alpha}_{j-1}(\tau_j), \\ \boldsymbol{\alpha}^+ &:= \boldsymbol{\alpha}_j(\tau_j), \\ \boldsymbol{\mu}^- &:= \boldsymbol{\mu}_{j-1}(\tau_j). \end{aligned}$$

Here, the $(\cdot)^+$ superscript indicates the right limit of event j . Rewriting (3.21) into

$$\mathbf{z}^+ = \frac{1}{\epsilon} (\mathbf{x}^+ - \boldsymbol{\alpha}^+) - \dot{\boldsymbol{\alpha}}^+ \Delta, \quad (3.29)$$

with $\mathbf{z}^+ := \mathbf{z}_j(\tau_j)$ and substituting (3.28) into (3.29), finally results in

$$\mathbf{z}^+ = D_1\mathbf{g}^- \cdot (\mathbf{z}^- + \dot{\boldsymbol{\alpha}}^- \Delta) + D_2\mathbf{g}^- \cdot (\mathbf{v}^- + \dot{\boldsymbol{\mu}}^- \Delta) + D_3\mathbf{g}^- \cdot \Delta - \dot{\boldsymbol{\alpha}}^+ \Delta, \quad (3.30)$$

By substituting (3.23) into (3.30), we find

$$\mathbf{z}^+ = D_1 \mathbf{g}^- \cdot \mathbf{z}^- + D_2 \mathbf{g}^- \cdot \mathbf{v}^- - (D_1 \mathbf{g}^- \cdot \mathbf{f}^- + D_2 \mathbf{g}^- \cdot \dot{\boldsymbol{\mu}}^- + D_3 \mathbf{g}^- \cdot 1 - \mathbf{f}^+) \frac{D_1 \gamma^- \cdot \mathbf{z}^- + D_2 \gamma^- \cdot \mathbf{v}^-}{\dot{\gamma}^-}, \quad (3.31)$$

which can be rewritten in compact form as

$$\mathbf{z}^+ = \mathbf{G}_j(\tau_j) \mathbf{z}^- + \mathbf{J}_j(\tau_j) \mathbf{v}^-, \quad (3.32)$$

with

$$\mathbf{G}_j(\tau_j) = D_1 \mathbf{g}^- - (\dot{\mathbf{g}}^- - \mathbf{f}^+) \frac{D_1 \gamma^-}{\dot{\gamma}^-}, \quad (3.33)$$

$$\mathbf{J}_j(\tau_j) = D_2 \mathbf{g}^- - (\dot{\mathbf{g}}^- - \mathbf{f}^+) \frac{D_2 \gamma^-}{\dot{\gamma}^-}, \quad (3.34)$$

where

$$\begin{aligned} \mathbf{f}^- &:= \mathbf{f}_{j-1}(\boldsymbol{\alpha}_{j-1}(\tau_j), \boldsymbol{\mu}_{j-1}(\tau_j), \tau_j), \\ \mathbf{f}^+ &:= \mathbf{f}_j(\boldsymbol{\alpha}_j(\tau_j), \boldsymbol{\mu}_j(\tau_j), \tau_j), \\ \dot{\mathbf{g}}^- &:= D_1 \mathbf{g}^- \cdot \mathbf{f}^- + D_2 \mathbf{g}^- \cdot \dot{\boldsymbol{\mu}}^- + D_3 \mathbf{g}^-. \end{aligned}$$

The jump gains in (3.33) and (3.34) consist of two terms. The first term in (3.33), $D_1 \mathbf{g}^-$, represents the effect of the ante-event state perturbation on the post-event perturbation. The perturbation does not only change the ante-event state, but also the time-instant the event takes place. The second term in (3.33), $-(\dot{\mathbf{g}}^- - \mathbf{f}^+) \frac{D_1 \gamma^-}{\dot{\gamma}^-}$, represents the effect of the difference in time, in comparison to the nominal event. Obviously, the same can be said for (3.34).

Equation (3.32) describes the relation between the post-event state perturbation \mathbf{z}^+ and the ante-event state and input perturbations \mathbf{z}^- and \mathbf{v}^- . The relation given in (3.32) is an extension on the results that have been obtained in [59]. The jump gain in [59] is derived with state-dependent guard functions γ and jump gains \mathbf{g} , whereas the jump gain \mathbf{G}_j in (3.32) is derived using state-and-input-dependent guard functions γ and jump gains \mathbf{g} . The second term in (3.32) describes the effect of the ante-event input perturbation \mathbf{v}^- on the post-event state perturbation \mathbf{z}^+ , which is a contribution of this work. This term is a result of the jump gains \mathbf{g} being state-and-input-dependent, where in previous work the jump gains were considered state-dependent.

3.2.2 Linear time-triggered hybrid system

The sensitivity analysis performed in the previous section will be used next to define the LTTHS associated to reference trajectory $\boldsymbol{\alpha}$ and the NSITHS defined in Definition 1. The LTTHS converts the state-triggered behavior of the NSITHS to a time-triggered behavior using an approximation of the state jumps, which we expect to be first order. Where the jump times of the NSITHS are unknown, the LTTHS jumps at the same event-times as the nominal trajectory $\boldsymbol{\alpha}$. Since the stability assessment of LTTHS is well established in literature, the LTTHS can then be used to conveniently assess the local asymptotic stability of the NSITHS. Let us now formally define the LTTHS.

Definition 2 (LTTHS). *The linear time-triggered hybrid system associated with the reference trajectory $\boldsymbol{\alpha}$ and the NSITHS (3.1)-(3.2) is given by*

$$\dot{\mathbf{z}}_j = \mathbf{A}_j(t) \mathbf{z}_j + \mathbf{B}_j(t) \mathbf{v}_j, \quad (t, j) \in \text{dom } \boldsymbol{\alpha}, \quad (3.35)$$

$$\mathbf{z}^+ = \mathbf{G}_{j+1}(t) \mathbf{z}^- + \mathbf{J}_{j+1}(t) \mathbf{v}^-, \quad (t, j) \in \text{eve } \boldsymbol{\alpha}, \quad (3.36)$$

with initial condition $\mathbf{z}(t_0, 0) = \mathbf{z}_0$, $\mathbf{z}^+ = \mathbf{z}(t, j + 1)$, $\mathbf{z}^- = \mathbf{z}(t, j)$,

$$\begin{aligned} \mathbf{A}_j(t) &= D_1 \mathbf{f}_j(\boldsymbol{\alpha}_j(t), \boldsymbol{\mu}_j(t), t), \\ \mathbf{B}_j(t) &= D_2 \mathbf{f}_j(\boldsymbol{\alpha}_j(t), \boldsymbol{\mu}_j(t), t), \\ \mathbf{G}_j &= D_1 \mathbf{g}^- - (\dot{\mathbf{g}}^- - \mathbf{f}^+) \frac{D_1 \gamma^-}{\dot{\gamma}^-}, \\ \mathbf{J}_j &= D_2 \mathbf{g}^- - (\dot{\mathbf{g}}^- - \mathbf{f}^+) \frac{D_2 \gamma^-}{\dot{\gamma}^-}, \end{aligned}$$

and

$$\begin{aligned} \dot{\boldsymbol{\mu}}^- &:= \dot{\boldsymbol{\mu}}_{j-1}(\tau_j), \\ \mathbf{f}^- &:= \mathbf{f}_{j-1}(\boldsymbol{\alpha}_{j-1}(\tau_j), \boldsymbol{\mu}_{j-1}(\tau_j), \tau_j), \\ \mathbf{f}^+ &:= \mathbf{f}_j(\boldsymbol{\alpha}_j(\tau_j), \boldsymbol{\mu}_j(\tau_j), \tau_j), \\ \mathbf{g}^- &:= \mathbf{g}_j(\boldsymbol{\alpha}_{j-1}(\tau_j), \boldsymbol{\mu}_{j-1}(\tau_j), \tau_j), \\ \dot{\mathbf{g}}^- &:= D_1 \mathbf{g}^- \cdot \mathbf{f}^- + D_2 \mathbf{g}^- \cdot \dot{\boldsymbol{\mu}}^- + D_3 \mathbf{g}^-, \\ \gamma^- &:= \gamma_j(\boldsymbol{\alpha}_{j-1}(\tau_j), \boldsymbol{\mu}_{j-1}(\tau_j), \tau_j), \\ \dot{\gamma}^- &:= D_1 \gamma^- \cdot \mathbf{f}^- + D_2 \gamma^- \cdot \dot{\boldsymbol{\mu}}^- + D_3 \gamma^-. \end{aligned}$$

The LTTHS of Definition 2 gives an approximation of the NSITHS about the state-input reference trajectory $(\boldsymbol{\alpha}, \boldsymbol{\mu})$. With a nominal trajectory $\boldsymbol{\alpha}$ with input $\boldsymbol{\mu}$, the perturbed trajectory $\mathbf{x}_j(\epsilon)$ is the trajectory starting from initial condition $\mathbf{x}_0(\epsilon) = \boldsymbol{\alpha}_0 + \epsilon \mathbf{z}_0$ and with input $\mathbf{u}_j(\epsilon) = \boldsymbol{\mu}_j + \epsilon \mathbf{v}_j$. The approximation is then defined as $\mathbf{x}_j(\epsilon) = \bar{\mathbf{a}}_j + \epsilon \bar{\mathbf{z}}_j + o(\epsilon)$, with \mathbf{z} defined by the LTTHS. The reader should be aware that the term \mathbf{v}^- is not an input that can be freely chosen. The ante-event input perturbation \mathbf{v}^- is directly related to \mathbf{v}_j , as it is a result of the input law implemented during the continuous segment before the event. Also, note that the approximation jumps at the same time instants as the nominal trajectory, with $(t, j) \in \text{eve } \boldsymbol{\alpha}$. This results in a trajectory which is generally infeasible around the jump times. However, due to the short timescales of the events, we are more interested in finding a good approximation of the continuous segments between the events, which is what the LTTHS achieves. In [55] a proof is given, which shows that stability of the LTTHS implies tracking of a NSTHS. The presumption is made that a similar proof exists, saying that stability of the LTTHS implies local stability of the NSITHS. Straightforward stability analysis tools for LTTHS are available in the literature, about which more can be read in Appendix C.3.

3.3 Summary

In this chapter, a linear approximation of the NSITHS is presented. The NSITHS is formally defined, which is a framework suitable for the dynamics defined in Chapter 2. Perturbations in the initial condition and input curve are introduced into this system, resulting in perturbed trajectories of which the event times differ from the nominal event times, and are not known beforehand. This mismatch in event time leads to a behavior called peaking. Reference spreading is then presented to eliminate peaking behavior. After posing assumptions on continuity of the vector fields, transversality of the guard activations, and differentiability of the jump maps, a sensitivity analysis is performed. The sensitivity analysis leads to an LTTHS describing the tracking error dynamics, which is used to generate an approximation of the perturbed state. While there is no proof available that the approximation generated by the LTTHS is first order, our claim is that such a proof exists. In addition, under the presumption that a proof exists that uniform asymptotic

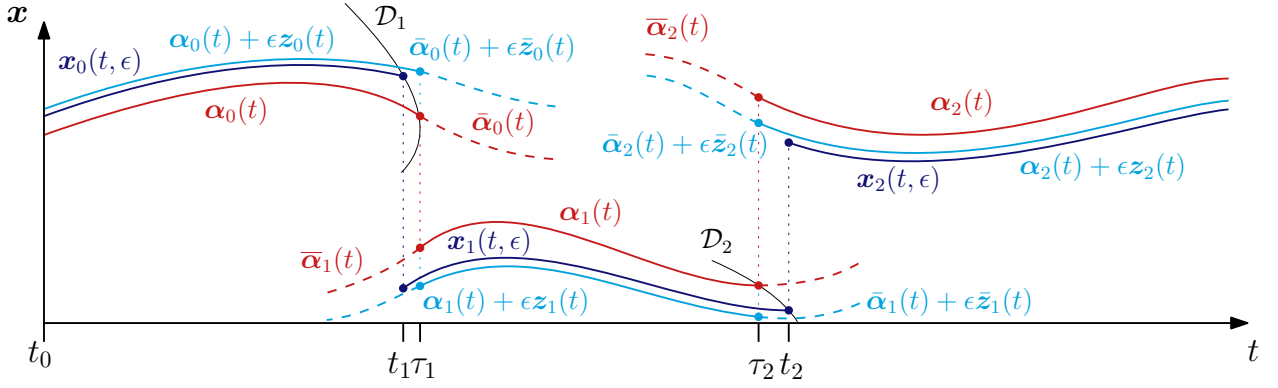


Figure 3.5: The approximation of the perturbed trajectory $\alpha + \epsilon z$ (cyan) generated by the LTTHS is illustrated besides the perturbed trajectory x (blue) and the nominal trajectory α (red). Note that the event times of the approximation are the same as those of the nominal trajectory.

stability of the LTTHS implies local asymptotic stability of the NSITHS, conventional stability analysis tools can be used to evaluate tracking of the nominal reference trajectory.

Chapter 4

Sensitivity Analysis with Simultaneous State-and-Input-Triggered Events

In this chapter, the analysis presented in Chapter 3 will be extended to be suitable for trajectories with simultaneous guard activations. Simultaneous guard activations are activations where a trajectory triggers two or more guard functions at the same time-instant. Take for example a box with two contact points, where both contacts are closed at the same time. When perturbations are introduced in these trajectories, the simultaneity of the event can be lost. Also, the order of activations can change depending on the perturbation. The box can first impact one contact point and then at the other, or the other way around. This complicates the definition of the approximation of the perturbed trajectory.

In this chapter, a novel notation introduced in [59] will be presented to describe trajectories with simultaneous guard functions. Reference spreading is applied to trajectories with simultaneous events, which is used as a basis to define a positively homogeneous jump gain which approximates the jump behavior of the perturbed trajectory. The positively homogeneous jump gain defines the *positively homogeneous time-triggered hybrid system* (PTTHS). This chapter extends the work presented in [59,67], making the approximation suitable for trajectories with input-dependent guard functions, and therefore mechanical systems experiencing dry friction and releasing motions.

4.1 Simultaneous guard-activation

To be able to perform a sensitivity analysis in the spirit of the one presented in Chapter 3 for trajectories with simultaneous guard activations, some adjustments need to be made to the notation of the system definition. In this section, a notation similar to the notation in [59] is presented, namely: the event character, micro and macro events, multiscale hybrid time, guard function index, mode descriptor, phantom segments, and historical notation. After this, reference spreading for simultaneous guard-activations is discussed. Note that the notation that will be presented in this section is not a contribution, but merely presented for completeness.

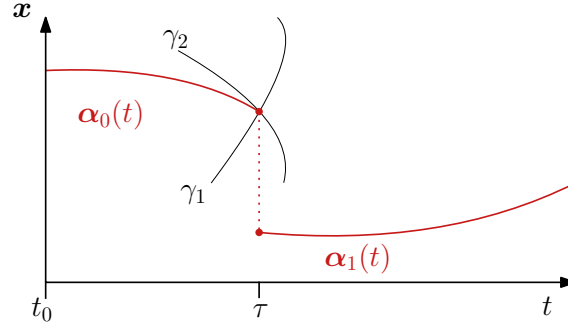


Figure 4.1: An illustration of a trajectory with a simultaneous event. At $t = \tau$, the trajectory activates two guard functions, γ_1 and γ_2 .

4.1.1 Adopted notation

In a simultaneous event, multiple guard functions are activated at the same time instant. In Figure 4.1, an example of a simultaneous activation of two guards is illustrated. The ante-event reference trajectory, $\alpha_0(t)$, activates two guard functions, γ_1 and γ_2 . The number of guard functions that are activated in a single nominal event is called the *event character*, and indicated with the letter c . In the example in Figure 4.1, the event character is two ($c = 2$).

When perturbations are introduced in an event with simultaneous activations, the number of events the system undergoes can change. Instead of a simultaneous activation of c guards, the guards can be activated in rapid succession. These events that are the result of loss of simultaneity are called *micro events*, where several micro events are associated to the same transition. Such a transition is called a *macro event*. When a macro event consists of simultaneous activations, one jump will be observed. Loss of simultaneity will generate micro events, resulting in that more jumps and flow segments can be observed in the state trajectory in comparison to the reference trajectory. To keep track of these segments, *multiscale hybrid time* is introduced. Multiscale hybrid time is denoted by (t, i, k) , where t is regular time, i the macro event counter, and k the micro event counter. The micro event counter k is incremented every time an event occurs, except when a macro event is completed by reaching the nominal post-event mode. The micro event counter k is then reset to zero, and the macro event counter i is incremented. One can now write $x(t, i, k)$ to make a distinction between all the segments that are generated as a result of loss of simultaneity. Multiscale hybrid time is directly related to the standard hybrid time as defined in Section 2.3.1, according to

$$j(i, k) = k + \sum_{\kappa=1}^i l_{\kappa}, \quad (4.1)$$

with l_{κ} the number of micro events in macro event κ . The perturbed event times of micro events are denoted by t_i^k , i.e., the event time of the k -th micro event of macro event i . A set of guard function indexes η is introduced to identify the several guard functions that are involved with an event. A guard function that is inactive is a guard function that is associated to a transition, but not yet activated. With c_i the event character of the i -th event, the index set of inactive guard functions is defined as

$$\{\eta = 2^{\nu} \mid \nu \in \{0, 1, \dots, c_i\}\}. \quad (4.2)$$

The index set of inactive guard functions η is written in the binary numeral system for a more intuitive notation of the different guard functions. The inactive guard functions can then be denoted

as γ^η . While the micro counter i and macro counter k are left out for readability, note that

$$\gamma^\eta = \gamma^\eta(\cdot, i, k), \quad (4.3)$$

meaning that the guard functions not only change with macro events, but also with micro events. Now an example is given to illustrate the relation between the set of guard functions γ^η and the guard functions defined in Section 2.3.3. Let us consider a block with two contact points not in contact, i.e., $\iota_1, \iota_2 \in \mathcal{I}_{\text{op}}$. We consider a nominal trajectory with a character-2 event ($c = 2$), where both contact points simultaneously close contact with a surface. The index set of inactive guards η before the event is, in this example, $\eta = \{01, 10\}$. The associated guard functions are then defined as

$$\gamma^{01} = \gamma_{\iota_1}^{\text{op} \rightarrow \text{cl}} = h_{n, \iota_1}(\mathbf{q}), \quad (4.4)$$

$$\gamma^{10} = \gamma_{\iota_2}^{\text{op} \rightarrow \text{cl}} = h_{n, \iota_2}(\mathbf{q}). \quad (4.5)$$

The mode of the system is indicated using the *mode descriptor* s_i^k . The mode descriptor s_i^k is associated to event i , similar to τ_i^1 . The micro segments associated to macro event i will be described using

$$s_i^k \mathbf{x}(t) := \mathbf{x}(t, i - 1, k), \quad (4.6)$$

with s_i^k the mode of the k -th micro event associated to macro event i . Note that s_i^k is a mode descriptor to describe the micro segments associated to macro event i . The macro segments, where $k = 0$, are still written as

$$\mathbf{x}_i(t) = \mathbf{x}(t, i, 0). \quad (4.7)$$

When the considered macro event is known from context, the macro counter i can be dropped to simplify the notation. From here on, we will also write the mode descriptor as s^k if the macro counter i is known. Similar to the inactive guard index set η , the mode descriptor is written in the binary numeral system. This binary numeral system is used as follows. When there is an event with character $c = 4$, four guard functions can be activated. When the mode of the system is described by $s^k = 1010$, this means that two guard functions are already activated, and two are still inactive. Namely, the guard functions that are still to be activated are those with index $\eta = \{0100, 0001\}$. The mode descriptor now intuitively shows which guard functions are inactive, as the zeros in the mode descriptor denote the inactive guard function indexes. The index of the guard function that is activated during event k is denoted by η_k . The superscript $(\cdot)^\epsilon$ is introduced for the state \mathbf{x} , to indicate that the state trajectory is perturbed, i.e.,

$$s_i^k \mathbf{x}^\epsilon(t) = \mathbf{x}(t, i - 1, k, \epsilon). \quad (4.8)$$

We will illustrate the adopted notation in an example. Let us consider a transition, depicted in Figure 4.2, with event character $c = 2$ and guard functions γ^{10} and γ^{01} . The state evolution of the system begins in the mode described by $s^0 = 00$, where $\gamma^{10} > 0$ and $\gamma^{01} > 0$. When the state activates one of the guard functions, in the example of Figure 4.2 $\gamma^{01} = 0$, the next mode is described by $s^1 = 01$. When the other guard function γ^{10} is activated as well, then the system completes its macro event with $s^2 = 11$. Note that the guard function can change when the system is in another mode, i.e., the guard function γ^{10} defined in s^0 is different from the guard function γ^{10} defined in s^1 .

¹The reader should be aware of the distinction between the event i and the hybrid time i . The hybrid time i indicates a segment of flow, whereas the event i indicates a point.

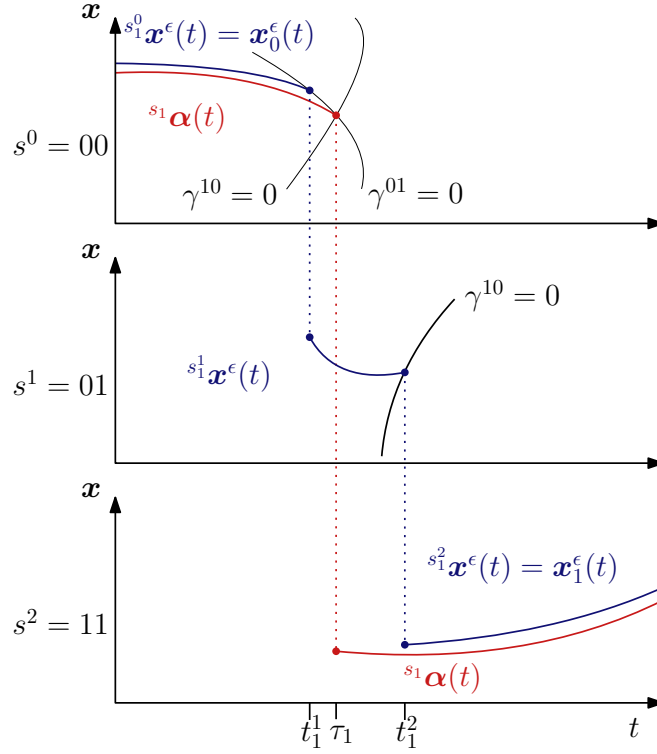


Figure 4.2: A reference trajectory going through a simultaneous event and a state trajectory experiencing loss of simultaneity. Where the reference trajectory activates γ^{10} and γ^{01} simultaneously, the state trajectory first activates γ^{01} at $t = t_1^1$, flows for $t \in [t_1^1, t_1^2]$, and then activates γ^{10} at $t = t_1^2$.

Depending on the perturbation, several mode sequences can achieve the expected nominal end mode when simultaneity is lost. The different mode sequences can generate a different post-event state, because of the flow phases in between the micro events. Therefore, it is useful to be able to indicate an entire mode sequence with one symbol. We call this notation the *historical notation*. We define the sequence for macro event i as

$$S_i^k = s_i^k \leftarrow s_i^{k-1} \leftarrow \dots \leftarrow s_i^0, \quad (4.9)$$

where $s_i^0 = 00 \dots 0$ with length c_i . Again, the macro counter i can be left out for convenience. A growing mode sequence is a sequence of micro events, where at each micro event another guard function is activated and no guard functions deactivated. We can now define $^{S^k} \mathbf{x}(t)$ as $^{s^k} \mathbf{x}(t)$ that is a result of the growing sequence S^k . The jump maps that are applied during such a sequence are given by

$$^p \mathbf{x} = ^{p \leftarrow a} \mathbf{g}(^a \mathbf{x}, ^a \mathbf{u}, t), \quad (4.10)$$

where p represents the post-event mode descriptor, and a the ante-event mode descriptor. For example, the state jump from s^k to s^{k+1} is given by $^{s^{k+1}} \mathbf{x} = ^{s^{k+1} \leftarrow s^k} \mathbf{g}(^{s^k} \mathbf{x}, ^{s^k} \mathbf{u}, t)$. Sequences with a particular order of events can also be expressed as

$$^{\nu_k \nu_{k-1} \dots \nu_1} S^k = s^k \leftarrow s^{k-1} \leftarrow \dots \leftarrow s^0, \quad (4.11)$$

where all mode descriptor entries are defined as $s^\kappa = s^{\kappa-1} + \eta_\kappa$, with $\eta_\kappa = 2^{\nu_\kappa - 1}$ and $\kappa = \{1, 2, \dots, k\}$. For a simultaneous activation during a micro event, the participating guard functions are placed within brackets. For example, for a character-4 ($c = 4$) growing sequence, we

write

$$^{23(14)}S^3 = 1111 \leftarrow 1101 \leftarrow 1001 \leftarrow 0000. \quad (4.12)$$

With the notation for trajectories experiencing simultaneous guard activations in place, reference spreading for such activations is presented in the next section.

4.1.2 Reference-spreading for simultaneous events

For trajectories with simultaneous activations, the perturbed state can experience more events than the reference trajectory. The perturbed state will enter intermediate modes and segments that are not entered by the reference trajectory. To be able to define a physically realistic comparison between the reference and state trajectories, the concept of reference trajectory has to be revised. This is achieved by means of introducing *nominal phantom modes* and *nominal phantom segments*. Phantom modes are modes defined in the reference trajectory that do not physically exist, but they allow for an approximation of the perturbed state to be defined during micro segments. Definition of these modes requires a property of the state jumps that we term associativity.

Assumption 6 (Jump map associativity). *We assume that the jump map $^p\mathbf{x} = ^{p \leftarrow a}\mathbf{g}(^a\mathbf{x}, ^a\mathbf{u}, t)$ is associative, meaning that taking an arbitrary growing sequence $s^k \leftarrow s^{k-1} \leftarrow \dots \leftarrow s^0$, finished by $p = s^k$ and entered by $a = s^0$, it holds that*

$$^{p \leftarrow a}\mathbf{g}(^a\mathbf{x}, ^a\mathbf{u}, t) = ^{p \leftarrow s^{k-1}}\mathbf{g}(\cdot, ^{s^{k-1}}\mathbf{u}, t) \circ ^{s^{k-1} \leftarrow s^{k-2}}\mathbf{g}(\cdot, ^{s^{k-2}}\mathbf{u}, t) \circ \dots \circ ^{s^1 \leftarrow a}\mathbf{g}(^a\mathbf{x}, ^a\mathbf{u}, t), \quad (4.13)$$

where \circ indicates the composition operator. Intuitively, this means that the simultaneous jump gain from a to p can be described with a sequence of jumps evaluated at the same time instant.

Using Assumption 6, the phantom modes can be defined. All micro modes, which the state can enter as a result of loss of simultaneity, are defined in the nominal trajectory. These modes are called the phantom modes in the nominal trajectory. The initial states associated to these modes are found by applying the corresponding jump maps $^{p \leftarrow a}\mathbf{g}$ to the nominal ante-event state,

$$\begin{aligned} s_i^1 \boldsymbol{\alpha} &= s_i^1 \leftarrow s_i^0 \mathbf{g}(s_i^0 \boldsymbol{\alpha}, s_i^0 \boldsymbol{\mu}, \tau_i) \\ s_i^2 \boldsymbol{\alpha} &= s_i^2 \leftarrow s_i^1 \mathbf{g}(s_i^1 \boldsymbol{\alpha}, s_i^1 \boldsymbol{\mu}, \tau_i) \\ &\vdots \\ s_i^k \boldsymbol{\alpha} &= s_i^k \leftarrow s_i^{k-1} \mathbf{g}(s_i^{k-1} \boldsymbol{\alpha}, s_i^{k-1} \boldsymbol{\mu}, \tau_i), \end{aligned} \quad (4.14)$$

resulting in the reference trajectory being defined in all modes that exist in the state trajectory. The analysis presented in [55] uses guard functions and jump maps that depend on the state \mathbf{x} and time t . As mentioned in Section 3.2.1, the sensitivity analysis in [55] is extended to be suitable for input-dependent guards. In (4.14), another contribution is made, in the sense that also the jump maps \mathbf{g} are input-dependent. The sensitivity analysis in this work is therefore suitable for both input-dependent guards and input-dependent jump maps.

Based on physical realization of the input, we limit ourselves to two options of the feedforward term $S_i^k \bar{\boldsymbol{\mu}}(t)$. We define *withdrawing phantom modes* and *pushing phantom modes*, which are defined by the feedforwards

$$\nearrow_i^k \bar{\boldsymbol{\mu}}(t) := \begin{cases} \bar{\boldsymbol{\mu}}_{i-1}(t), & k = 0 \\ \bar{\boldsymbol{\mu}}_i(t), & k \neq 0 \end{cases}, \quad (4.15)$$

and

$$\searrow_i^k \bar{\boldsymbol{\mu}}(t) := \begin{cases} \bar{\boldsymbol{\mu}}_{i-1}(t), & k \neq l_i \\ \bar{\boldsymbol{\mu}}_i(t), & k = l_i \end{cases}, \quad (4.16)$$

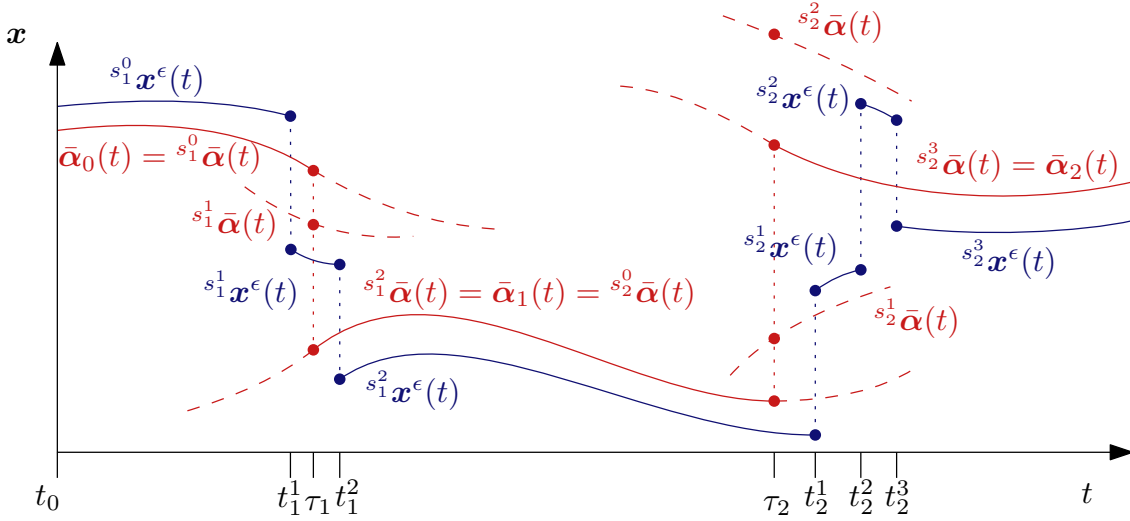


Figure 4.3: The state evolution of the reference trajectory and state trajectory. The reference trajectory is enriched with phantom segments, to which the micro segments of the state trajectory can be compared.

where \nearrow indicates a withdrawing feedforward and \searrow indicates a pushing feedforward, and l_i is the number of micro events associated with macro event i . For each event it should be specified whether a withdrawing or pushing phantom mode is used.

Since the micro segments of the state trajectory are defined over a time-interval rather than a time instant, the points in (4.14) should be integrated forwards and backwards to define the phantom segments over a time-interval. Using the initial states $S_i^k \alpha$ defined in (4.14) and inputs $S_i^k \bar{\mu}$ defined in (4.16), the vector field $S_i^k f$ can be integrated forward and backward to find the (pushing or withdrawing) phantom segments corresponding to the phantom modes. These phantom modes and segments are illustrated in Figure 4.3, where $s_1^0 \bar{\alpha}(t)$, $s_1^1 \bar{\alpha}(t)$, $s_2^1 \bar{\alpha}(t)$ are examples of phantom segments.

4.2 Approximating perturbed trajectories with simultaneous guard-activations

Using the notation presented in Section 4.1.1, an approximation of the NSITHS will be derived for trajectories with simultaneous activations. First, a sensitivity analysis is presented for a simultaneous event with character 2. The result is used to define a jump gain that approximates the behavior of a simultaneous event with an arbitrary event-character, which holds for a particular sequence of events. Since multiple sequences of events are feasible in a simultaneous event, multiple jump gains can be associated with such an event. These jump gains are used to define a positively homogeneous jump gain, which is a state- and input-dependent jump gain that describes the jumping behavior of the state near (α, μ) . Finally, the PTTHS is formally defined, which is an approximation of the NSITHS near the reference trajectory. Similar to the LTTHS presented in Section 3.2, we presume that the PTTHS is a first-order approximation of the NSITHS. The proof that the approximation is first order is not yet available, however.

4.2.1 Sensitivity analysis for simultaneous guard-activation

Similar to the sensitivity analysis for trajectories with isolated events presented in Section 3.2.1, the continuous macro segments ($k = 0$) of the state trajectory can be approximated as

$$\mathbf{x}_i^\epsilon(t) = \bar{\boldsymbol{\alpha}}_i + \epsilon \bar{\mathbf{z}}_i + o(\epsilon), \quad (4.17)$$

where the subscript $(\cdot)^\epsilon$ indicates that the variable is dependent on ϵ and \mathbf{z}_i satisfies

$$\dot{\mathbf{z}}_i = \mathbf{A}_i(t)\mathbf{z}_i + \mathbf{B}_i(t)\mathbf{v}_i, \quad i \in \text{dom } \boldsymbol{\alpha} \quad (4.18)$$

with

$$\begin{aligned} \mathbf{A}_i(t) &= D_1 \mathbf{f}_i(\boldsymbol{\alpha}_i, \boldsymbol{\mu}_i, t), \\ \mathbf{B}_i(t) &= D_2 \mathbf{f}_i(\boldsymbol{\alpha}_i, \boldsymbol{\mu}_i, t). \end{aligned}$$

We will now derive an approximation of the jump map of a simultaneous event with character $c_i = 2$. A more thorough derivation can be found in Appendix C.2. In this chapter, the macro counter i is dropped for the sake of readability. By posing ${}^{s^{k+1}}\mathbf{g} := {}^{s^{k+1} \leftarrow s^k} \mathbf{g}$, the perturbed post-event state associated with micro event $k + 1$ is given by

$${}^{s^{k+1}}\mathbf{x}^\epsilon(t^{k+1}) = {}^{s^{k+1}}\mathbf{g}({}^{s^k}\mathbf{x}^\epsilon(t^{k+1}), {}^{s^k}\mathbf{u}^\epsilon(t^{k+1}), t^{k+1}), \quad (4.19)$$

with

$${}^{s^k}\mathbf{x}^\epsilon(t^{k+1}) = \int_{t^k}^{t^{k+1}} \left[{}^{s^k}\mathbf{f} \left({}^{s^k}\mathbf{x}^\epsilon(t), {}^{s^k}\mathbf{u}^\epsilon(t), t \right) \right] dt + {}^{s^k}\mathbf{g}({}^{s^{k-1}}\mathbf{x}^\epsilon(t^k), {}^{s^{k-1}}\mathbf{u}^\epsilon(t^k), t^k). \quad (4.20)$$

Here the left superscript ${}^{s^k}(\cdot)$ indicates that the variable is in micro segment k and t^k represents the event-time of micro event k . Similar to (3.23), we define the micro event time as

$$\Delta^k := \left. \frac{dt^k}{d\epsilon} \right|_{\epsilon=0} = - \frac{D_1 {}^{s^k}\boldsymbol{\gamma} \cdot {}^{s^{k-1}}\bar{\mathbf{z}}(\tau) + D_2 {}^{s^k}\boldsymbol{\gamma} \cdot {}^{s^{k-1}}\bar{\mathbf{v}}(\tau)}{{}^{s^k}\dot{\boldsymbol{\gamma}}}, \quad (4.21)$$

with

$$\begin{aligned} {}^{s^k}\boldsymbol{\gamma} &:= {}^{s^k}\boldsymbol{\gamma}({}^{s^{k-1}}\boldsymbol{\alpha}(\tau), {}^{s^{k-1}}\boldsymbol{\mu}(\tau), \tau), \\ {}^{s^k}\dot{\boldsymbol{\gamma}} &:= D_1 {}^{s^k}\boldsymbol{\gamma} \cdot {}^{s^{k-1}}\dot{\boldsymbol{\alpha}} + D_2 {}^{s^k}\boldsymbol{\gamma} \cdot {}^{s^{k-1}}\dot{\boldsymbol{\mu}} + D_3 \boldsymbol{\gamma}^-. \end{aligned}$$

The right-hand side of (4.19) is expanded with respect to ϵ , to find

$${}^{s^{k+1}}\mathbf{x}^\epsilon(t^{k+1}) = {}^{s^{k+1}}\boldsymbol{\alpha}(\tau) + \epsilon \left. \frac{\partial {}^{s^{k+1}}\mathbf{g}}{\partial \epsilon} \right|_{\epsilon=0} + o(\epsilon), \quad (4.22)$$

where, similar to the expansion of $\mathbf{g}_j(\mathbf{x}^-, \mathbf{u}^-, t_j)$ in (3.28),

$$\begin{aligned} \left. \frac{\partial {}^{s^{k+1}}\mathbf{g}}{\partial \epsilon} \right|_{\epsilon=0} &= D_1 {}^{s^{k+1}}\mathbf{g} \cdot \left({}^{s^k}\dot{\boldsymbol{\alpha}}(\Delta^{k+1} - \Delta^k) + D_1 {}^{s^k}\mathbf{g} \cdot \left({}^{s^{k-1}}\mathbf{z} + {}^{s^{k-1}}\dot{\boldsymbol{\alpha}}\Delta^k \right) + D_2 {}^{s^k}\mathbf{g} \cdot \left({}^{s^{k-1}}\mathbf{v} + {}^{s^{k-1}}\dot{\boldsymbol{\mu}}\Delta^k \right) \right. \\ &\quad \left. + D_3 {}^{s^k}\mathbf{g} \cdot \Delta^k \right) + D_2 {}^{s^{k+1}}\mathbf{g} \cdot \left({}^{s^k}\mathbf{v} + {}^{s^k}\dot{\boldsymbol{\mu}}\Delta^{k+1} \right) + D_3 {}^{s^{k+1}}\mathbf{g} \cdot \Delta^{k+1}, \quad (4.23) \end{aligned}$$

with

$$\begin{aligned} {}^{s^k}\mathbf{f} &:= {}^{s^k}\mathbf{f}({}^{s^k}\boldsymbol{\alpha}(\tau), {}^{s^k}\boldsymbol{\mu}(\tau), \tau), \\ {}^{s^k}\mathbf{g} &:= {}^{s^k}\mathbf{g}({}^{s^{k-1}}\boldsymbol{\alpha}(\tau), {}^{s^{k-1}}\boldsymbol{\mu}(\tau), \tau), \\ {}^{s^k}\dot{\mathbf{g}} &:= D_1 {}^{s^k}\mathbf{g} \cdot {}^{s^{k-1}}\mathbf{f} + D_2 {}^{s^k}\mathbf{g} \cdot {}^{s^{k-1}}\dot{\boldsymbol{\mu}} + D_3 {}^{s^k}\mathbf{g}. \end{aligned}$$

In (4.23), the expansion of the post-event state ${}^{s^{k+1}}\mathbf{x}^\epsilon(t^{k+1})$ is expressed in terms of ${}^{s^k}$ and ${}^{s^{k-1}}$. This is done to find a relation between the ante-event state and input perturbation and the post-event state perturbation. By expanding the left-hand side of (4.19) with respect to ϵ , we find

$${}^{s^{k+1}}\mathbf{x}^\epsilon(t^{k+1}) = {}^{s^{k+1}}\bar{\boldsymbol{\alpha}}(t^{k+1}) + \epsilon {}^{s^{k+1}}\bar{\mathbf{z}}(t^{k+1}) + o(\epsilon), \quad (4.24)$$

$$= {}^{s^{k+1}}\boldsymbol{\alpha}(\tau) + \epsilon {}^{s^{k+1}}\dot{\boldsymbol{\alpha}}(\tau)\Delta^{k+1} + \epsilon {}^{s^{k+1}}\mathbf{z}(\tau) + o(\epsilon). \quad (4.25)$$

From the work in Section 3.2.1, the jump gains \mathbf{G} and \mathbf{J} are derived for single events. With ${}^{s^k}\mathbf{G}(t) := {}^{s^k \leftarrow s^{k-1}}\mathbf{G}(t)$ and ${}^{s^k}\mathbf{J}(t) := {}^{s^k \leftarrow s^{k-1}}\mathbf{J}(t)$, these jump gains translate to the micro-event case as

$${}^{s^k}\mathbf{G}(\tau) = D_1 {}^{s^k}\mathbf{g} - ({}^{s^k}\dot{\mathbf{g}} - {}^{s^k}\mathbf{f}) \frac{D_1 {}^{s^k}\gamma}{{}^{s^k}\dot{\gamma}}, \quad (4.26)$$

$${}^{s^k}\mathbf{J}(\tau) = D_2 {}^{s^k}\mathbf{g} - ({}^{s^k}\dot{\mathbf{g}} - {}^{s^k}\mathbf{f}) \frac{D_2 {}^{s^k}\gamma}{{}^{s^k}\dot{\gamma}}. \quad (4.27)$$

Using (4.22) and (4.25), an expression for ${}^{s^{k+1}}\mathbf{z}(\tau)$ is found, which is

$$\begin{aligned} {}^{s^{k+1}}\mathbf{z}(\tau) &= D_1 {}^{s^{k+1}}\mathbf{g} \cdot {}^{s^k}\mathbf{f}\Delta^{k+1} - D_1 {}^{s^{k+1}}\mathbf{g} \cdot {}^{s^k}\mathbf{f}\Delta^k + D_1 {}^{s^{k+1}}\mathbf{g} \cdot \left(D_1 {}^{s^k}\mathbf{g} \cdot ({}^{s^{k-1}}\mathbf{z} + {}^{s^{k-1}}\mathbf{f}\Delta^k) \right. \\ &\quad \left. + D_2 {}^{s^k}\mathbf{g} \cdot ({}^{s^{k-1}}\mathbf{v} + {}^{s^{k-1}}\dot{\boldsymbol{\mu}}\Delta^k) + D_3 {}^{s^k}\mathbf{g} \cdot \Delta^k \right) + D_2 {}^{s^{k+1}}\mathbf{g} \cdot ({}^{s^k}\mathbf{v} + {}^{s^k}\dot{\boldsymbol{\mu}}\Delta^{k+1}) + (D_3 {}^{s^{k+1}}\mathbf{g} - {}^{s^{k+1}}\mathbf{f}) \Delta^{k+1}. \end{aligned} \quad (4.28)$$

which can be rewritten to

$$\begin{aligned} {}^{s^{k+1}}\mathbf{z}(\tau) &= \left(D_1 {}^{s^{k+1}}\mathbf{g} - \left(D_1 {}^{s^{k+1}}\mathbf{g} \cdot {}^{s^k}\mathbf{f} + D_2 {}^{s^{k+1}}\mathbf{g} \cdot {}^{s^k}\dot{\boldsymbol{\mu}} + D_3 {}^{s^{k+1}}\mathbf{g} - {}^{s^{k+1}}\mathbf{f} \right) \frac{D_1 {}^{s^{k+1}}\gamma}{{}^{s^{k+1}}\dot{\gamma}} \right) {}^{s^k}\mathbf{G} {}^{s^{k-1}}\mathbf{z} \\ &\quad + \left(D_1 {}^{s^{k+1}}\mathbf{g} - \left(D_1 {}^{s^{k+1}}\mathbf{g} \cdot {}^{s^k}\mathbf{f} + D_2 {}^{s^{k+1}}\mathbf{g} \cdot {}^{s^k}\dot{\boldsymbol{\mu}} + D_3 {}^{s^{k+1}}\mathbf{g} - {}^{s^{k+1}}\mathbf{f} \right) \frac{D_1 {}^{s^{k+1}}\gamma}{{}^{s^{k+1}}\dot{\gamma}} \right) {}^{s^k}\mathbf{J} {}^{s^{k-1}}\mathbf{v} \\ &\quad + \left(D_2 {}^{s^{k+1}}\mathbf{g} - \left(D_1 {}^{s^{k+1}}\mathbf{g} \cdot {}^{s^k}\mathbf{f} + D_2 {}^{s^{k+1}}\mathbf{g} \cdot {}^{s^k}\dot{\boldsymbol{\mu}} + D_3 {}^{s^{k+1}}\mathbf{g} - {}^{s^{k+1}}\mathbf{f} \right) \frac{D_2 {}^{s^{k+1}}\gamma}{{}^{s^{k+1}}\dot{\gamma}} \right) {}^{s^k}\mathbf{v}, \end{aligned} \quad (4.29)$$

which is equal to

$${}^{s^{k+1}}\mathbf{z}(\tau) = {}^{s^{k+1}}\mathbf{G} {}^{s^k}\mathbf{G} {}^{s^{k-1}}\mathbf{z} + {}^{s^{k+1}}\mathbf{G} {}^{s^k}\mathbf{J} {}^{s^{k-1}}\mathbf{v} + {}^{s^{k+1}}\mathbf{J} {}^{s^k}\mathbf{v}. \quad (4.30)$$

An important realization is that (4.30) is also found by evaluating two single jumps at τ , and taking the post-event state of the first jump as the ante-event state of the second jump. These two jumps are given by

$${}^{s^k}\mathbf{z}(\tau) = {}^{s^k}\mathbf{G} {}^{s^{k-1}}\mathbf{z} + {}^{s^k}\mathbf{J} {}^{s^{k-1}}\mathbf{v}, \quad (4.31)$$

$${}^{s^{k+1}}\mathbf{z}(\tau) = {}^{s^{k+1}}\mathbf{G} {}^{s^k}\mathbf{z} + {}^{s^{k+1}}\mathbf{J} {}^{s^k}\mathbf{v}, \quad (4.32)$$

respectively. This implies that the approximation of the post-impact state of two simultaneous jumps at τ can be found by evaluating the two jumps separately. For an arbitrary number of micro events k , the approximation of the post-event state can be found to be

$$S^k \mathbf{z}(\tau) = {}^{s^k \leftarrow s^0} \mathbf{G} {}^{s^0} \mathbf{z}(\tau) + \sum_{\iota=0}^{k-1} {}^{s^k \leftarrow s^{\iota+1}} \mathbf{G} {}^{s^{\iota+1} \leftarrow s^{\iota}} \mathbf{J} {}^{s^{\iota}} \mathbf{v}(\tau), \quad (4.33)$$

where ${}^{p \leftarrow a} \mathbf{G}$ and ${}^{p \leftarrow a} \mathbf{J}$ are defined as

$${}^{p \leftarrow a} \mathbf{G} := {}^p \mathbf{G} {}^{p-1} \mathbf{G} \dots {}^a \mathbf{G}, \quad (4.34)$$

$${}^{p \leftarrow a} \mathbf{J} := {}^p \mathbf{J} {}^{p-1} \mathbf{J} \dots {}^a \mathbf{J}, \quad (4.35)$$

for a sequence $p \leftarrow p-1 \leftarrow \dots \leftarrow a$, with slight abuse of notation, in the sense that $p-1$ indicates the mode descriptor associated to the mode before p . The relation between the post-event state perturbation ${}^{s^{k+1}} \mathbf{z}(\tau)$ and the ante-event state and input perturbation ${}^{s^{k-1}} \mathbf{z}$ and \mathbf{v} in (4.33) is the main result of this section. Using that result, the effect of a perturbation on the jumping behavior of the system can be approximated. For a more complete derivation, consult Appendix C.2. The first term in (4.33) represents the effect of the perturbed ante-event state on the perturbed post-event state. This term is already found in [59], where a sensitivity analysis is presented without input-dependent guards and jump maps. The summation in (4.33) is a contribution of this work, which represents the effects of the chosen feedback during micro-segments.

Note that the approximation of the post-event state (4.33) shares an algebraic similarity with the impulse response of linear discrete time systems. With $\mathbf{x}_d(t)$ the state, $\mathbf{u}_d(t)$ the input, and $\mathbf{y}_d(t)$ the output of a discrete system, the discrete impulse response is in the form of

$$\mathbf{y}_d(t) = \mathbf{C} \mathbf{x}_d(0) + \sum_{j=0}^t \mathbf{D}(j) \mathbf{u}_d(t-j), \quad (4.36)$$

where $\mathbf{y}_d(t) := \mathbf{y}_d(\mathbf{x}_d(0), \mathbf{u}(t), t)$, and \mathbf{C} and \mathbf{D} some matrices defined by the discrete systems dynamics [68]. Note that, similar to the discrete impulse response \mathbf{y}_d , the post-event perturbation ${}^{S^k} \mathbf{z}$ is also dependent on the ante-event state perturbation ${}^{s^0} \mathbf{z}$, the entire evolution of the input \mathbf{u} , and the time t , i.e., ${}^{S^k} \mathbf{z}(\tau) := {}^{S^k} \mathbf{z}({}^{s^0} \mathbf{z}, \mathbf{v}, \tau)$.

When \mathbf{v} is considered a feedback term that is turned off when the first micro event is detected, then the approximation of the post-event state perturbation can be simplified to

$${}^{S^k} \mathbf{z}(\tau) = {}^{S^k} \mathbf{L} \begin{bmatrix} {}^{s^0} \mathbf{z}(\tau) \\ {}^{s^0} \mathbf{v}(\tau) \end{bmatrix}, \text{ with } {}^{S^k} \mathbf{L} = \begin{bmatrix} {}^{S^k} \mathbf{G} & {}^{S^{k-1}} \mathbf{G} {}^{S^{1 \leftarrow 0}} \mathbf{J} \end{bmatrix}, \quad (4.37)$$

since only the ante-event feedback term will be non-zero. The jump gain ${}^{S^k} \mathbf{L}$ defined in (4.37) is defined for a particular order of guard activations. When considering a simultaneous event, different trajectories close to $(\boldsymbol{\alpha}, \boldsymbol{\mu})$ can be associated to different sequences of guard-activations. Since the sensitivity analysis considers all trajectories close to $(\boldsymbol{\alpha}, \boldsymbol{\mu})$, several sequences of guard-activations, and therefore several jumps gains as in (4.37), can be associated with a simultaneous event. In the next section, the jump gain (4.37) associated to an a priori known mode sequence is used to define a state-dependent jump gain, which covers all possible mode sequences.

Note that the description of the jump gain given in (4.37) is less complicated than jump gain (4.33) for a micro event where feedback is nonzero. Since the micro events usually happen too rapidly to control on, feedback is often turned off when micro events are taking place. Therefore, only situations with zero feedback during micro events are considered in this work. Under these considerations the jump gain in (4.37) is used from here on to define ${}^{S^k} \mathbf{L}$.

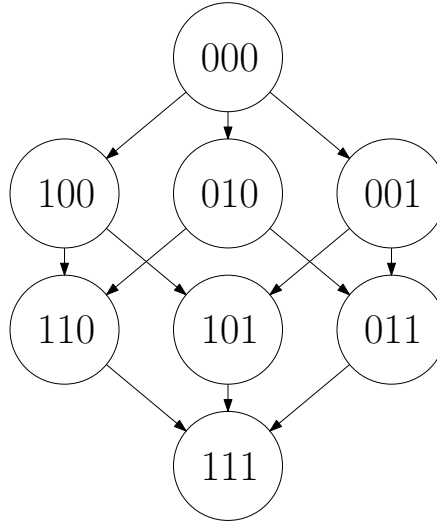


Figure 4.4: An example of the possible modes in a character-3 event ($c = 3$) illustrated with a graph. When the mode sequences are growing, the edges between the modes are unidirectional, resulting in a finite amount of paths to the post-event mode described by $s = 111$.

4.2.2 The positively homogeneous jump map

As mentioned in Section 4.1, an event with simultaneous guard activation will experience loss of simultaneity when perturbations are introduced. Due to the loss of simultaneity, the order of events is unknown. For that reason, one simultaneous event has several feasible event sequences associated with it. For there to be a finite amount of possibilities of event sequences, all sequences should be growing. A graph of growing mode sequences is illustrated for a character-3 event ($c = 3$) in Figure 4.4, where the nodes represent the possible system modes and the edges represent the possible transitions. When the mode sequences are growing, the edges are unidirectional. Therefore a finite number of paths can be found from the ante-event mode described by $s = 000$ to the post-event mode described by $s = 111$. When the mode sequences are not growing, the edges are bidirectional. One can then travel both ways over each edge, resulting in an infinite number of possible mode sequences.

To be able to define a jump map, only a finite number of sequences can be considered. Therefore, an assumption is posed that the mode sequences should be growing.

Assumption 7 (Growing mode sequences). *We assume, locally at each macro event, that all considered mode sequences are growing. Namely, at each micro event, all activated guards will remain active. In other words, considering one macro event, we assume that $s^0 < s^1 < \dots < s^l$, where $s^0 = 00 \dots 0$ and $s^l = 11 \dots 1$, and l is the number of micro events in the considered macro event.*

For example, when we consider a block with two contact points ι_1 and ι_2 executing a pushing motion towards a surface, with $s^0 = 00$ is both contact points open and $s^l = 11$ is both contact points in closed contact stick. Let us say we are in mode $s^1 = 10$, i.e., ι_1 is in closed contact stick and ι_2 is still open. The system goes through the second micro event by activating γ_2^{01} . Under Assumption 7, the event can not cause ι_1 to release contact, i.e., $\Gamma_{\iota_1}^{\text{cl} \rightarrow \text{op}} > 0$, $\Gamma_{\iota_1}^{\text{st} \rightarrow \text{sl}} > 0$, $\gamma_{\iota_1}^{\text{cl} \rightarrow \text{op}} > 0$ and $\gamma_{\iota_1}^{\text{st} \rightarrow \text{sl}} > 0$ when solving the state reinitialization and mode selection presented in Section 2.3.4. Under Assumption 7, all mode sequences in a neighborhood of α, μ will be growing and a finite number of jump gains are possible for a range of perturbations. Let us now pose an assumption on

the association between guard functions and transitions.

Assumption 8 (Guard-transition association). *We assume that activation of a guard will result in a transition associated with that guard, i.e., the guard function γ^{η_k} activated in mode s^{k-1} , will result in a post-event mode of which the mode descriptor satisfies $s^k = s^{k-1} + \eta_k$. Here η_k is the index of the guard function that is activated during micro event k .*

Remark. *Considering mechanical systems, Assumption 8 is easily verified for most guard functions. Because $\gamma_\iota^{\text{op} \rightarrow \text{cl}} = h_{n,\iota}(\mathbf{q})$ is defined on position level, under Assumption 7 it will always be contact point ι that will change mode when $\gamma_\iota^{\text{op} \rightarrow \text{cl}}$ is activated. For guard functions defined on acceleration level, i.e.,*

$$\begin{aligned}\gamma^{\text{st} \rightarrow \text{sl}} &= \mu_\iota^2 \lambda_{n,\iota} - \lambda_{t,\iota}^T \lambda_{t,\iota}, \\ \gamma^{\text{cl} \rightarrow \text{op}} &= \lambda_{n,\iota},\end{aligned}$$

the situation is different. The feasible post-event mode is determined by the post-event acceleration for these guard functions. It is therefore possible that a guard function is activated in mode s^{k-1} , but is inactive in mode s^k . Under Assumption 8 this is not possible. Therefore a constraint is introduced on the post-event acceleration, which can be determined by the set of equations, called the mode selection in Section 2.3.4,

$$\begin{aligned}\ddot{\mathbf{q}}^+ &= \mathbf{M}^{-1} [\mathbf{S}\mathbf{u}^+ - \mathbf{C} + \mathbf{W}_n \lambda_n^+ + \mathbf{W}_t \lambda_t^+], \\ \mathbf{w}_{n,\iota}^T \ddot{\mathbf{q}}^+ + \dot{\mathbf{w}}_{n,\iota}^T \dot{\mathbf{q}}^+ &= 0, & \forall \iota \in \mathcal{I}_{cl}, \\ \lambda_{t,\iota}^+ \|\mathbf{W}_{t,\iota}^T \dot{\mathbf{q}}^+\| + \mu \lambda_{n,\iota}^+ \mathbf{W}_{t,\iota}^T \dot{\mathbf{q}}^+ &= 0, & \forall \iota \in \mathcal{I}_{sl}, \\ \mathbf{W}_{t,\iota}^T \ddot{\mathbf{q}}^+ + \dot{\mathbf{W}}_{t,\iota}^T \dot{\mathbf{q}}^+ &= 0. & \forall \iota \in \mathcal{I}_{st},\end{aligned}$$

From the mode selection we can conclude that the post-event acceleration $\ddot{\mathbf{q}}$ is directly dependent on the post-event input \mathbf{u}^+ . Therefore, the post-event input \mathbf{u}^+ should be chosen in such a way that Assumption 8 is met.

A state-dependent jump gain for all possible mode sequences associated to a simultaneous event will be defined in the following. This jump gain should consider all growing sequences that can take place for that range of perturbations. Therefore, a state-dependent matrix gain is defined, in the form of

$$p^{\leftarrow a} \mathbf{H}({}^a \mathbf{z}(\tau), {}^a \mathbf{v}(\tau), \tau) = \begin{cases} \mathbf{H}^1(s^0 \mathbf{z}, s^0 \mathbf{v}, \tau), & \text{if condition 1 is true,} \\ \mathbf{H}^2(s^0 \mathbf{z}, s^0 \mathbf{v}, \tau), & \text{if condition 2 is true,} \\ \vdots & \vdots \\ \mathbf{H}^r(s^0 \mathbf{z}, s^0 \mathbf{v}, \tau), & \text{if condition } r \text{ is true,} \end{cases} \quad (4.38)$$

where r the number of possible mode sequences in a macro event. The jump map \mathbf{H} is presented later in this section for a character-2 event ($c = 2$). While it is possible to construct a straightforward algorithm that defines \mathbf{H} for any character c , this is left as future work. We will now derive the jump maps and associated conditions in (4.38) to obtain an explicit expression. Note that the several jump gains \mathbf{H} in (4.38) all coincide with a particular sequence of events.

For a certain perturbation, only a specific order of micro events is feasible. This order can be found by determining the perturbed jump time of all possible micro events, and selecting the micro event with the earliest event time as the next event. The perturbed event-time of the next micro event

$s^{k+1} \leftarrow S^k t^\epsilon$ can be approximated at first order as

$$t^{k+1} = \tau + \epsilon \Delta^{k+1} + o(\epsilon), \quad (4.39)$$

$$= \tau + \epsilon \left(S^{k+1} \mathbf{a}^T S^k \mathbf{z} + S^{k+1} \mathbf{b}^T S^k \mathbf{v} \right) + o(\epsilon), \quad (4.40)$$

with

$$\begin{aligned} S^k \mathbf{a} &:= -\frac{1}{\dot{\gamma} \eta_k} D_1 \gamma^{\eta_k} (s^{k-1} \boldsymbol{\alpha}, s^{k-1} \boldsymbol{\mu}, \tau), \\ S^k \mathbf{b} &:= -\frac{1}{\dot{\gamma} \eta_k} D_2 \gamma^{\eta_k} (s^{k-1} \boldsymbol{\alpha}, s^{k-1} \boldsymbol{\mu}, \tau). \end{aligned}$$

Defining the set mode descriptors related to all possible post-event modes

$$\mathcal{S} := \{s^+ = s^- + \eta_+ \mid \eta_+ \in \eta\}, \quad (4.41)$$

the mode descriptor of the next mode can be written as

$$s^{k+1} = \underset{s^*}{\operatorname{argmin}} \left\{ t^{k+1} \mid s^* \in \mathcal{S} \right\}. \quad (4.42)$$

Since the minimization of the impact-time does not depend on τ and ϵ , we can rewrite (4.42) to

$$s^{k+1} = \underset{s^*}{\operatorname{argmin}} \left\{ S^{k+1} \mathbf{a}^T S^k \mathbf{z} + S^{k+1} \mathbf{b}^T S^k \mathbf{v} \mid s^* \in \mathcal{S} \right\}, \quad (4.43)$$

which can be written as

$$s^{k+1} = s^k + \eta_{k+1}, \quad (4.44)$$

with

$$\eta_{k+1} = \underset{\eta^*}{\operatorname{argmin}} \left\{ -\frac{D_1 \gamma^{\eta^*} (s^k \boldsymbol{\alpha}, s^k \boldsymbol{\mu}, \tau) \cdot S^k \mathbf{z} + D_2 \gamma^{\eta^*} (s^k \boldsymbol{\alpha}, s^k \boldsymbol{\mu}, \tau) \cdot S^k \mathbf{v}}{\dot{\gamma} \eta^*} \mid \eta^* \in \eta \right\}. \quad (4.45)$$

Here η is the index set of inactive guard functions as defined in (4.2) and η_{k+1} is the identifier of the guard that is activated during micro event $k+1$. Finally, (4.45) can be rewritten as

$$\eta_{k+1} = \underset{\eta^*}{\operatorname{argmin}} \left(S^* \mathbf{a}^T S^k \mathbf{z} + S^* \mathbf{b}^T S^k \mathbf{v} \right), \quad (4.46)$$

with

$$\begin{aligned} S^* \mathbf{a} &:= -\frac{1}{\dot{\gamma} \eta^*} D_1 \gamma^{\eta^*} (s^k \boldsymbol{\alpha}, s^k \boldsymbol{\mu}, \tau), \\ S^* \mathbf{b} &:= -\frac{1}{\dot{\gamma} \eta^*} D_2 \gamma^{\eta^*} (s^k \boldsymbol{\alpha}, s^k \boldsymbol{\mu}, \tau). \end{aligned}$$

By checking (4.45) for every micro event, we can determine what the post-event mode of each micro-event will be. With that knowledge, we can decide which jump gains we should apply in (4.33) to find the correct jump gain.

We now pose an example to illustrate the positively homogeneous jump gain. Let us consider a system with $c_i = 2$, $s^1 \mathbf{v} = s^2 \mathbf{v} = \dots = s^l \mathbf{v} = 0$, and with a macro event starting in $s^0 = 00$ and ending in $s^l = 11$, this gives

$${}^{11 \leftarrow 00} \mathbf{H}(s^0 \mathbf{z}(\tau), s^0 \mathbf{v}(\tau), \tau) = \begin{cases} \begin{bmatrix} {}^{11 \leftarrow 00} \mathbf{G}, & {}^{11 \leftarrow 00} \mathbf{J} \end{bmatrix}, & \text{if (I),} \\ \begin{bmatrix} {}^{11 \leftarrow 01} \mathbf{G}_2 S^1, & {}^{01 \leftarrow 00} \mathbf{G}, & {}^{11 \leftarrow 01} \mathbf{G}_2 S^1 \mathbf{J} \end{bmatrix}, & \text{if (II),} \\ \begin{bmatrix} {}^{11 \leftarrow 10} \mathbf{G}_2 S^1, & {}^{10 \leftarrow 00} \mathbf{G}, & {}^{11 \leftarrow 10} \mathbf{G}_2 S^1 \mathbf{J} \end{bmatrix}, & \text{if (III),} \end{cases} \quad (4.47)$$

with

$$\begin{aligned}
 \text{(I)} : & \quad {}^2S^1 \mathbf{a}^T s^0 \mathbf{z} + {}^2S^1 \mathbf{b}^T s^0 \mathbf{v} = {}^1S^1 \mathbf{a}^T s^0 \mathbf{z} + {}^1S^1 \mathbf{b}^T s^0 \mathbf{v}, \\
 \text{(II)} : & \quad {}^2S^1 \mathbf{a}^T s^0 \mathbf{z} + {}^2S^1 \mathbf{b}^T s^0 \mathbf{v} > {}^1S^1 \mathbf{a}^T s^0 \mathbf{z} + {}^1S^1 \mathbf{b}^T s^0 \mathbf{v}, \\
 \text{(III)} : & \quad {}^2S^1 \mathbf{a}^T s^0 \mathbf{z} + {}^2S^1 \mathbf{b}^T s^0 \mathbf{v} < {}^1S^1 \mathbf{a}^T s^0 \mathbf{z} + {}^1S^1 \mathbf{b}^T s^0 \mathbf{v}.
 \end{aligned} \tag{4.48}$$

The jump gain in (4.47) is called a positively homogeneous jump gain for character-2 events ($c = 2$). Due to the behavior of the simultaneous events, the linearity property of the jump gain is lost. This is shown in Appendix D.2. Instead, the jump gain is positively homogeneous, which is now formally defined.

Definition 3 (Positive homogeneity). *Suppose that $\mathbf{f}(\mathbf{x}, \mathbf{u}, t)$ is a continuously differentiable function. The function \mathbf{f} is positively homogeneous of degree k in \mathbf{x} and \mathbf{u} , and uniform in t , if*

$$\mathbf{f}(a\mathbf{x}, a\mathbf{u}, t) = a^k \mathbf{f}(\mathbf{x}, \mathbf{u}, t), \tag{4.49}$$

for all $a > 0$ [69].

The reader should be aware that the positively homogeneous jump gain (4.47) is non-unique. Due to the simultaneous activation of two guards γ^{01} and γ^{10} , the term $\begin{bmatrix} {}^{11\leftarrow 00}S^1 \mathbf{G} & {}^{11\leftarrow 00}S^1 \mathbf{J} \end{bmatrix}$ can be defined using either γ^{01} or γ^{10} . However, this gain is only applied under the condition that

$${}^2S^1 \mathbf{a}^T s^0 \mathbf{z} + {}^2S^1 \mathbf{b}^T s^0 \mathbf{v} = {}^1S^1 \mathbf{a}^T s^0 \mathbf{z} + {}^1S^1 \mathbf{b}^T s^0 \mathbf{v}, \tag{4.50}$$

which means that the positively homogeneous jump map ${}^{11\leftarrow 00}\mathbf{H} \begin{bmatrix} s^0 \mathbf{z} & s^0 \mathbf{v} \end{bmatrix}^T$ is unique. For this reason, despite the jump gain ${}^{11\leftarrow 00}\mathbf{H}$ being non-unique, the post-event state perturbation $s^k \mathbf{z}$ resulting from the positively homogeneous jump gain is unique.

The conditions that decide which jump gain to use are illustrated in Figure 4.5. Since the conditions are linear in \mathbf{z} and \mathbf{v} , they appear as lines in the state space of \mathbf{z} and \mathbf{v} . When we introduce more conditions, we will find several cones that relate a certain jump gain to a \mathbf{z}, \mathbf{v} pair. When we look at the vector $\mathbf{r}(\mathbf{z}, \mathbf{v})$ in Figure 4.5, it can be noticed that when \mathbf{r} is multiplied with a positive constant a , the same jump gain is applied. Therefore, the positively homogeneous jump gain (4.47) is positively homogeneous of order zero. The non-uniqueness of ${}^{11\leftarrow 00}\mathbf{H}$ appears on the dashed line associated with condition (I), depicted in Figure 4.5.

4.2.3 The positively homogeneous time-triggered hybrid system

With the positively homogeneous jump gain presented in the previous section, the PTTHS can be defined. The PTTHS forms an approximation of the NSITHS defined in Definition 1. We presume this approximation to be first order. The PTTHS will jump at the same time as the nominal trajectory $\boldsymbol{\alpha}$, and will also experience the same number of jumps. This means that a controller designed on the PTTHS will only switch once during a macro event, and not on every micro event. This is desired behavior, as the micro events will likely happen too rapidly to control on. We now define the PTTHS formally, with the positively homogeneous jump gain being defined for a character-2 event ($c = 2$, with $a = 00$ and $p = 11$) for brevity reasons.

Definition 4 (PTTHS). *The positively homogeneous time-triggered hybrid system associated with the NSITHS and the associative and transversal reference trajectory $(\boldsymbol{\alpha}(t, i), \boldsymbol{\mu}(t, i))$ is given by*

$$\dot{\mathbf{z}} = \mathbf{A}_i(t)\mathbf{z} + \mathbf{B}_i(t)\mathbf{v}, \quad (t, i) \in \text{dom } \boldsymbol{\alpha}, \tag{4.51}$$

$$\mathbf{z}^+ = \mathbf{H}_{i+1} \begin{bmatrix} \mathbf{z}^- \\ \mathbf{v}^- \end{bmatrix}, \quad (t, i) \in \text{eve } \boldsymbol{\alpha}, \tag{4.52}$$

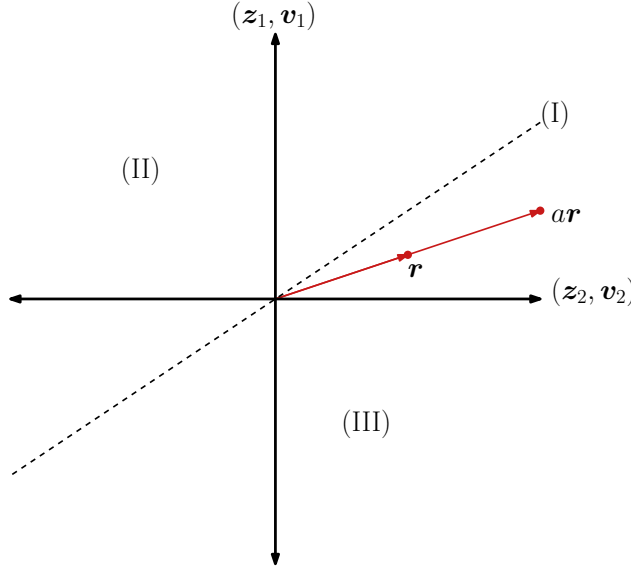


Figure 4.5: An illustration of the conditions in (4.48), and how they result in a order zero positively homogeneous jump gain. The areas (I), (II), and (III) coincide with the conditions (I), (II), and (III) in (4.48).

where $\mathbf{H}_{i+1} := {}^{p \leftarrow a} \mathbf{H}(\mathbf{z}^-, \mathbf{v}^-, t)$ is a positively homogeneous jump gain of order zero,

$$\begin{aligned} \mathbf{A}_i(t) &:= D_1 \mathbf{f}(\boldsymbol{\alpha}(t, i), \boldsymbol{\mu}(t, i), t, i), \\ \mathbf{B}_i(t) &:= D_2 \mathbf{f}(\boldsymbol{\alpha}(t, i), \boldsymbol{\mu}(t, i), t, i), \\ \mathbf{v}^- &:= {}^a \mathbf{v} = \mathbf{v}(t, i), \\ \mathbf{z}^- &:= {}^a \mathbf{z} = \mathbf{z}(t, i), \\ \mathbf{z}^+ &:= {}^p \mathbf{z} = \mathbf{z}(t, i + 1), \end{aligned}$$

with $a = s_i^0 = 00 \dots 0$ and $p = s_i^l = 11 \dots 1$ where l is the amount of micro events in the growing sequence $p \leftarrow \dots \leftarrow a$. The domain $\text{dom } \boldsymbol{\alpha}$ and event set $\text{eve } \boldsymbol{\alpha}$ are defined as

$$\text{dom } \boldsymbol{\alpha} := \bigcup_{i=0}^N [\tau_i, \tau_{i+1}] \times \{i\}, \quad (4.53)$$

$$\text{eve } \boldsymbol{\alpha} := \bigcup_{i=1}^N \{\tau_i\} \times \{i - 1\}, \quad (4.54)$$

with $\tau_0 = t_0$. The positively homogeneous jump gain ${}^{p \leftarrow a} \mathbf{H}$ for a character-2 event ($c = 2$), with the macro counter i omitted for readability, is given by

$${}^{11 \leftarrow 00} \mathbf{H}(s^0 \mathbf{z}(\tau), s^0 \mathbf{v}(\tau), \tau) = \begin{cases} \begin{bmatrix} {}^{11 \leftarrow 00} \mathbf{G}, & {}^{11 \leftarrow 00} \mathbf{J} \end{bmatrix}, & \text{if (I),} \\ \begin{bmatrix} {}^{11 \leftarrow 01} \mathbf{G}_2^{01 \leftarrow 00}, & {}^{11 \leftarrow 01} \mathbf{G}_2^{01 \leftarrow 00} \mathbf{J} \end{bmatrix}, & \text{if (II),} \\ \begin{bmatrix} {}^{11 \leftarrow 10} \mathbf{G}_2^{10 \leftarrow 00}, & {}^{11 \leftarrow 10} \mathbf{G}_2^{10 \leftarrow 00} \mathbf{J} \end{bmatrix}, & \text{if (III),} \end{cases} \quad (4.55)$$

with

$$\begin{aligned} (I) : & {}^2 S^1 \mathbf{a}^T s^0 \mathbf{z} + {}^2 S^1 \mathbf{b}^T s^0 \mathbf{v} = {}^1 S^1 \mathbf{a}^T s^0 \mathbf{z} + {}^1 S^1 \mathbf{b}^T s^0 \mathbf{v}, \\ (II) : & {}^2 S^1 \mathbf{a}^T s^0 \mathbf{z} + {}^2 S^1 \mathbf{b}^T s^0 \mathbf{v} > {}^1 S^1 \mathbf{a}^T s^0 \mathbf{z} + {}^1 S^1 \mathbf{b}^T s^0 \mathbf{v}, \\ (III) : & {}^2 S^1 \mathbf{a}^T s^0 \mathbf{z} + {}^2 S^1 \mathbf{b}^T s^0 \mathbf{v} < {}^1 S^1 \mathbf{a}^T s^0 \mathbf{z} + {}^1 S^1 \mathbf{b}^T s^0 \mathbf{v}. \end{aligned} \quad (4.56)$$

The jump gains ${}^{s^+ \leftarrow s^-}_{S^k} \mathbf{G}$ and ${}^{s^+ \leftarrow s^-}_{S^k} \mathbf{J}$ in (4.55), with $s^+ = s^k$ and $s^- = s^0$ and $S^k = s^k \leftarrow s^{k-1} \leftarrow \dots \leftarrow s^0$, are given by

$${}^{s^+ \leftarrow s^-}_{S^k} \mathbf{G} := D_1 \mathbf{g}^- - (\dot{\mathbf{g}}^- - \mathbf{f}^+) \frac{D_1 \gamma^-}{\dot{\gamma}^-}, \quad (4.57)$$

$${}^{s^+ \leftarrow s^-}_{S^k} \mathbf{J} := D_2 \mathbf{g}^- - (\dot{\mathbf{g}}^- - \mathbf{f}^+) \frac{D_2 \gamma^-}{\dot{\gamma}^-}, \quad (4.58)$$

and

$$\begin{aligned} \mathbf{f}^- &:= {}^{s^-} \mathbf{f} \left({}^{S^-} \boldsymbol{\alpha}(\tau), {}^{S^-}_{\rightarrow} \boldsymbol{\mu}(\tau), \tau \right), \\ \mathbf{f}^+ &:= {}^{s^+} \mathbf{f} \left({}^{S^+} \boldsymbol{\alpha}(\tau), {}^{S^+}_{\rightarrow} \boldsymbol{\mu}(\tau), \tau \right), \\ \mathbf{g}^- &:= {}^{s^+ \leftarrow s^-} \mathbf{g} \left({}^{S^-} \boldsymbol{\alpha}(\tau), {}^{S^-}_{\rightarrow} \boldsymbol{\mu}(\tau), \tau \right), \\ \gamma^- &:= \gamma^{\eta(s^+ \leftarrow s^-)} \left({}^{S^-} \boldsymbol{\alpha}(\tau), {}^{S^-}_{\rightarrow} \boldsymbol{\mu}(\tau), \tau \right), \\ \dot{\mathbf{g}}^- &:= D_1 \mathbf{g}^- \cdot \mathbf{f}^- + D_2 \mathbf{g}^- \cdot \dot{\boldsymbol{\mu}}^- + D_3 \mathbf{g}^-, \\ \dot{\gamma}^- &:= D_1 \gamma^- \cdot \mathbf{f}^- + D_2 \gamma^- \cdot \dot{\boldsymbol{\mu}}^- + D_3 \gamma^-, \end{aligned}$$

where the \rightarrow left subscript should be interpreted as \searrow or \nearrow to indicate whether the feedforward is pushing or withdrawing, respectively. $\gamma^{\eta(s^+ \leftarrow s^-)}$ is the guard function that is activated during the transition $s^+ \leftarrow s^-$. If the transition $s^+ \leftarrow s^-$ is associated with multiple guard functions, one of the guard functions can be chosen, as it will have no effect on the jump gain. For example, during the transition $11 \leftarrow 00$, γ^{01} or γ^{10} should be used for defined the jump gain. Finally, the vectors ${}^{S^k} \mathbf{a}$ and ${}^{S^k} \mathbf{b}$ in (4.56) are given by

$$\begin{aligned} {}^{S^k} \mathbf{a} &= -\frac{1}{\dot{\gamma}^-} D_1 \gamma^-, \\ {}^{S^k} \mathbf{b} &= -\frac{1}{\dot{\gamma}^-} D_2 \gamma^-. \end{aligned}$$

4.3 Summary

An approximation for nonlinear state-and-input-triggered systems with input-dependent guard experiencing simultaneous impacts is presented. Simultaneous guard activations are introduced and the adopted notation required to deal with such activations is presented and elaborated. Assumptions on the reference trajectory are presented, which reduce the complexity of the problem while maintaining practical usability. Then, reference spreading is extended to transitions with simultaneous events. After that, a sensitivity analysis is presented, to find an approximation of the behavior of the NSITHS near $(\boldsymbol{\alpha}, \boldsymbol{\mu})$, where so-called loss of simultaneity occurs. Similar to the result presented in Chapter 3, we presume the approximation being first order, despite the proof not yet being available. A state-and-input dependent jump gain, called the positively homogeneous jump gain, is used to define the positively homogeneous time-triggered hybrid system (PTTHS). The PTTHS is expected to be suitable for assessing the local asymptotic stability of a nonlinear state-and-input triggered hybrid system with simultaneous guard activations.

Chapter 5

Numerical Validation

Chapter 6

Conclusions and Recommendations

The research goals that have been addressed in this work are:

Simultaneous impacts with friction

Find a model suitable to describe mechanical systems with unilateral constraints and spatial friction. The sensitivity analysis and mathematical notation presented in [67] shall be extended to be compatible with such models.

Simultaneous releases

Extending the sensitivity analysis presented in [67] such that it is suitable for input-triggered events.

6.1 Conclusions

To analyze mechanical systems with unilateral constraints and spatial friction, a suitable model needed to be found. The hybrid system formulation using guard functions has been previously used in modeling mechanical systems with trajectories experiencing impact [67]. In Chapter 2, a hybrid system formulation using guard functions is presented for mechanical systems with trajectories experiencing frictional impacts, releasing motions, and stick-slip transitions. We name this model the nonlinear state-and-input-triggered hybrid system (NSITHS). The contribution made in Chapter 2 is:

A model, suitable to describe mechanical systems with unilateral constraints and spatial friction, is found and presented in the form an NSITHS.

The model presented in Chapter 2 is used to analyze the effect of perturbations on trajectories of mechanical systems with unilateral constraints and spatial friction. This is achieved by performing a sensitivity analysis, which results in a model that describes the response on perturbations of the system. Since the model presented in Chapter 2 contains input-dependent guard functions, the sensitivity analysis presented in [55] does not suffice. Therefore, the sensitivity analysis is extended to be suitable for input-dependent guard functions and jump maps. This sensitivity analysis defines a linear time-triggered hybrid system (LTTHS), which approximates the behavior of the NSITHS for trajectories with isolated events. The contribution made in Chapter 3 is:

The sensitivity analysis and notation presented in [67] is extended to be compatible with the NSITHS, for trajectories with isolated events.

- PTTHS for systems with input dependent guards

- First steps in simulations
- Summary of contribution can accomplish

6.2 Recommendations

- Trajectory generation
- Numerical Validation (also slip to stick guard function suitable for simulations)
- Missing proofs (Induction proof of \mathbf{G} and \mathbf{J} , stability of LTTHS/PTTHS implies stability of NSITHS, approximation is first order)
- Impacts at the border between stick and slip

Bibliography

- [1] Virginia Tech Robotics and Mechatronics Lab. Simlab quadruped. <http://www.me.vt.edu/research/laboratories/rmlab/>, 2018.
- [2] ABB Robotics. Irb 360 flexpicker. <https://new.abb.com/products/robotics/industrial-robots/irb-360>, 2018.
- [3] Remco I. Leine and Henk Nijmeijer. *Dynamics and Bifurcations of Non-Smooth Mechanical Systems*. Springer-Verlag, Berlin, Heidelberg, 1st edition, 2004.
- [4] A. F. Fillippov. *Differential Equations with Discontinuous Righthand Sides*. Springer-Science, Dordrecht, 1st edition, 1988.
- [5] Remco I. Leine and Nathan Van De Wouw. Uniform Convergence of Monotone Measure Differential Inclusions: With Application To the Control of Mechanical Systems With Unilateral Constraints. *International Journal of Bifurcation and Chaos*, 18(5):1435–1457, 2008.
- [6] J. J. Moreau and P. O. Panagiotopoulos. *Nonsmooth Mechanics and Applications*. Springer-Verlag, Wien, 1st edition, 1988.
- [7] Bernard Brogliato. *Nonsmooth Mechanics*. Springer, 3rd edition, 1999.
- [8] N Van De Wouw. An introduction to Time-Stepping: a Numerical Technique for Mechanical Systems with Unilateral Constraints. pages 1–27, 2004.
- [9] A. J. Van Der Schaft and J. M. Schumacher. Complementarity modeling of hybrid systems. *IEEE Transactions on Automatic Control*, 43(4):483–490, 1998.
- [10] W. Heemels. *Linear complementarity systems: a study in hybrid dynamics*. PhD thesis, Eindhoven University of Technology, 1999.
- [11] Christoph Glocker. *Set-Valued Force Laws: Dynamics of Non-Smooth Systems*, volume 1. Springer, Zürich, 1 edition, 2001.
- [12] Jean-Matthieu Bourgeot and Bernard Brogliato. Passivity-based tracking control of multiconstraint complementarity Lagrangian systems. *International Journal of Bifurcation and Chaos*, 15(6):1839–1866, 2005.
- [13] Irinel-Constantin Morarescu and Bernard Brogliato. Tracking Control of Multiconstraint Complementarity Lagrangian Systems. *International Journal of Bifurcation and Chaos*, 55(6):1300–1313, 2010.
- [14] Dong Jin Hyun, Sangok Seok, Jongwoo Lee, and Sangbae Kim. High speed trot-running: Implementation of a hierarchical controller using proprioceptive impedance control on the MIT Cheetah. *International Journal of Robotics Research*, 33(11):1417–1445, 2014.

- [15] Benjamin Morris and Jessy W. Grizzle. Hybrid invariant manifolds in systems with impulse effects with application to periodic locomotion in bipedal robots. *IEEE Transactions on Automatic Control*, 54(8):1751–1764, 2009.
- [16] Rafal Goebel, Ricardo G. Sanfelice, and Andrew R. Teel. Hybrid dynamical systems. *IEEE Control Systems Magazine*, 29(2):28–93, 2009.
- [17] Jerry Ding, Jeremy H Gillula, Haomiao Huang, Michael P Vitus, Wei Zhang, and Claire J Tomlin. Hybrid Systems in Robotics: Toward Reachability-Based Controller Design. *IEEE Robotics & Automation Magazine*, 18(3):33–43, 2011.
- [18] Hui Ye and a. N. Michel. Stability theory for hybrid dynamical systems. *IEEE Transactions on Automatic Control*, 43(4):461–474, 1998.
- [19] J. Lygeros, K.H. Johansson, S.N. Simic, and S.S. Sastry. Dynamical properties of hybrid automata. *IEEE Transactions on Automatic Control*, 48(1):2–17, 2003.
- [20] F. L. Pereira and G. N. Silva. Lyapunov stability of measure driven impulsive systems. *Differential Equations*, 40(8):1122–1130, 2004.
- [21] Bernard Brogliato. Absolute stability and the Lagrange-Dirichlet theorem with monotone multivalued mappings. *Systems and Control Letters*, 51(5):343–353, 2004.
- [22] R.I. Leine and N. van de Wouw. *Stability and Convergence of Mechanical Systems with Unilateral Constraints*, volume 36. Springer, 2008.
- [23] M Kanat Camlibel, Jong-Shi Pang, and Jinglai Shen. Lyapunov Stability of Complementarity and Extended Systems. *SIAM Journal on Optimization*, 17(4):1056–1101, 2007.
- [24] M. Kanat Camlibel and Nathan Van De Wouw. On the Convergence of Linear Passive Complementarity Systems. *IEEE Conference on Decision and Control*, 46th:5886–5891, 2007.
- [25] Marc H. Raibert. Hopping in Legged Systems - Modeling and Simulation for the Two-Dimensional One-Legged Case. *IEEE Transactions on Systems, Man and Cybernetics*, SMC-14(3):451–463, 1984.
- [26] Andrés Lebaudy, Joseph Prosser, and Moshe Kam. Control Algorithms for a Vertically-Constrained One-Legged Hopping Machine. *Proceedings of the 32nd Conference on Decision and Control*, pages 2688–2693, 1993.
- [27] H. Michalska, M. Ahmadi, and M. Buehler. Vertical motion control of a hopping robot. *Proceedings of IEEE International Conference on Robotics and Automation*, 3(April):2712–2717, 1996.
- [28] Pedro Gregorio, Mojtaba Ahmadi, and Martin Buehler. Design, control, and energetics of an electrically actuated legged robot. *IEEE Transactions on Systems, Man, and Cybernetics, Part B: Cybernetics*, 27(4):626–634, 1997.
- [29] Jesse W. Grizzle, Gabriel Abba, and Franck Plestan. Asymptotically stable walking for biped robots: Analysis via systems with impulse effects. *IEEE Transactions on Automatic Control*, 46(1):51–64, 2001.
- [30] Aaron D. Ames. Human-inspired control of Bipedal walking robots. *IEEE Transactions on Automatic Control*, 59(5):1115–1130, 2014.

- [31] Jacob Reher, Eric A. Cousineau, Ayonga Hereid, Christian M. Hubicki, and Aaron D. Ames. Realizing dynamic and efficient bipedal locomotion on the humanoid robot DURUS. *Proceedings - IEEE International Conference on Robotics and Automation*, 2016-June:1794–1801, 2016.
- [32] Agility Robotics. Cassie. <http://www.agilityrobotics.com/robots/#cassie>, 2018.
- [33] Jessy W. Grizzle, Christine Chevallereau, Ryan W. Sinnet, and Aaron D. Ames. Models, feedback control, and open problems of 3D bipedal robotic walking. *Automatica*, 50(8):1955–1988, 2014.
- [34] Nathan van de Wouw and Remco I Leine. Tracking control for a class of measure differential inclusions. *Proceedings IEEE Conference on Decision and Control*, pages 2526–2532, 2008.
- [35] Nathan Van De Wouw and Remco I Leine. Stability and Control of Lur’e-type Measure Differential Inclusions. pages 129–151, 2010.
- [36] Roberto Naldi and Ricardo G. Sanfelice. Passivity-based control for hybrid systems with applications to mechanical systems exhibiting impacts. *Automatica*, 49(5):1104–1116, 2013.
- [37] Ricardo G. Sanfelice, J. J. Benjamin Biemond, Nathan Van De Wouw, and W. P. Maurice H. Heemels. Tracking control for hybrid systems via embedding of known reference trajectories. *Proceedings of the 2011 American Control Conference*, pages 869–874, 2011.
- [38] Ricardo G. Sanfelice, J. J. Benjamin Biemond, Nathan Van De Wouw, and W. P. Maurice H. Heemels. An embedding approach for the design of state-feedback tracking controllers for references with jumps. *International Journal of Robust and Nonlinear Control*, 24:1585–1608, 2014.
- [39] Michael Posa, Mark Tobenkin, and Russ Tedrake. Stability Analysis and Control of Rigid Body Systems with Impacts and Friction. *IEEE TRANSACTIONS ON AUTOMATIC CONTROL*, 61(6):1423–1437, 2016.
- [40] Ye Zhao, Benito R. Fernandez, and Luis Sentis. A Framework for Planning and Controlling Non-Periodic Bipedal Locomotion. 2015.
- [41] J J B Biemond, N Van De Wouw, W P M H Heemels, and H Nijmeijer. Tracking Control for Hybrid Systems with State-Triggered Jumps. *IEEE Transactions on Automatic Control*, 58(257462):876–890, 2013.
- [42] Laura Menini and Antonia Tornambè. Asymptotic tracking of periodic trajectories for a simple mechanical system subject to nonsmooth impacts. *IEEE Transactions on Automatic Control*, 46(7):1122–1126, 2001.
- [43] S. Galeani, L. Menini, A. Potini, and A. Tornambè. Trajectory tracking for a particle in elliptical billiards. *International Journal of Control*, 81(2):189–213, 2008.
- [44] Fulvio Forni, Andrew R. Teel, and Luca Zaccarian. Follow the bouncing ball: Global results on tracking and state estimation with impacts. *IEEE Transactions on Automatic Control*, 58(6):1470–1485, 2013.
- [45] J. J. Benjamin Biemond, W. P. Maurice H. Heemels, Ricardo G. Sanfelice, and Nathan van de Wouw. Distance function design and Lyapunov techniques for the stability of hybrid trajectories. *Automatica*, 73:38–46, 2016.

- [46] Michael Baumann, J. J. Benjamin Biemond, Remco I. Leine, and Nathan van de Wouw. Synchronization of impacting mechanical systems with a single constraint. *Physica D: Nonlinear Phenomena*, 362:9–23, 2018.
- [47] Jisu Kim, Hyungbo Shim, and Jin Heon Seo. Tracking control for hybrid systems with state jumps using gluing function. *2016 IEEE 55th Conference on Decision and Control, CDC 2016*, pages 3006–3011, 2016.
- [48] Ting Yang, Fen Wu, and Lixian Zhang. Tracking control of hybrid systems with state-triggered jumps and stochastic events and its application. *IET Control Theory & Applications*, 11(7):1024–1033, 2017.
- [49] Alessandro Saccon, Nathan van de Wouw, and Henk Nijmeijer. Sensitivity analysis of hybrid systems with state jumps with application to trajectory tracking. *Proceedings of the 53rd IEEE Conference on Decision and Control*, pages 3065–3070, 2014.
- [50] Mark Rijnen, Alessandro Saccon, and Henk Nijmeijer. On Optimal Trajectory Tracking for Mechanical Systems with Unilateral Constraints. *2015 IEEE 54th Annual Conference on Decision and Control (CDC)*, pages 2561–2566, 2015.
- [51] Hassan K. Khalil. *Nonlinear Systems*. Prentice-Hall, Englewood Cliffs, NJ, 3rd edition, 1996.
- [52] Gian Paolo Incremona, Alessandro Saccon, Antonella Ferrara, and Henk Nijmeijer. Trajectory tracking of mechanical systems with unilateral constraints: Experimental results of a recently introduced hybrid PD feedback controller. *Proceedings of the IEEE Conference on Decision and Control*, 54rd IEEE(Cdc):920–925, 2015.
- [53] M. W.L.M. Rijnen, A. T. van Rijn, H. Dallali, A. Saccon, and H. Nijmeijer. Hybrid Trajectory Tracking for a Hopping Robotic Leg. *IFAC-PapersOnLine*, 49(14):107–112, 2016.
- [54] N. G. Tsagarakis, S. Morfey, H. Dallali, G. A. Medrano-Cerda, and D. G. Caldwell. An asymmetric compliant antagonistic joint design for high performance mobility. *IEEE International Conference on Intelligent Robots and Systems*, pages 5512–5517, 2013.
- [55] M.W.L.M. Rijnen, J.J.B. Biemond, N. van de Wouw, A. Saccon, and H. Nijmeijer. Hybrid Systems with State-Triggered Jumps: Sensitivity-Based Stability Analysis with Application to Trajectory Tracking. pages 1–16, 2017.
- [56] Mark Rijnen, Eric De Mooij, Silvio Traversaro, Francesco Nori, Nathan Van De Wouw, Alessandro Saccon, and Henk Nijmeijer. Control of humanoid robot motions with impacts: Numerical experiments with reference spreading control. *Proceedings - IEEE International Conference on Robotics and Automation*, pages 4102–4107, 2017.
- [57] Huihua Zhao, Jonathan Horn, Jacob Reher, Victor Paredes, and Aaron D. Ames. A hybrid systems and optimization-based control approach to realizing multi-contact locomotion on transfemoral prostheses. *Proceedings of the IEEE Conference on Decision and Control*, 54(2):1607–1612, 2015.
- [58] Hao Liang Chen. *Trajectory tracking control for mechanical systems experiencing simultaneous impacts*. Master’s thesis, Eindhoven University of Technology, 2018.
- [59] Mark Rijnen, Hao Liang Chen, Nathan Van De Wouw, Alessandro Saccon, and Henk Nijmeijer. Sensitivity analysis for trajectories of nonsmooth mechanical systems with simultaneous impacts : a hybrid systems perspective. 2018.

- [60] Christoph Glocker. Energetic consistency conditions for standard impacts: Part I: Newton-type inequality impact laws and Kane’s example. *Multibody System Dynamics*, 32(4):445–509, 2014.
- [61] Anthom van Rijn. *Hybrid trajectory tracking for hopping robots*. Master’s thesis, Eindhoven University of Technology, 2016.
- [62] N. van de Wouw. *Multibody and Nonlinear Dynamics Lecture Notes*. University of Technology Eindhoven, Eindhoven, 2016.
- [63] Mihai Anitescu. Optimization-based simulation of nonsmooth rigid multibody dynamics. *Math. Program., Ser. A*, 105:113–143, 2006.
- [64] Vincent Acary and Bernard Brogliato. *Numerical Methods for Nonsmooth Dynamical Systems: Applications in Mechanics and Electronics*, volume 35. Springer, Montbonnot, 2008.
- [65] Wassim M Haddad, VijaySekhar Chellaboina, and Sergey G. Nersesov. *Impulsive and Hybrid Dynamical Systems*. Princeton University Press, New Jersey, 1st edition, 2006.
- [66] Étienne Delassus. Mémoire sur la théorie des liaisons finies unilatérales. *Annales scientifiques de l’É.N.S.*, 34(3rd):95–179, 1917.
- [67] M.W.L.M. Rijnen. *Enabling motions with impacts in robotic and mechatronic systems*. Technische Universiteit Eindhoven, Eindhoven, 2018.
- [68] Joao P. Hespanha. *Linear Systems Theory*. Princeton Press, Princeton, New Jersey, 2018. ISBN13: 9780691179575.
- [69] TM Apostol. *Multi-Variable Calculus and Linear Algebra with Applications*, volume 2. John Wiley & Sons, New York, 2nd edition, 1967.

Appendix A

Nonsmooth modeling

A.1 Hybrid system formulation for mechanical systems

A.1.1 Continuous dynamics derivation

A.1.2 Discrete event set derivation

In this section the discrete event sets D are defined. When the state or input of the system enters a discrete event set, contact points can change set and a reinitialization of the state can take place. In this work the assumption is made that all contact points in closed contact are in the same set, i.e., in either \mathcal{I}_{sl} or \mathcal{I}_{st} .

More elaboration on why the conditions that are chosen are chosen (i.e., why $\|\zeta_{t,i}\| = 0$)

Recap each paragraph using section D and mentioning γ 's again.

Open to stick/slip

When a contact point is "open", it can trigger a guard function $\gamma_{op \rightarrow cl}$ to go from open to closed. This guard is defined using the contact distance h_{n,i_c} . When $h_{n,i_c} > 0$, the contact point is in open-contact. When $h_{n,i_c} = 0$ with $\dot{h}_{n,i_c} < 0$, the contact point enters the closed-contact mode with a non-zero ante-impact velocity. Therefore the guard function $\gamma_{op \rightarrow cl}$ is given by

$$\gamma_{op \rightarrow cl} = h_{n,i_c}(\mathbf{q}). \quad (\text{A.1})$$

The plane that spans $\gamma = 0$ is divided in two regions: a region where the post-impact state is in slip and a region where the post-impact state is in stick. **I** This region is defined by Γ_{i_c} , where $\Gamma_{i_c} < 0$ in the region where the contact point goes to slip and $\Gamma_{i_c} > 0$ in the region where the contact point goes to stick. When $\Gamma_{i_c} = 0$ the system is right at the border between a slip post-impact state and a stick post-impact state. This is illustrated in Figure A.1.

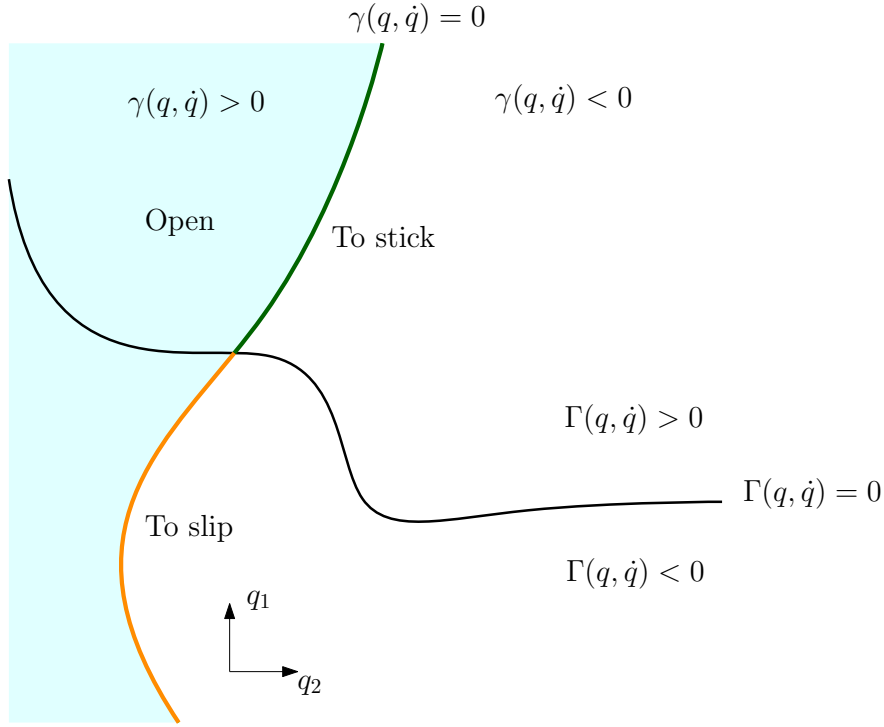


Figure A.1: The functions $\gamma(\mathbf{q}, \dot{\mathbf{q}})$ and $\Gamma(\mathbf{q}, \dot{\mathbf{q}})$ illustrated in the state space of $\mathbf{q} \in \mathbb{R}^2$. The light blue area is the state space where the contact is open, and goes the closed when it triggers $\gamma = 0$. If it triggers $\gamma = 0$ in the area where $\Gamma < 0$ (orange), then the contact will go to slip. If it triggers $\gamma = 0$ in the area where $\Gamma \geq 0$ (green), then the contact will go to stick.

For slip, we know that $\mu\Lambda_{n,i_c} - \|\Lambda_{t,i_c}\| = 0$ and for stick, we know that $\mu\Lambda_{n,i_c} - \|\Lambda_{t,i_c}\| \geq 0$. From this we can derive the guard function

$$\Gamma_{i_c} = \mu^2 \underline{\Lambda}_{n,i_c}^2(\underline{\mathbf{q}}, \underline{\dot{\mathbf{q}}}) - \underline{\Lambda}_{t,i_c}(\underline{\mathbf{q}}, \underline{\dot{\mathbf{q}}}) \underline{\Lambda}_{t,i_c}^T(\underline{\mathbf{q}}, \underline{\dot{\mathbf{q}}}). \quad (\text{A.2})$$

The underlined variables are virtual states, meaning that they do not necessarily have a physical meaning. The way (A.2) is given, it is defined in both open and closed contact. This map is only physically realistic during an event from open to closed contact. However, by using virtual states we obtain a differentiable guard function Γ_{i_c} . This guard function Γ_{i_c} satisfies the requirements that $\Gamma_{i_c} < 0$ in the region where the contact point goes to slip, $\Gamma_{i_c} > 0$ in the region where the contact point goes to stick and $\Gamma_{i_c} = 0$ at the border. We now find expressions for Λ_{n,i_c} and Λ_{t,i_c} by looking at the jump map to stick, given in (??) to (??).

We can rewrite (??) to

$$\dot{\mathbf{q}} = \mathbf{M}^{-1} \mathbf{W}_n \underline{\Lambda}_n + \mathbf{M}^{-1} \mathbf{W}_t \underline{\Lambda}_t + \underline{\dot{\mathbf{q}}}, \quad (\text{A.3})$$

and (??), (??) to

$$\mathbf{W}_n^T \underline{\dot{\mathbf{q}}} = 0, \quad (\text{A.4})$$

$$\mathbf{W}_t^T \underline{\dot{\mathbf{q}}} = 0, \quad (\text{A.5})$$

with

$$\mathbf{W}_n = [\mathbf{w}_{n,i_1}, \mathbf{w}_{n,i_2}, \dots, \mathbf{w}_{n,i_c}] \in \mathbb{R}^{n \times C}, \quad (\text{A.6})$$

$$\mathbf{W}_t = [\mathbf{w}_{t,i_1}, \mathbf{w}_{t,i_2}, \dots, \mathbf{w}_{t,i_c}] \in \mathbb{R}^{n \times 2C}, \quad (\text{A.7})$$

$$\underline{\mathbf{A}}_n = [\underline{\mathbf{A}}_{n,i_1}; \underline{\mathbf{A}}_{n,i_2}; \dots; \underline{\mathbf{A}}_{n,i_c}] \in \mathbb{R}^C, \quad (\text{A.8})$$

$$\underline{\mathbf{A}}_t = [\underline{\mathbf{A}}_{t,i_1}; \underline{\mathbf{A}}_{t,i_2}; \dots; \underline{\mathbf{A}}_{t,i_c}] \in \mathbb{R}^{2C}. \quad (\text{A.9})$$

Substituting (A.3) into (A.4) and (A.5) leads to

$$\mathbf{W}_n^T \mathbf{M}^{-1} \mathbf{W}_n \underline{\mathbf{A}}_n + \mathbf{W}_n^T \mathbf{M}^{-1} \mathbf{W}_t \underline{\mathbf{A}}_t + \underline{\boldsymbol{\zeta}}_n = 0 \quad (\text{A.10})$$

$$\mathbf{W}_t^T \mathbf{M}^{-1} \mathbf{W}_n \underline{\mathbf{A}}_n + \mathbf{W}_t^T \mathbf{M}^{-1} \mathbf{W}_t \underline{\mathbf{A}}_t + \underline{\boldsymbol{\zeta}}_t = 0, \quad (\text{A.11})$$

respectively, with

$$\underline{\boldsymbol{\zeta}}_n = \mathbf{W}_n^T \dot{\mathbf{q}}, \quad (\text{A.12})$$

$$\underline{\boldsymbol{\zeta}}_t = \mathbf{W}_t^T \dot{\mathbf{q}}. \quad (\text{A.13})$$

This is now rewritten to

$$\begin{bmatrix} \mathbf{W}_n^T \mathbf{M}^{-1} \mathbf{W}_n & \mathbf{W}_n^T \mathbf{M}^{-1} \mathbf{W}_t \\ \mathbf{W}_t^T \mathbf{M}^{-1} \mathbf{W}_n & \mathbf{W}_t^T \mathbf{M}^{-1} \mathbf{W}_t \end{bmatrix} \begin{bmatrix} \underline{\mathbf{A}}_n \\ \underline{\mathbf{A}}_t \end{bmatrix} + \begin{bmatrix} \underline{\boldsymbol{\zeta}}_n \\ \underline{\boldsymbol{\zeta}}_t \end{bmatrix} = 0, \quad (\text{A.14})$$

which is in turn rewritten to

$$\begin{bmatrix} \underline{\mathbf{A}}_n \\ \underline{\mathbf{A}}_t \end{bmatrix} = -\mathbf{D}^{-1} \begin{bmatrix} \underline{\boldsymbol{\zeta}}_n \\ \underline{\boldsymbol{\zeta}}_t \end{bmatrix}, \quad \text{with } \mathbf{D} = \begin{bmatrix} \mathbf{W}_n^T \mathbf{M}^{-1} \mathbf{W}_n & \mathbf{W}_n^T \mathbf{M}^{-1} \mathbf{W}_t \\ \mathbf{W}_t^T \mathbf{M}^{-1} \mathbf{W}_n & \mathbf{W}_t^T \mathbf{M}^{-1} \mathbf{W}_t \end{bmatrix}. \quad (\text{A.15})$$

The matrix \mathbf{D} is often called a Delassus-matrix. We now have expressions for $\underline{\mathbf{A}}_n$ and $\underline{\mathbf{A}}_t$ which are continuous and differentiable in $(\mathbf{q}, \dot{\mathbf{q}})$. It is straightforward that $\Gamma(\mathbf{q}, \dot{\mathbf{q}})$ is continuous and differentiable as well. In this work only trajectories where all closed contacts are in the same mode are considered. This means that when (A.2) is smaller than zero, i.e., the reaction forces are infeasible for a stick post-impact mode, all contact points have a feasible slip post-impact mode. For trajectories where different contact points can be in slip and in stick at the same time, this conclusion can not be drawn. One should then iterate over all possible post-impact modes until a post-impact mode is found which has feasible reaction forces.

Slip to stick/open

When a contact point is in closed-contact slip, it can transition to closed-contact stick and it can transition to open-contact. A slipping contact transitions to sticking when the tangential velocity of the contact point is zero, i.e.,

$$\|\boldsymbol{\zeta}_{t,\ell}\| = 0. \quad (\text{A.16})$$

A guard function that can be used to describe this set is

$$\gamma_{\text{sl} \rightarrow \text{st}} = \boldsymbol{\zeta}_{t,\ell}^T \boldsymbol{\zeta}_{t,\ell}, \quad (\text{A.17})$$

which is equal to zero when $\|\boldsymbol{\zeta}_{t,i_c}\| = 0$, greater than zero when $\|\boldsymbol{\zeta}_{t,i_c}\| > 0$, smaller than zero when $\|\boldsymbol{\zeta}_{t,i_c}\| < 0$, and it is globally differentiable. The time derivative of the guard function is then given by

$$\dot{\gamma}^{\text{sl} \rightarrow \text{st}} = \frac{\dot{\boldsymbol{\zeta}}_{t,1} + \dot{\boldsymbol{\zeta}}_{t,2}}{\sqrt{\boldsymbol{\zeta}_{t,1}^2 + \boldsymbol{\zeta}_{t,2}^2}}. \quad (\text{A.18})$$

For $\gamma^{\text{sl} \rightarrow \text{st}} = 0$, $\dot{\gamma}^{\text{sl} \rightarrow \text{st}}$ is undefined because of a division by zero. But we can take the left limit of $\dot{\gamma}^{\text{sl} \rightarrow \text{st}}$ to find the direction at which the guard is activated. Using a Taylor expansion w.r.t. the time we can define the limits

$$\dot{\zeta}_{t,1}(\tau + s) = a_1 s + o(s), \quad (\text{A.19})$$

$$\dot{\zeta}_{t,2}(\tau + s) = a_2 s + o(s), \quad (\text{A.20})$$

where τ is the event time where $\gamma = 0$. Note that the Taylor expansions are only physically realistic for $s < 0$. We can then write

$$\dot{\gamma}^{\text{sl} \rightarrow \text{st}}(\tau + s) = \frac{(a_1 + a_2)s + o(s)}{\sqrt{(a_1^2 + a_2^2)s^2 + o(s^2)}} \approx \text{Sign}(s)(a_1 + a_2). \quad (\text{A.21})$$

Since we're interested in the left limit, we get

$$\lim_{s \rightarrow 0^-} \dot{\gamma}^{\text{sl} \rightarrow \text{st}}(\tau + s) = -(a_1^2 + a_2^2), \quad (\text{A.22})$$

which will be non-zero when the guard is activated transversally. This guard function can be used to perform the positive homogenization. For simulations we have to find another solution, because $\gamma^{\text{sl} \rightarrow \text{st}}$ cannot become negative. This will lead to problems when we use zero-border crossing detection.

For a slipping contact transitioning to open-contact an acceleration based guard function is necessary, since the normal velocity of the contact point is constrained in the continuous dynamics of a slipping contact. Therefore, a slipping contact point transitions to open-contact when

$$\lambda_{n,i_c} = 0. \quad (\text{A.23})$$

Similarly to the expression found for Λ_n and Λ_t , we can use (2.37) and (??) to define the vector λ_n . With

$$\underline{\lambda}_n = [\underline{\lambda}_{n,i_1}; \underline{\lambda}_{n,i_2}; \dots; \underline{\lambda}_{n,i_C}] \in \mathbb{R}^C, \quad (\text{A.24})$$

$$\underline{\lambda}_t = [\underline{\lambda}_{t,i_1}; \underline{\lambda}_{t,i_2}; \dots; \underline{\lambda}_{t,i_C}] \in \mathbb{R}^{2C}, \quad (\text{A.25})$$

the dynamics and constraints for a system with all closed contact points in slip are defined as

$$\ddot{\mathbf{q}} = \mathbf{M}^{-1} [\mathbf{S}\mathbf{u} - \mathbf{H} + \mathbf{W}_n \lambda_n + \mathbf{W}_t \lambda_t], \quad (\text{A.26})$$

$$\mathbf{W}_n^T \ddot{\mathbf{q}} + \dot{\mathbf{W}}_n^T \dot{\mathbf{q}} = 0, \quad (\text{A.27})$$

$$\lambda_t = -\mu \mathbf{Z}_t \lambda_n, \quad (\text{A.28})$$

with

$$\mathbf{Z}_t = \begin{bmatrix} \langle \zeta_{t,i_1} \rangle & \mathbf{0} & \dots & \mathbf{0} \\ \mathbf{0} & \langle \zeta_{t,i_2} \rangle & \dots & \mathbf{0} \\ \vdots & \vdots & \ddots & \vdots \\ \mathbf{0} & \mathbf{0} & \dots & \langle \zeta_{t,i_C} \rangle \end{bmatrix}, \quad \in \mathbb{R}^{2C \times C} \quad (\text{A.29})$$

where $\langle \zeta_t \rangle = [\langle \zeta_{t,i_1} \rangle, \langle \zeta_{t,i_2} \rangle, \dots, \langle \zeta_{t,i_C} \rangle]^T$, with $\langle \zeta_{t,i_c} \rangle$ the unit vector ζ_{t,i_c} . (A.26)-(A.28) can be rewritten into

$$\lambda_n = -[\mathbf{W}_n^T \mathbf{M}^{-1} (\mathbf{W}_n - \mu \mathbf{W}_t \mathbf{Z}_t)]^{-1} \mathbf{W}_n^T \mathbf{M}^{-1} [\mathbf{S}\mathbf{u} - \mathbf{H}] - \dot{\mathbf{W}}_n^T \dot{\mathbf{q}}, \quad (\text{A.30})$$

which can be used to define the guard function (A.23).

Stick to slip/open

When a contact point is in closed-contact stick, it can transition to closed-contact slip and it can transition to open-contact. A slipping contact transitions to sticking when the tangential reaction force becomes equal to the normal reaction force at that contact point times the friction coefficient, i.e.,

$$\mu\lambda_{n,i_c} = \|\lambda_{t,i_c}\|. \quad (\text{A.31})$$

A guard function that can be used to describe this set is

$$\gamma_{\text{st} \rightarrow \text{sl}} = \mu^2 \lambda_{n,i_c}^2 - \lambda_{t,i_c} \lambda_{t,i_c}^T, \quad (\text{A.32})$$

which is equal to zero when $\mu^2 \lambda_{n,i_c}^2 = \|\lambda_{t,i_c}\|^2$, greater than zero when $\mu^2 \lambda_{n,i_c}^2 > \|\lambda_{t,i_c}\|^2$, and it is globally differentiable. It is physically impossible that $\mu^2 \lambda_{n,i_c}^2 < \|\lambda_{t,i_c}\|^2$, meaning that $\gamma_{\text{st} \rightarrow \text{sl}}$ will never be smaller than zero. The dynamics and constraints of a system with all contact points in stick are defined as

$$\ddot{\mathbf{q}} = \mathbf{M}^{-1} [\mathbf{S}\mathbf{u} - \mathbf{H} + \mathbf{W}_n \lambda_n + \mathbf{W}_t \lambda_t], \quad (\text{A.33})$$

$$\mathbf{W}_n^T \ddot{\mathbf{q}} + \dot{\mathbf{W}}_n^T \dot{\mathbf{q}} = 0, \quad (\text{A.34})$$

$$\mathbf{W}_t^T \ddot{\mathbf{q}} + \dot{\mathbf{W}}_t^T \dot{\mathbf{q}} = 0, \quad (\text{A.35})$$

Substituting (A.33) into (A.34) and (A.35) leads to

$$\mathbf{W}_n^T \mathbf{M}^{-1} \mathbf{W}_n \lambda_n + \mathbf{W}_n^T \mathbf{M}^{-1} \mathbf{W}_t \lambda_t = \mathbf{W}_n^T \mathbf{M}^{-1} [\mathbf{S}\mathbf{u} - \mathbf{H}] - \dot{\mathbf{W}}_n^T \dot{\mathbf{q}}, \quad (\text{A.36})$$

$$\mathbf{W}_t^T \mathbf{M}^{-1} \mathbf{W}_n \lambda_n + \mathbf{W}_t^T \mathbf{M}^{-1} \mathbf{W}_t \lambda_t = \mathbf{W}_t^T \mathbf{M}^{-1} [\mathbf{S}\mathbf{u} - \mathbf{H}] - \dot{\mathbf{W}}_t^T \dot{\mathbf{q}}, \quad (\text{A.37})$$

which can be rewritten to

$$\begin{bmatrix} \lambda_n \\ \lambda_t \end{bmatrix} = -\mathbf{D}^{-1} \begin{bmatrix} \mathbf{W}_n^T \mathbf{M}^{-1} [\mathbf{S}\mathbf{u} - \mathbf{H}] - \dot{\mathbf{W}}_n^T \dot{\mathbf{q}} \\ \mathbf{W}_t^T \mathbf{M}^{-1} [\mathbf{S}\mathbf{u} - \mathbf{H}] - \dot{\mathbf{W}}_t^T \dot{\mathbf{q}} \end{bmatrix}. \quad (\text{A.38})$$

Using (A.38) the guard function (A.32) is defined.

A.1.3 Discrete dynamics derivation

In this section the discrete dynamics are defined, describing the state reinitialization when a discrete event set is entered. These dynamics are defined by a jump map \mathbf{g} , which is defined differently for each post-event mode.

Slip post-impact mode $\dot{\mathbf{q}}^+ = \mathbf{g}_{\rightarrow \text{sl}}(\dot{\mathbf{q}}^-)$

The discrete dynamics of a transition with a slip post-impact mode are given by

$$\mathbf{M}[\dot{\mathbf{q}}^+ - \dot{\mathbf{q}}^-] = \mathbf{W}_n \Lambda_n + \mathbf{W}_t \Lambda_t, \quad (\text{A.39})$$

$$\mathbf{W}_n^T \dot{\mathbf{q}}^+ = 0, \quad (\text{A.40})$$

$$\Lambda_t = -\mu \mathbf{Z}_t^- \Lambda_n, \quad (\text{A.41})$$

with \mathbf{Z}_t^- defined as in (A.29) using the unit vector of the ante-impact tangential velocity $\langle \zeta_t^- \rangle$. After substituting (A.41) into (A.39) and rewriting to

$$\dot{\mathbf{q}}^+ = [\mathbf{M}^{-1} \mathbf{W}_n - \mu \mathbf{M}^{-1} \mathbf{W}_t \mathbf{Z}_t^-] \Lambda_n + \dot{\mathbf{q}}^-, \quad (\text{A.42})$$

and expression for Λ_n can be found by substituting this into (A.40), which is

$$\Lambda_n = - [\mathbf{W}_n^T \mathbf{M}^{-1} \mathbf{W}_n - \mu \mathbf{W}_n^T \mathbf{M}^{-1} \mathbf{W}_t \mathbf{Z}_t^-]^{-1} \mathbf{W}_n^T \dot{\mathbf{q}}^-, \quad (\text{A.43})$$

The jump map $\dot{\mathbf{q}}^+ = \mathbf{g}_{\rightarrow \text{sl}}(\dot{\mathbf{q}}^-)$ is then found by substituting (A.43) into (A.42),

$$\dot{\mathbf{q}}^+ = - [\mathbf{M}^{-1} \mathbf{W}_n - \mu \mathbf{M}^{-1} \mathbf{W}_t \mathbf{Z}_t^-] [\mathbf{W}_n^T \mathbf{M}^{-1} \mathbf{W}_n - \mu \mathbf{W}_n^T \mathbf{M}^{-1} \mathbf{W}_t \mathbf{Z}_t^-]^{-1} \mathbf{W}_n^T \dot{\mathbf{q}}^- + \dot{\mathbf{q}}^-. \quad (\text{A.44})$$

Note that when there is a transition from stick to slip, i.e., there is no impact, the post-event velocity is $\dot{\mathbf{q}}^+ = \dot{\mathbf{q}}^-$.

Stick post-impact mode $\dot{\mathbf{q}}^+ = \mathbf{g}_{\rightarrow \text{st}}(\dot{\mathbf{q}}^-)$

The discrete dynamics of a transition with a stick post-impact mode are given by

$$\mathbf{M}[\dot{\mathbf{q}}^+ - \dot{\mathbf{q}}^-] = \mathbf{W}_n \Lambda_n + \mathbf{W}_t \Lambda_t, \quad (\text{A.45})$$

$$\mathbf{W}_n^T \dot{\mathbf{q}}^+ = 0, \quad (\text{A.46})$$

$$\mathbf{W}_t^T \dot{\mathbf{q}}^+ = 0. \quad (\text{A.47})$$

After rewriting (A.45) into

$$\dot{\mathbf{q}}^+ = \mathbf{M}^{-1} \mathbf{W}_n \Lambda_n + \mathbf{M}^{-1} \mathbf{W}_t \Lambda_t + \dot{\mathbf{q}}^-, \quad (\text{A.48})$$

substituting this into (A.46) and (A.47) results in

$$\mathbf{W}_n^T \mathbf{M}^{-1} \mathbf{W}_n \Lambda_n + \mathbf{W}_n^T \mathbf{M}^{-1} \mathbf{W}_t \Lambda_t + \mathbf{W}_n^T \dot{\mathbf{q}}^- = 0 \quad (\text{A.49})$$

$$\mathbf{W}_t^T \mathbf{M}^{-1} \mathbf{W}_n \Lambda_n + \mathbf{W}_t^T \mathbf{M}^{-1} \mathbf{W}_t \Lambda_t + \mathbf{W}_t^T \dot{\mathbf{q}}^- = 0. \quad (\text{A.50})$$

This can be rewritten into a definition of Λ_n and Λ_t , given by

$$\begin{bmatrix} \Lambda_n \\ \Lambda_t \end{bmatrix} = -\mathbf{D}^{-1} \begin{bmatrix} \mathbf{W}_n^T \dot{\mathbf{q}}^- \\ \mathbf{W}_t^T \dot{\mathbf{q}}^- \end{bmatrix}, \quad \text{with } \mathbf{D} = \begin{bmatrix} \mathbf{W}_n^T \mathbf{M}^{-1} \mathbf{W}_n & \mathbf{W}_n^T \mathbf{M}^{-1} \mathbf{W}_t \\ \mathbf{W}_t^T \mathbf{M}^{-1} \mathbf{W}_n & \mathbf{W}_t^T \mathbf{M}^{-1} \mathbf{W}_t \end{bmatrix}. \quad (\text{A.51})$$

Substituting Λ_n and Λ_t into (A.48) results in the jump map $\dot{\mathbf{q}}^+ = \mathbf{g}_{\rightarrow \text{st}}(\dot{\mathbf{q}}^-)$,

$$\dot{\mathbf{q}}^+ = \mathbf{M}^{-1} \mathbf{W}_n \Lambda_n + \mathbf{M}^{-1} \mathbf{W}_t \Lambda_t + \dot{\mathbf{q}}^-, \quad (\text{A.52})$$

Similarly to the stick to slip case, note that when there is a transition from slip to stick the post-event velocity is $\dot{\mathbf{q}}^+ = \dot{\mathbf{q}}^-$.

Open-contact post-impact mode $\dot{\mathbf{q}}^+ = \mathbf{g}_{\rightarrow \text{op}}(\dot{\mathbf{q}}^-)$

The discrete dynamics of a transition with a slip post-impact mode are given by

$$\mathbf{M}(\dot{\mathbf{q}}^+ - \dot{\mathbf{q}}^-) = 0. \quad (\text{A.53})$$

In this case there are no impulsive reaction forces, and it is trivial to see that the jump map $\dot{\mathbf{q}}^+ = \mathbf{g}_{\rightarrow \text{op}}(\dot{\mathbf{q}}^-)$ is given by

$$\dot{\mathbf{q}}^+ = \dot{\mathbf{q}}^-. \quad (\text{A.54})$$

A.2 Proximal Point Formulation

The contact law and friction law defined in the complementarity condition formulation can be redefined to a proximal point formulation. This makes the system compatible with simulation methods as timestepping [64, Chapter 10]. More information on the definition of the proximal point formulation of contact laws and friction laws can be found in [22, Section 5.3].

A.2.1 Signorini's contact law and Poisson's impact law

In Figure A.2 a convex set C is illustrated. The normal cone $N_C(\mathbf{x})$ of a point \mathbf{x} is $N_C(\mathbf{x}) = 0$ if $\mathbf{x} \in \text{int}(C)$, where $\text{int}(\cdot)$ is the interior of a set. An example of this is point \mathbf{x}_3 in Figure A.2. Defining $\text{bd}(\cdot)$ as the boundary of the set, when $\mathbf{x} \in \text{bd}(C)$ there are two options. When \mathbf{x} is on a smooth part of $\text{bd}(C)$, then $N_C(\mathbf{x})$ is a ray normal to $\text{bd}(C)$ at point \mathbf{x} as depicted in at point \mathbf{x}_1 . When \mathbf{x} is on a nonsmooth part of $\text{bd}(C)$, then $N_C(\mathbf{x})$ is a cone starting on the point \mathbf{x} whose sides are normal to the left and right approximation of the point \mathbf{x} on $\text{bd}(C)$. This is illustrated at point \mathbf{x}_2 . The proximal point $\text{prox}_C(\mathbf{z})$ of a point \mathbf{z} , is the point in C closest to the point \mathbf{z} . The point \mathbf{x} is the proximal point to all points $\mathbf{z} \in N_C(\mathbf{x})$. For a point $\mathbf{z} \in C$, $\text{prox}_C(\mathbf{z}) = \mathbf{z}$ i.e. \mathbf{x}_3 in Figure A.2.

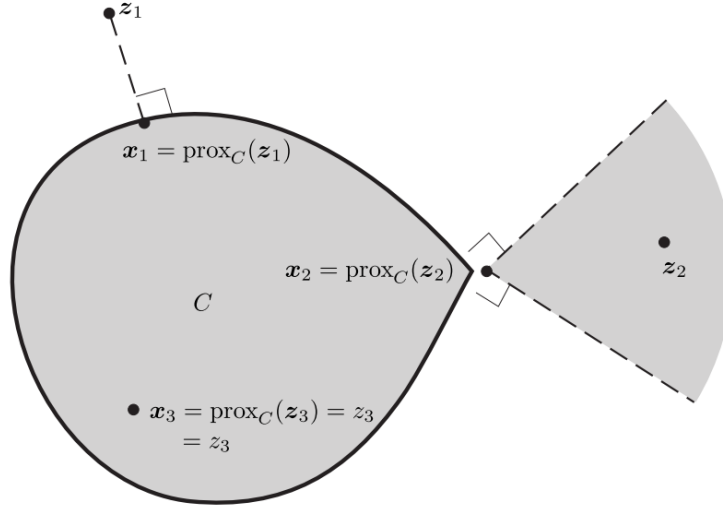


Figure A.2

This formulation can be used to define Signorini's contact law, which is defined as (2.19). The normal cone formulation, as illustrated in Figure A.2, of the contact is given by

$$-h_{n,i} \in N_{C_{n,i}}(\lambda_{n,i}), \quad \text{with } C_{n,i} = (\mathbb{R}^n)^+. \quad (\text{A.55})$$

The set $C_{n,i}$ is the set of admissible normal forces according to Signorini's law. See Figure 2.2a for an illustration of the set $C_{n,i}$ with $\lambda_{n,i} \in C_{n,i}$ and $h_{n,i} \in N_{C_{n,i}}(\lambda_{n,i})$. Now using the fact that

$$\mathbf{x} = \text{prox}_C(\mathbf{x} - r\mathbf{y}), r > 0 \iff -\mathbf{y} \in N_C(\mathbf{x}), \quad (\text{A.56})$$

rewriting (A.55) to a proximal point formulation gives

$$\lambda_{n,i} = \text{prox}_{C_{n,i}}(\lambda_{n,i} - rh_{n,i}), \quad \text{with } C_{n,i} = (\mathbb{R}^n)^+ \text{ and } r > 0. \quad (\text{A.57})$$

Similarly for the Poisson's impact law illustrated in Figure ??, we find the proximal point formulation

$$\Lambda_{n,i} = \text{prox}_{C_{n,i}}(\Lambda_{n,i} - r\zeta_{n,i}^+), \quad \text{with } C_{n,i} = (\mathbb{R}^n)^+ \text{ and } r > 0. \quad (\text{A.58})$$

A.2.2 Coulomb's friction law

Now we define the normal cone formulation of Coulomb's friction law

$$-\zeta_{t,i} \in N_{C_{t,i}}(\lambda_{t,i}) \quad \forall i \in \mathcal{I}_a, \quad \text{with } C_{t,i}(\lambda_{n,i}) = \{\lambda_{t,i} \mid \|\lambda_{t,i}\| \leq \mu\lambda_{n,i}\}, \quad (\text{A.59})$$

which is illustrated in Figure A.3.

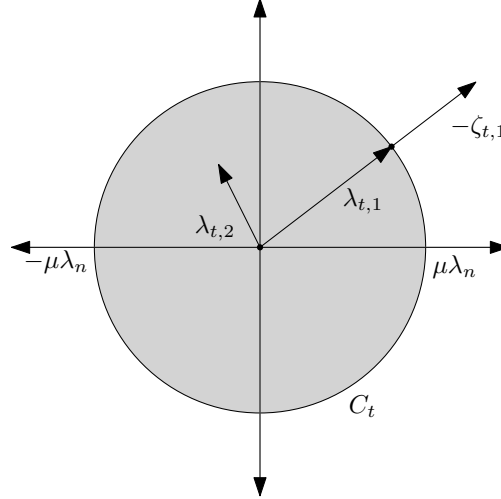


Figure A.3: The friction disk with two separate friction forces $\lambda_{t,1}$ and $\lambda_{t,2}$. $\lambda_{t,1} = \mu\lambda_{n,1}$, resulting in a tangential velocity $\zeta_{t,i} > 0$. $\lambda_{t,2} < \mu\lambda_{n,2}$, leading to a tangential velocity $\zeta_{t,i} = 0$.

C_t is the set of all admitted friction forces. The tangential velocity $\zeta_{t,i}$ is directed opposite to the friction force $\lambda_{t,i}$ for isotropic friction.

Now using the fact that

$$\mathbf{x} = \text{prox}_C(\mathbf{x} - r\mathbf{y}), r > 0 \iff -\mathbf{y} \in N_C(\mathbf{x}), \quad (\text{A.60})$$

we can rewrite the normal cone to a proximal point formulation

$$\lambda_{t,i} = \text{prox}_{C_{t,i}}(\lambda_{t,i} - r\zeta_{t,i}) \quad \text{with } C_{t,i}(\lambda_{n,i}) = \{\lambda_{t,i} \mid \|\lambda_{t,i}\| \leq \mu\lambda_{n,i}\} \text{ and } r > 0. \quad (\text{A.61})$$

Similarly, for the impact dynamics we can formulate

$$\Lambda_{t,i} = \text{prox}_{C_{t,i}}(\Lambda_{t,i} - r\zeta_{t,i}^+) \quad \text{with } C_{t,i}(\lambda_{n,i}) = \{\Lambda_{t,i} \mid \|\Lambda_{t,i}\| \leq \mu\Lambda_{n,i}\} \text{ and } r > 0. \quad (\text{A.62})$$

A.2.3 System dynamics with contact law and friction law

The flow dynamics is then described by

$$M(q)\dot{\xi} + H(q, \xi) = S(q)u + \sum_{i \in \mathcal{I}_c} (w_{n,i}(q)\lambda_{n,i} + W_{t,i}(q)\lambda_{t,i}), \quad (\text{A.63})$$

$$\lambda_{n,i} = \text{prox}_{C_{n,i}}(\lambda_{n,i} - rh_{n,i}), \quad (\text{A.64})$$

$$\lambda_{t,i} = \text{prox}_{C_{t,i}}(\lambda_{t,i} - r\zeta_{t,i}), \quad (\text{A.65})$$

with

$$C_{n,i} = (\mathbb{R}^n)^+ \text{ and } r > 0, \quad (\text{A.66})$$

$$C_{t,i}(\lambda_{n,i}) = \{\lambda_{t,i} \mid \|\lambda_{t,i}\| \leq \mu\lambda_{n,i}\} \text{ and } r > 0. \quad (\text{A.67})$$

The impulsive dynamics that take place when a contact point opens or closes contact is described by

$$\mathbf{M}(\mathbf{q})(\boldsymbol{\xi}^+ - \boldsymbol{\xi}^-) = \sum_{i \in \mathcal{I}_c} (\mathbf{w}_{n,i}(\mathbf{q})\boldsymbol{\Lambda}_{n,i} + \mathbf{W}_{t,i}(\mathbf{q})\boldsymbol{\Lambda}_{t,i}), \quad (\text{A.68})$$

$$\boldsymbol{\Lambda}_{n,i} = \text{prox}_{C_{n,i}}(\boldsymbol{\Lambda}_{n,i} - r\boldsymbol{\zeta}_{n,i}^+), \quad (\text{A.69})$$

$$\boldsymbol{\Lambda}_{t,i} = \text{prox}_{C_{t,i}}(\boldsymbol{\Lambda}_{t,i} - r\boldsymbol{\zeta}_{t,i}^+) \quad (\text{A.70})$$

with

$$C_{n,i} = (\mathbb{R}^n)^+ \text{ and } r > 0, \quad (\text{A.71})$$

$$C_{t,i}(\lambda_{n,i}) = \{\boldsymbol{\Lambda}_{t,i} \mid \|\boldsymbol{\Lambda}_{t,i}\| \leq \mu\boldsymbol{\Lambda}_{n,i}\} \text{ and } r > 0. \quad (\text{A.72})$$

Appendix B

Spatial Friction in Mechanical Systems with Unilateral Constraints

B.1 Reference trajectories with impact away from slip-stick border

Now we look at the case where a contact point goes from open to closed, away from $\Gamma = 0$. This is illustrated in Figure B.1. The goal is to prove that for an event away from Γ , a sufficiently small perturbation cannot cause the trajectory to hit $\gamma = 0$ at a perturbed ante-impact state $\mathbf{x}_\epsilon^-(t_\epsilon)$ where Γ changes sign in comparison with the unperturbed ante-impact state $\boldsymbol{\alpha}^-(\tau)$. From [59, p. 6] we know that based on the continuity property of γ and \mathbf{f} , the perturbed impact state can be written as

$$\mathbf{x}_\epsilon(t_\epsilon) = \boldsymbol{\alpha}(\tau) + \epsilon \dot{\boldsymbol{\alpha}}(\tau) \frac{\partial t_\epsilon}{\partial \epsilon} + \epsilon \mathbf{z}(\tau) + o(\epsilon), \quad (\text{B.1})$$

for sufficiently small ϵ . The shortest distance between $\Gamma = \Gamma(\boldsymbol{\alpha}(\tau))$ and $\Gamma = 0$ on the plane where $\gamma = 0$ is defined as the constant δ_Γ , which is also illustrated in Figure B.1.

Let's define a point in the state $\mathbf{x}_{\gamma=0, \Gamma=0}$ where $\gamma(\mathbf{x}_{\gamma=0, \Gamma=0}) = 0$ and $\Gamma(\mathbf{x}_{\gamma=0, \Gamma=0}) = 0$. We are evaluating nominal trajectories which impact away from $\Gamma = 0$, i.e. $\Gamma(\boldsymbol{\alpha}(\tau)) \neq \Gamma(\mathbf{x}_{\gamma=0, \Gamma=0})$. From Section ?? we know that Γ is continuously differentiable, which implies that it is Lipschitz-continuous and therefore satisfies the Lipschitz-continuity condition

$$\|\mathbf{f}(\mathbf{x}) - \mathbf{f}(\mathbf{y})\| \leq \kappa \|\mathbf{x} - \mathbf{y}\|, \quad \forall \mathbf{x}, \mathbf{y} \in \mathbb{R}^n, \quad (\text{B.2})$$

where $\kappa > 0$ [22]. By applying (B.2) to the function value of Γ at impact for the nominal trajectory and the perturbed trajectory, we find

$$\|\Gamma(\boldsymbol{\alpha}(\tau)) - \Gamma(\mathbf{x}_{\gamma=0, \Gamma=0})\| \leq \kappa \|\boldsymbol{\alpha}(\tau) - \mathbf{x}_{\gamma=0, \Gamma=0}\|. \quad (\text{B.3})$$

Now, since $\Gamma(\boldsymbol{\alpha}(\tau)) \neq \Gamma(\mathbf{x}_{\gamma=0, \Gamma=0})$, we know that $\|\Gamma(\boldsymbol{\alpha}(\tau)) - \Gamma(\mathbf{x}_{\gamma=0, \Gamma=0})\| > 0$ and therefore from (B.3) that $\|\boldsymbol{\alpha}(\tau) - \mathbf{x}_{\gamma=0, \Gamma=0}\| > 0$, i.e. $\delta_\Gamma > 0$. Finally, from (B.1), we find

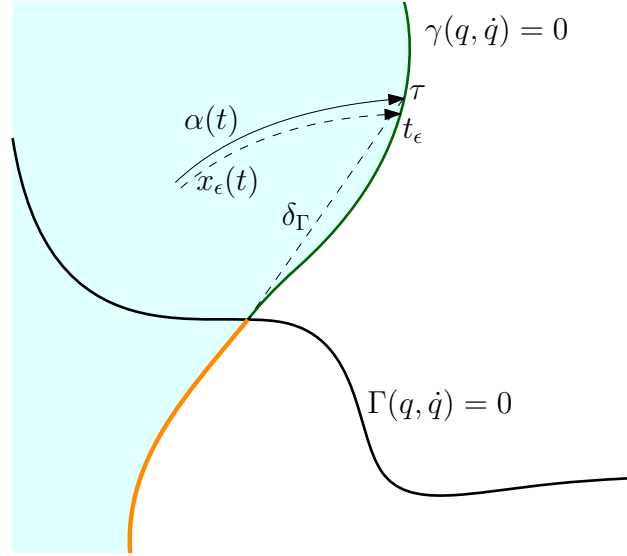


Figure B.1: The guard functions γ and Γ in the state space of \mathbf{q} . A transition from open to closed is made away from Γ . $\alpha(t)$ is the nominal trajectory and $\mathbf{x}_\epsilon(t)$ a perturbed trajectory of the contact point up to the transition.

$$\|\mathbf{x}_\epsilon(t_\epsilon) - \alpha(\tau)\| = \|\epsilon \dot{\alpha}(\tau) \frac{\partial t_\epsilon}{\partial \epsilon} + \epsilon \mathbf{z}(\tau) + o(\epsilon)\|. \quad (\text{B.4})$$

Since $\delta_\Gamma > 0$ and $\lim_{\epsilon \rightarrow 0} \|\mathbf{x}_\epsilon(t_\epsilon) - \alpha(\tau)\| = 0$, there always exists an ϵ such that $\|\mathbf{x}_\epsilon(t_\epsilon) - \alpha(\tau)\| < \delta_\Gamma$. In other words, this proves that if \mathbf{f} , γ and Γ are continuous and the nominal trajectory makes impact away from the slip-stick post-impact mode border $\Gamma = 0$, then there always exists a range of ϵ such that the perturbed state will have the same post-impact mode as the nominal trajectory.

B.2 Reference trajectories with impact at the slip-stick border

- Consider as simultaneous trigger of open-closed guard and slip-stick guard. However, it is not entirely the same, as the slip-stick guard cannot be triggered before the open-closed guard.
- The trigger should be transversal, in both closed-open guard and slip-stick guard.
- If we can show continuity of post-impact state, then we can define a jump gain like H , which uses one jump map for the open to stick domain and another jump map for the open to slip domain.

B.3 Post-impact accelerations in open-to-stick transitions

The mode transition from stick to slip happens when a guard is triggered at acceleration level,

$$\text{slip} \leftarrow \text{stick} \gamma = \mu^2 \lambda_{n,i}^2 - \lambda_{t,i} \lambda_{t,i}^T, \quad (\text{B.5})$$

and the post-impact mode is determined by the guard function defined at velocity level

$$\Gamma = \mu^2 \Lambda_{n,i}^2(\mathbf{q}, \dot{\mathbf{q}}^-) - \Lambda_{t,i}(\mathbf{q}, \dot{\mathbf{q}}^-) \Lambda_{t,i}^T(\mathbf{q}, \dot{\mathbf{q}}^-). \quad (\text{B.6})$$

Since the jump map from open to stick is

$$\mathbf{M}(\mathbf{q})(\dot{\mathbf{q}}^+ - \dot{\mathbf{q}}^-) = \mathbf{w}_{n,i}(\mathbf{q})\Lambda_{n,i} + \mathbf{W}_{t,i}(\mathbf{q})\Lambda_{t,i}, \quad (\text{B.7})$$

$$\zeta_{n,i}^+ = 0, \quad (\text{B.8})$$

$$\zeta_{t,i}^+ = 0, \quad (\text{B.9})$$

which is on velocity level, the post-impact reaction forces of the open-to-stick event can be in the stick-to-slip jump set, causing an immediate transition to slip. This is demonstrated using the flow dynamics of the stick mode at the time-instant of the transition,

$$\mathbf{M}(\mathbf{q}^+)\ddot{\mathbf{q}}^+ + \mathbf{H}(\mathbf{q}^+, \dot{\mathbf{q}}^+) = \mathbf{S}(\mathbf{q}^+)\mathbf{u}^+ + \sum_{i \in \mathcal{I}_c} \left(\mathbf{w}_{n,i}(\mathbf{q}^+)\lambda_{n,i}^+ + \mathbf{W}_{t,i}(\mathbf{q}^+)\lambda_{t,i}^+ \right), \quad (\text{B.10})$$

$$\mathbf{w}_{n,i}^T(\mathbf{q}^+)\ddot{\mathbf{q}}^+ + \dot{\mathbf{w}}_{n,i}^T(\mathbf{q}^+)\dot{\mathbf{q}}^+ = 0, \quad (\text{B.11})$$

$$\mathbf{W}_{t,i}^T(\mathbf{q}^+)\ddot{\mathbf{q}}^+ + \dot{\mathbf{W}}_{t,i}^T(\mathbf{q}^+)\dot{\mathbf{q}}^+ = 0. \quad (\text{B.12})$$

We can deduce from (B.8)-(B.9) and (B.11)-(B.12) that the normal acceleration of the transition contact point $\mathbf{w}_{n,i}^T(\mathbf{q}^+)\ddot{\mathbf{q}}^+$ and the tangential acceleration of the transitioning contact point $\mathbf{W}_{t,i}^T(\mathbf{q}^+)\ddot{\mathbf{q}}^+$ are both equal to zero. From (B.10) we then notice that $\lambda_{n,i}^+$ and $\lambda_{t,i}^+$ depend continuously on \mathbf{u}^+ and can therefore instantly lead to $\mu^2\lambda_{n,i}^2 - \lambda_{t,i}^+(\lambda_{t,i}^+)^T > 0$ for certain \mathbf{u}^+ . For these inputs the contact point will immediately start slipping after the open-to-stick transition. These areas are illustrated in Figure B.2

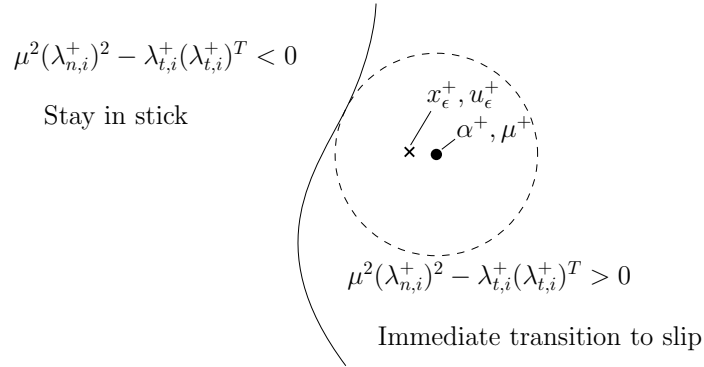


Figure B.2: The border between an open-to-stick event that stays in stick and an open-to-stick event that immediately starts slipping is illustrated in this figure. The post event state and input indicated in the figure is in the $\mu^2(\lambda_{n,i}^+)^2 - \lambda_{t,i}^+(\lambda_{t,i}^+)^T > 0$ area, causing the contact point to immediately start slipping.

Using the continuity of the system's flow dynamics and the function $\mu^2(\lambda_{n,i}^+)^2 - \lambda_{t,i}^+(\lambda_{t,i}^+)^T$, we can show that if we choose μ^+ such that α^+, μ^+ is not on $\mu^2(\lambda_{n,i}^+)^2 - \lambda_{t,i}^+(\lambda_{t,i}^+)^T = 0$ then there always exists a range of perturbations ϵ such that the perturbed post-impact is on the same side of $\mu^2(\lambda_{n,i}^+)^2 - \lambda_{t,i}^+(\lambda_{t,i}^+)^T = 0$ as the unperturbed trajectory similarly to Section B.1.

B.4 Slip-stick transition in closed-contact

Appendix C

Sensitivity Analysis for Input-Dependent Guards

C.1 Linearization for single jumps

The perturbed state is defined as

$$\mathbf{x}(t, \epsilon) = \mathbf{x}(t_0, \epsilon) + \int_{t_0}^t \mathbf{f}(\mathbf{x}(s, \epsilon), \mathbf{u}(s, \epsilon), s) ds. \quad (\text{C.1})$$

Then

$$\frac{\partial \mathbf{x}(t, \epsilon)}{\partial \epsilon} = \frac{\partial \mathbf{x}_0}{\partial \epsilon} + \int_{t_0}^t \left(\frac{\partial \mathbf{f}}{\partial \mathbf{x}} \frac{\partial \mathbf{x}}{\partial \epsilon} + \frac{\partial \mathbf{f}}{\partial \mathbf{u}} \frac{\partial \mathbf{u}}{\partial \epsilon} \right) ds, \quad (\text{C.2})$$

$$\frac{\partial^2 \mathbf{x}}{\partial t \partial \epsilon} = \frac{\partial \mathbf{f}}{\partial \mathbf{x}} \frac{\partial \mathbf{x}}{\partial \epsilon} + \frac{\partial \mathbf{f}}{\partial \mathbf{u}} \frac{\partial \mathbf{u}}{\partial \epsilon}, \quad (\text{C.3})$$

which we can write as

$$\frac{\partial^2 \mathbf{x}}{\partial t \partial \epsilon} = D_1 \mathbf{f}(\mathbf{x}(t, \epsilon), \mathbf{u}(t, \epsilon), t) \cdot \frac{\partial \mathbf{x}}{\partial \epsilon} + D_2 \mathbf{f}(\mathbf{x}(t, \epsilon), \mathbf{u}(t, \epsilon), t) \cdot \frac{\partial \mathbf{u}}{\partial \epsilon}, \quad (\text{C.4})$$

with $D_i \mathbf{f}$ the derivative of \mathbf{f} wrt the i th term of \mathbf{f} . Evaluating (C.4) at $\epsilon = 0$ results in the flow dynamics of the positive homogenization

$$\dot{\mathbf{z}} = D_1 \mathbf{f}(\boldsymbol{\alpha}(t), \boldsymbol{\mu}(t), t) \cdot \mathbf{z}(t) + D_2 \mathbf{f}(\boldsymbol{\alpha}(t), \boldsymbol{\mu}(t), t) \cdot \mathbf{v}(t), \quad (\text{C.5})$$

where

$$\mathbf{z}(t) = \left. \frac{\partial \mathbf{x}(t, \epsilon)}{\partial \epsilon} \right|_{\epsilon=0}, \text{ and } \mathbf{v}(t) = \left. \frac{\partial \mathbf{u}(t, \epsilon)}{\partial \epsilon} \right|_{\epsilon=0}. \quad (\text{C.6})$$

When we consider a single jump

$$\mathbf{x}_\epsilon^+(t_\epsilon, \epsilon) = \mathbf{g}(\mathbf{x}_\epsilon^-(t_\epsilon, \epsilon), t_\epsilon), \quad (\text{C.7})$$

using a Taylor approximation on the left-hand side of (C.7) with respect to ϵ and around $\epsilon = 0$, we can write

$$\mathbf{x}_\epsilon^+(t_\epsilon, \epsilon) = \boldsymbol{\alpha}^+(t_\epsilon) + \epsilon \mathbf{z}^+(t_\epsilon) + o(\epsilon), \quad (\text{C.8})$$

$$\mathbf{u}_\epsilon^+(t_\epsilon, \epsilon) = \boldsymbol{\mu}^+(t_\epsilon) + \epsilon \mathbf{v}^+(t_\epsilon) + o(\epsilon), \quad (\text{C.9})$$

where $\alpha(t)$ is a nominal reference trajectory that satisfies the dynamics of the system and $\mu(t)$ an input that achieves this reference trajectory. Now we expand this in terms of ϵ , so with

$$\Delta = \left. \frac{\partial t_\epsilon}{\partial \epsilon} \right|_{\epsilon=0}, \quad (\text{C.10})$$

we get

$$\alpha^+(t_\epsilon) = \alpha^+(\tau) + \epsilon \dot{\alpha}^+(\tau) \Delta + o(\epsilon), \quad (\text{C.11})$$

$$\mu^+(t_\epsilon) = \mu^+(\tau) + \epsilon \dot{\mu}^+(\tau) \Delta + o(\epsilon), \quad (\text{C.12})$$

$$z^+(t_\epsilon) = z^+(\tau) + \epsilon \dot{z}^+(\tau) \Delta + o(\epsilon), \quad (\text{C.13})$$

$$v^+(t_\epsilon) = v^+(\tau) + \epsilon \dot{v}^+(\tau) \Delta + o(\epsilon), \quad (\text{C.14})$$

which when substituted into (C.8) and (C.9) gives,

$$x_\epsilon^+(t_\epsilon, \epsilon) = \alpha^+(\tau) + \epsilon \dot{\alpha}^+(\tau) \Delta + \epsilon z^+(\tau) + o(\epsilon). \quad (\text{C.15})$$

$$u_\epsilon^+(t_\epsilon, \epsilon) = \mu^+(\tau) + \epsilon \dot{\mu}^+(\tau) \Delta + \epsilon v^+(\tau) + o(\epsilon). \quad (\text{C.16})$$

To find Δ , we evaluate the ante impact guard function

$$\gamma^-(x_\epsilon^-(t_\epsilon), u_\epsilon^-(t_\epsilon), t_\epsilon) = 0. \quad (\text{C.17})$$

In previous work, the guard function γ was not dependent on $u_\epsilon(t_\epsilon)$ because friction and release was not considered. We now expand $\gamma(x_\epsilon(t_\epsilon), u_\epsilon(t_\epsilon), t_\epsilon)$ wrt ϵ , giving

$$\gamma(x_\epsilon(t_\epsilon), u_\epsilon(t_\epsilon), t_\epsilon) = \gamma(\alpha(\tau), \mu(\tau), \tau) + \epsilon \left[\frac{\partial \gamma}{\partial \epsilon}(\alpha(\tau), \mu(\tau), \tau) \right]_{\epsilon=0} + o(\epsilon), \quad (\text{C.18})$$

$$= \gamma(\alpha(\tau), \mu(\tau), \tau) + \epsilon \left[\frac{\partial \gamma}{\partial \mathbf{x}} \left(\frac{\partial \mathbf{x}}{\partial \epsilon} + \frac{\partial \mathbf{x}}{\partial t_\epsilon} \frac{dt_\epsilon}{d\epsilon} \right) + \frac{\partial \gamma}{\partial \mathbf{u}} \left(\frac{\partial \mathbf{u}}{\partial \epsilon} + \frac{\partial \mathbf{u}}{\partial t_\epsilon} \frac{dt_\epsilon}{d\epsilon} \right) + \frac{\partial \gamma}{\partial t_\epsilon} \frac{dt_\epsilon}{d\epsilon} \right]_{\epsilon=0} + o(\epsilon). \quad (\text{C.19})$$

By definition $\gamma(\tau) = 0$, so we can rewrite (C.19) to

$$\gamma(x_\epsilon(t_\epsilon), u_\epsilon(t_\epsilon), t_\epsilon) = \epsilon [D_1 \gamma \cdot (\bar{z}(\tau) + \dot{\alpha}(\tau) \Delta) + D_2 \gamma \cdot (\bar{v}(\tau) + \dot{\mu}(\tau) \Delta) + D_3 \cdot \gamma \Delta] \quad (\text{C.20})$$

Now we can evaluate (C.19) using (C.20), which gives

$$\epsilon [D_1 \gamma^- \cdot (z^-(\tau) + \dot{\alpha}^-(\tau) \Delta) + D_2 \gamma^- \cdot (v^-(\tau) + \dot{\mu}^-(\tau) \Delta) + D_3 \gamma^- \cdot \Delta] = 0. \quad (\text{C.21})$$

From (C.21) we can determine the expression for Δ ,

$$\Delta = - \frac{D_1 \gamma^- \cdot z^-(\tau) + D_2 \gamma^- \cdot v^-(\tau)}{\dot{\gamma}^-}, \quad (\text{C.22})$$

with

$$\gamma^- = \gamma^-(\alpha^-(\tau), \mu^-(\tau), \tau), \quad (\text{C.23})$$

$$\dot{\gamma}^- = D_1 \gamma^- \cdot \dot{\alpha}^- + D_2 \gamma^- \cdot \dot{\mu}^- + D_3 \gamma^-. \quad (\text{C.24})$$

To find the expression for the right hand side of (C.7), we now expand $g(x_\epsilon^-(t_\epsilon, \epsilon), u_\epsilon^-(t_\epsilon, \epsilon), t_\epsilon)$ with respect to ϵ as

$$\mathbf{g}(\mathbf{x}_\epsilon^-, \mathbf{u}_\epsilon^-, t_\epsilon) = \mathbf{g}(\boldsymbol{\alpha}^-(\tau), \tau) + \epsilon \left[\frac{\partial \mathbf{g}}{\partial \epsilon} \right] + o(\epsilon), \quad (\text{C.25})$$

$$= \boldsymbol{\alpha}^+(\tau) + \epsilon \left[\frac{\partial \mathbf{g}}{\partial \mathbf{x}} \left(\frac{\partial \mathbf{x}}{\partial \epsilon} + \frac{\partial \mathbf{x}}{\partial t_\epsilon} \frac{dt_\epsilon}{d\epsilon} \right) + \frac{\partial \mathbf{g}}{\partial \mathbf{u}} \left(\frac{\partial \mathbf{u}}{\partial \epsilon} + \frac{\partial \mathbf{u}}{\partial t_\epsilon} \frac{dt_\epsilon}{d\epsilon} \right) + \frac{\partial \mathbf{g}}{\partial t_\epsilon} \frac{dt_\epsilon}{d\epsilon} \right]_{\epsilon=0} + o(\epsilon), \quad (\text{C.26})$$

$$= \boldsymbol{\alpha}^+(\tau) + \epsilon [D_1 \mathbf{g} \cdot (\mathbf{z}^- + \dot{\boldsymbol{\alpha}}^- \Delta) + D_2 \mathbf{g} \cdot (\mathbf{v}^- + \dot{\boldsymbol{\mu}}(\tau) \Delta) + D_3 \mathbf{g} \cdot \Delta] + o(\epsilon). \quad (\text{C.27})$$

Jump maps are impulsive by definition, and since impulsive inputs do not exist it is impossible for the jump map to be dependent on \mathbf{u} . For small ϵ , we can rewrite (C.7), (C.22) and (C.27) to a general jump map with counter k as

$$\mathbf{x}_\epsilon^k(t_\epsilon, \epsilon) = \mathbf{g}^k(\mathbf{x}_\epsilon^{k-1}, \mathbf{u}_\epsilon^{k-1}, t_\epsilon), \quad (\text{C.28})$$

$$\Delta^k = - \frac{D_1 \gamma^k \cdot {}^{s^{k-1}}\mathbf{z}(\tau) + D_2 \gamma^k \cdot {}^{s^{k-1}}\mathbf{v}(\tau)}{\dot{\gamma}^k}, \quad (\text{C.29})$$

$$\mathbf{g}^k(\mathbf{x}_\epsilon^{k-1}, \mathbf{u}_\epsilon^{k-1}, t_\epsilon) = \boldsymbol{\alpha}^k(\tau) + \epsilon [D_1 \mathbf{g}^k \cdot ({}^{s^{k-1}}\mathbf{z}(\tau) + \dot{\boldsymbol{\alpha}}^{k-1} \Delta^k) + D_2 \mathbf{g}^k \cdot ({}^{s^{k-1}}\mathbf{v}(\tau) + {}^{s^{k-1}}\dot{\boldsymbol{\mu}} \Delta^k) + D_3 \mathbf{g}^k \cdot \Delta^k]. \quad (\text{C.30})$$

From (C.15) we get

$${}^{s^k}\mathbf{z}(\tau) = \frac{1}{\epsilon} \left(\mathbf{x}_\epsilon^k(t_\epsilon) - \boldsymbol{\alpha}^k(\tau) \right) - \dot{\boldsymbol{\alpha}}^k(\tau) \Delta^k, \quad (\text{C.31})$$

and by equating (C.28) and (C.30) we find an expression for $\bar{\mathbf{x}}_\epsilon^k(t_\epsilon, \epsilon)$ which we can substitute into (C.31) resulting in

$${}^{s^k}\mathbf{z}(\tau) = D_1 \mathbf{g}^k \cdot ({}^{s^{k-1}}\mathbf{z}(\tau) + \dot{\boldsymbol{\alpha}}^{k-1} \Delta^k) + D_2 \mathbf{g}^k \cdot ({}^{s^{k-1}}\mathbf{v}(\tau) + {}^{s^{k-1}}\dot{\boldsymbol{\mu}} \Delta^k) + D_3 \mathbf{g}^k \cdot \Delta^k - \dot{\boldsymbol{\alpha}}^k(\tau) \Delta^k. \quad (\text{C.32})$$

Now, by substituting (C.29) into (C.32), we get

$$\begin{aligned} {}^{s^k}\mathbf{z}(\tau) &= D_1 \mathbf{g}^k \cdot {}^{s^{k-1}}\mathbf{z} + D_2 \mathbf{g}^k \cdot {}^{s^{k-1}}\mathbf{v} \\ &\quad - \left(D_1 \mathbf{g}^k \cdot \mathbf{f}^{k-1} + D_2 \mathbf{g}^k \cdot {}^{s^{k-1}}\dot{\boldsymbol{\mu}} + D_3 \mathbf{g}^k \cdot 1 - \mathbf{f}^k \right) \frac{D_1 \gamma^k \cdot {}^{s^{k-1}}\mathbf{z} + D_2 \gamma^k \cdot {}^{s^{k-1}}\mathbf{v}}{\dot{\gamma}^k}, \end{aligned} \quad (\text{C.33})$$

$${}^{s^k}\mathbf{z}(\tau) = \left(\frac{\mathbf{f}^k - \dot{\mathbf{g}}^k}{\dot{\gamma}^k} D_1 \gamma^k + D_1 \mathbf{g}^k \right) \cdot {}^{s^{k-1}}\mathbf{z} + \left(\frac{\mathbf{f}^k - \dot{\mathbf{g}}^k}{\dot{\gamma}^k} D_2 \gamma^k + D_2 \mathbf{g}^k \right) \cdot {}^{s^{k-1}}\mathbf{v}, \quad (\text{C.34})$$

with

$$\dot{\mathbf{g}}^k = D_1 \mathbf{g}^k \cdot \mathbf{f}^{k-1} + D_2 \mathbf{g}^k \cdot {}^{s^{k-1}}\dot{\boldsymbol{\mu}} + D_3 \mathbf{g}^k \cdot 1, \quad (\text{C.35})$$

$$\mathbf{f}^k = {}^{s^k}\mathbf{f}(\boldsymbol{\alpha}^k(\tau), \boldsymbol{\mu}^k(\tau), \tau). \quad (\text{C.36})$$

Now, using

$$\mathbf{G}^k(\tau) = \frac{\mathbf{f}^k - \dot{\mathbf{g}}^k}{\dot{\gamma}^k} D_1 \gamma^k \cdot 1 + D_1 \mathbf{g}^k \cdot 1, \quad (\text{C.37})$$

$$\mathbf{J}^k(\tau) = \frac{\mathbf{f}^k - \dot{\mathbf{g}}^k}{\dot{\gamma}^k} D_2 \gamma^k \cdot 1 + D_2 \mathbf{g}^k \cdot 1, \quad (\text{C.38})$$

we can write

$${}^{s^k} \mathbf{z}(\tau) = \mathbf{G}^{ks^{k-1}} \mathbf{z} + \mathbf{J}^{ks^{k-1}} \mathbf{v}. \quad (\text{C.39})$$

C.2 Linearization for multiple jumps

We now assume that we find the first order approximation of the perturbed post-impact state of two simultaneous jumps, by considering these jumps after each other as

$${}^{s^{k+1}} \mathbf{z}(\tau) = \mathbf{G}^{k+1s^k} \mathbf{z} + \mathbf{J}^{k+1s^k} \mathbf{v} \quad (\text{C.40})$$

$${}^{s^{k+1}} \mathbf{z}(\tau) = \mathbf{G}^{k+1} \left(\mathbf{G}^{ks^{k-1}} \mathbf{z} + \mathbf{J}^{ks^{k-1}} \mathbf{v} \right) + \mathbf{G}^{k+1s^k} \mathbf{v}, \quad (\text{C.41})$$

$$= \mathbf{G}^{k+1} \mathbf{G}^{ks^{k-1}} \mathbf{z} + \mathbf{G}^{k+1} \mathbf{J}^{ks^{k-1}} \mathbf{v} + \mathbf{J}^{k+1s^k} \mathbf{v}. \quad (\text{C.42})$$

We prove that this is true by deriving an expression for the post-impact state of two simultaneous jumps, and comparing it with (C.42). Now we evaluate the jump map of two jumps at the same time instant τ ,

$${}^{s^{k+1}} \mathbf{x}^\epsilon(t^{k+1}) = {}^{s^{k+1} \leftarrow s^k} \mathbf{g}({}^{s^k} \mathbf{x}^\epsilon(t^{k+1}), {}^{s^k} \mathbf{u}^\epsilon(t_\epsilon^{k+1}), t_\epsilon^{k+1}), \quad (\text{C.43})$$

with

$${}^{s^k} \mathbf{x}^\epsilon(t^{k+1}) = \int_{t^k}^{t^{k+1}} \left[{}^{s^k} \mathbf{f} \left({}^{s^k} \mathbf{x}^\epsilon(t), {}^{s^k} \mathbf{u}^\epsilon(t) \right) \right] dt + {}^{s^k} \mathbf{g}({}^{s^{k-1}} \mathbf{x}^\epsilon(t^k), {}^{s^{k-1}} \mathbf{u}^\epsilon(t^k), t^k). \quad (\text{C.44})$$

We rewrite the integral in (C.44) to

$$\int_{t^k}^{t^{k+1}} {}^{s^k} \mathbf{f}(t, \epsilon) dt = \mathbf{F}(t^{k+1}, \epsilon) - \mathbf{F}(t^k, \epsilon) = \Phi(t^k, t^{k+1}, \epsilon), \quad (\text{C.45})$$

where ${}^{s^k} \mathbf{f} \left({}^{s^k} \mathbf{x}^\epsilon(t), {}^{s^k} \mathbf{u}^\epsilon(t) \right)$ can be written as ${}^{s^k} \mathbf{f}(t, \epsilon)$, because \mathbf{x}^ϵ and \mathbf{u}^ϵ depend solely on t and ϵ . We now expand Φ with respect to ϵ , which results in

$$\Phi(t^k, t^{k+1}, \epsilon) = \Phi(t^k, t^{k+1}, 0) + \epsilon \left. \frac{\partial \Phi}{\partial \epsilon} \right|_{\epsilon=0} + o(\epsilon), \quad (\text{C.46})$$

$$= \mathbf{F}(t^k, 0) - \mathbf{F}(t^k, 0) + \left[{}^{s^k} \mathbf{f}(t^{k+1}, \epsilon) \frac{dt^{k+1}}{d\epsilon} - {}^{s^k} \mathbf{f}(t^k, \epsilon) \frac{dt^k}{d\epsilon} + \int_{t^k}^{t^{k+1}} \frac{\partial {}^{s^k} \mathbf{f}}{\partial \epsilon} dt \right]_{\epsilon=0}, \quad (\text{C.47})$$

$$= {}^{s^k} \mathbf{f}(\Delta^{k+1} - \Delta^k), \quad (\text{C.48})$$

since $\tau^k = \tau^{k+1} = \tau$, and $\int_{t^k}^{t^{k+1}} \frac{\partial s^k \mathbf{f}(t, \epsilon)}{\partial \epsilon} dt \Big|_{\epsilon=0} = 0$. Here $s^k \mathbf{f} = s^k \mathbf{f}(s^k \boldsymbol{\alpha}(\tau), s^k \boldsymbol{\mu}(\tau), \tau)$. Note that ϵ is assumed sufficiently small, such that we can write t as a function of ϵ . By expanding (C.43) with respect to ϵ , we find

$$s^{k+1} \mathbf{x}^\epsilon(t^{k+1}) = s^{k+1} \boldsymbol{\alpha}(\tau) + \epsilon \frac{\partial s^{k+1} \mathbf{g}(s^k \mathbf{x}^\epsilon(t^{k+1}), s^k \mathbf{u}^\epsilon(t^{k+1}), t^{k+1})}{\partial \epsilon} \Big|_{\epsilon=0} + o(\epsilon), \quad (\text{C.49})$$

with

$$\frac{\partial s^{k+1} \mathbf{g}}{\partial \epsilon} \Big|_{\epsilon=0} = \left[\frac{\partial s^{k+1} \mathbf{g}}{\partial \mathbf{x}} \left(\frac{\partial s^k \mathbf{x}}{\partial \epsilon} + \frac{\partial s^k \mathbf{x}}{\partial t} \frac{dt^{k+1}}{d\epsilon} \right) + \frac{\partial s^{k+1} \mathbf{g}}{\partial \mathbf{u}} \left(\frac{\partial s^k \mathbf{u}}{\partial \epsilon} + \frac{\partial s^k \mathbf{u}}{\partial t} \frac{dt^{k+1}}{d\epsilon} \right) + \frac{\partial s^{k+1} \mathbf{g}}{\partial t} \frac{dt^{k+1}}{d\epsilon} \right]_{\epsilon=0}, \quad (\text{C.50})$$

$$\begin{aligned} \frac{\partial s^{k+1} \mathbf{g}}{\partial \epsilon} \Big|_{\epsilon=0} = & \left[D_1^{s^{k+1}} \mathbf{g} \left(\frac{\partial \Phi}{\partial \epsilon} + D_1^{s^k} \mathbf{g} \left(\frac{\partial s^{k-1} \mathbf{x}}{\partial \epsilon} + \frac{\partial s^{k-1} \mathbf{x}}{\partial t} \frac{dt^k}{d\epsilon} \right) + D_2^{s^k} \mathbf{g} \left(\frac{\partial s^{k-1} \mathbf{u}}{\partial \epsilon} + \frac{\partial s^{k-1} \mathbf{u}}{\partial t} \frac{dt^k}{d\epsilon} \right) \right. \right. \\ & \left. \left. + D_3^{s^k} \mathbf{g} \frac{dt^k}{d\epsilon} \right) + D_2^{s^{k+1}} \mathbf{g} \left(\frac{\partial s^k \mathbf{u}}{\partial \epsilon} + \frac{\partial s^k \mathbf{u}}{\partial t} \frac{dt^{k+1}}{d\epsilon} \right) + D_3^{s^{k+1}} \mathbf{g} \frac{dt^{k+1}}{d\epsilon} \right]_{\epsilon=0}, \quad (\text{C.51}) \end{aligned}$$

$$\begin{aligned} \frac{\partial s^{k+1} \mathbf{g}}{\partial \epsilon} \Big|_{\epsilon=0} = & D_1^{s^{k+1}} \mathbf{g} \cdot \left(s^k \dot{\boldsymbol{\alpha}}(\Delta^{k+1} - \Delta^k) + D_1^{s^k} \mathbf{g} \cdot \left(s^{k-1} \mathbf{z} + s^{k-1} \dot{\boldsymbol{\alpha}} \Delta^k \right) + D_2^{s^k} \mathbf{g} \cdot \left(s^{k-1} \mathbf{v} + s^{k-1} \dot{\boldsymbol{\mu}} \Delta^k \right) \right. \\ & \left. + D_3^{s^k} \mathbf{g} \cdot \Delta^k \right) + D_2^{s^{k+1}} \mathbf{g} \cdot \left(s^k \mathbf{v} + s^k \dot{\boldsymbol{\mu}} \Delta^{k+1} \right) + D_3^{s^{k+1}} \mathbf{g} \cdot \Delta^{k+1}. \quad (\text{C.52}) \end{aligned}$$

We now substitute (C.52) into (C.49), which we in turn substitute into (C.31) to get

$$\begin{aligned} s^{k+1} \mathbf{z}(\tau) = & D_1^{s^{k+1}} \mathbf{g} \cdot s^k \mathbf{f} \Delta^{k+1} - D_1^{s^{k+1}} \mathbf{g} \cdot s^k \mathbf{f} \Delta^k + D_1^{s^{k+1}} \mathbf{g} \cdot \left(D_1^{s^k} \mathbf{g} \cdot \left(s^{k-1} \mathbf{z} + s^{k-1} \mathbf{f} \Delta^k \right) \right. \\ & \left. + D_2^{s^k} \mathbf{g} \cdot \left(s^{k-1} \mathbf{v} + s^{k-1} \dot{\boldsymbol{\mu}} \Delta^k \right) + D_3^{s^k} \mathbf{g} \cdot \Delta^k \right) + D_2^{s^{k+1}} \mathbf{g} \cdot \left(s^k \mathbf{v} + s^k \dot{\boldsymbol{\mu}} \Delta^{k+1} \right) + \left(D_3^{s^{k+1}} \mathbf{g} - s^{k+1} \mathbf{f} \right) \Delta^{k+1}, \quad (\text{C.53}) \end{aligned}$$

with $s^k \mathbf{f} = s^k \mathbf{f}(s^k \boldsymbol{\alpha}(\tau), s^k \boldsymbol{\mu}(\tau), \tau)$. The five terms in (C.53) can be rewritten into

$$D_1^{s^{k+1}} \mathbf{g} \cdot s^k \mathbf{f} \Delta^{k+1} = - \frac{D_1^{s^{k+1}} \mathbf{g} \cdot s^{k+1} \mathbf{f}}{\dot{\gamma}^{k+1}} \left(D_1 \gamma^{k+1} \cdot \left(\mathbf{G}^{ks^{k-1}} \mathbf{z} + \mathbf{J}^{ks^{k-1}} \mathbf{v} \right) + D_2 \gamma^{k+1} \cdot s^k \mathbf{v} \right), \quad (\text{C.54})$$

$$- D_1^{s^{k+1}} \mathbf{g} \cdot s^k \mathbf{f} \Delta^k = \frac{D_1^{s^{k+1}} \mathbf{g} \cdot s^k \mathbf{f}}{\dot{\gamma}^k} \left(D_1 \gamma^k \cdot s^{k-1} \mathbf{z} + D_2 \gamma^k \cdot s^{k-1} \mathbf{v} \right), \quad (\text{C.55})$$

$$\begin{aligned} D_1^{s^{k+1}} \mathbf{g} \cdot \left(D_1^{s^k} \mathbf{g} \cdot \left(s^{k-1} \mathbf{z} + s^{k-1} \mathbf{f} \Delta^k \right) + D_2^{s^k} \mathbf{g} \cdot \left(s^{k-1} \mathbf{v} + s^{k-1} \dot{\boldsymbol{\mu}} \Delta^k \right) + D_3^{s^k} \mathbf{g} \cdot \Delta^k \right) = \\ D_1^{s^{k+1}} \mathbf{g} \cdot \left(- \frac{D_1^{s^k} \mathbf{g} \cdot s^{k-1} \mathbf{f}}{\dot{\gamma}^k} D_1 \gamma^k - \frac{D_2^{s^k} \mathbf{g} \cdot s^{k-1} \dot{\boldsymbol{\mu}}}{\dot{\gamma}^k} D_1 \gamma^k - \frac{D_3^{s^k} \mathbf{g} \cdot 1}{\dot{\gamma}^k} D_1 \gamma^k + D_1^{s^k} \mathbf{g} \right) \cdot s^{k-1} \mathbf{z} \\ + D_1^{s^{k+1}} \mathbf{g} \cdot \left(- \frac{D_1^{s^k} \mathbf{g} \cdot s^{k-1} \mathbf{f}}{\dot{\gamma}^k} D_2 \gamma^k - \frac{D_2^{s^k} \mathbf{g} \cdot s^{k-1} \dot{\boldsymbol{\mu}}}{\dot{\gamma}^k} D_2 \gamma^k - \frac{D_3^{s^k} \mathbf{g} \cdot 1}{\dot{\gamma}^k} D_2 \gamma^k + D_2^{s^k} \mathbf{g} \right) \cdot s^{k-1} \mathbf{v}, \quad (\text{C.56}) \end{aligned}$$

$$\begin{aligned}
 D_2^{s^{k+1}} \mathbf{g} \cdot \left({}^{s^k} \mathbf{v} + {}^{s^k} \dot{\boldsymbol{\mu}} \Delta^{k+1} \right) &= -\frac{D_2^{s^{k+1}} \mathbf{g} \cdot {}^{s^k} \dot{\boldsymbol{\mu}}}{\dot{\gamma}^{k+1}} D_1 \gamma^{k+1} \cdot \mathbf{G}^{ks^{k-1}} \mathbf{z} - \frac{D_2^{s^{k+1}} \mathbf{g} \cdot {}^{s^k} \dot{\boldsymbol{\mu}}}{\dot{\gamma}^{k+1}} D_1 \gamma^{k+1} \cdot \mathbf{J}^{ks^{k-1}} \mathbf{v} \\
 &\quad + \left(D_2^{s^{k+1}} \mathbf{g} - \frac{D_2^{s^{k+1}} \mathbf{g} \cdot {}^{s^k} \dot{\boldsymbol{\mu}}}{\dot{\gamma}^{k+1}} D_2 \gamma^{k+1} \right) \cdot {}^{s^k} \mathbf{v}, \quad (\text{C.57})
 \end{aligned}$$

$$\left(D_3^{s^{k+1}} \mathbf{g} \cdot \mathbf{1} - {}^{s^{k+1}} \mathbf{f} \right) \Delta^{k+1} = -\frac{D_3^{s^{k+1}} \mathbf{g} \cdot \mathbf{1} + {}^{s^{k+1}} \mathbf{f}}{\dot{\gamma}^{k+1}} \left(D_1 \gamma^{k+1} \cdot \left(\mathbf{G}^{ks^{k-1}} \mathbf{z} + \mathbf{J}^{ks^{k-1}} \mathbf{v} \right) + D_2 \gamma^{k+1} \cdot {}^{s^k} \mathbf{v} \right). \quad (\text{C.58})$$

When we substitute the equations above into (C.53), after reordering the expression we get

$$\begin{aligned}
 {}^{s^{k+1}} \mathbf{z}(\tau) &= \left(\frac{{}^{s^{k+1}} \mathbf{f} - D_1^{s^{k+1}} \mathbf{g} \cdot {}^{s^k} \mathbf{f} - D_2^{s^{k+1}} \mathbf{g} \cdot {}^{s^k} \dot{\boldsymbol{\mu}} - D_3^{s^{k+1}} \mathbf{g} \cdot \mathbf{1}}{\dot{\gamma}^{k+1}} D_1 \gamma^{k+1} \cdot \mathbf{G}^k \right. \\
 &\quad \left. + D_1^{s^{k+1}} \mathbf{g} \cdot \frac{{}^{s^k} \mathbf{f} - D_1^{s^k} \mathbf{g} \cdot {}^{s^{k-1}} \mathbf{f} - D_2^{s^k} \mathbf{g} \cdot {}^{s^{k-1}} \dot{\boldsymbol{\mu}} - D_3^{s^k} \mathbf{g} \cdot \mathbf{1}}{\dot{\gamma}^k} D_1 \gamma^{k+1} + D_1^{s^{k+1}} \mathbf{g} D_1^{s^k} \mathbf{g} \cdot \mathbf{1} \right) {}^{s^{k-1}} \mathbf{z} \\
 &\quad + \left(\frac{{}^{s^{k+1}} \mathbf{f} - D_1^{s^{k+1}} \mathbf{g} \cdot {}^{s^k} \mathbf{f} - D_2^{s^{k+1}} \mathbf{g} \cdot {}^{s^k} \dot{\boldsymbol{\mu}} - D_3^{s^{k+1}} \mathbf{g} \cdot \mathbf{1}}{\dot{\gamma}^{k+1}} D_1 \gamma^{k+1} \cdot \mathbf{J}^k \right. \\
 &\quad \left. + D_1^{s^{k+1}} \mathbf{g} \cdot \frac{{}^{s^k} \mathbf{f} - D_1^{s^k} \mathbf{g} \cdot {}^{s^{k-1}} \mathbf{f} - D_2^{s^k} \mathbf{g} \cdot {}^{s^{k-1}} \dot{\boldsymbol{\mu}} - D_3^{s^k} \mathbf{g} \cdot \mathbf{1}}{\dot{\gamma}^k} D_2 \gamma^{k+1} + D_1^{s^{k+1}} \mathbf{g} D_2^{s^k} \mathbf{g} \cdot \mathbf{1} \right) {}^{s^{k-1}} \mathbf{v} \\
 &\quad + \left(\frac{{}^{s^{k+1}} \mathbf{f} - D_1^{s^{k+1}} \mathbf{g} \cdot {}^{s^k} \mathbf{f} - D_2^{s^{k+1}} \mathbf{g} \cdot {}^{s^k} \dot{\boldsymbol{\mu}} - D_3^{s^{k+1}} \mathbf{g} \cdot \mathbf{1}}{\dot{\gamma}^{k+1}} D_2 \gamma^{k+1} \right) {}^{s^k} \mathbf{v}, \quad (\text{C.59})
 \end{aligned}$$

from which we can isolate \mathbf{G}^k , and \mathbf{J}^k resulting in

$$\begin{aligned}
 {}^{s^{k+1}} \mathbf{z}(\tau) &= \left(\frac{{}^{s^{k+1}} \mathbf{f} - D_1^{s^{k+1}} \mathbf{g} \cdot {}^{s^k} \mathbf{f} - D_2^{s^{k+1}} \mathbf{g} \cdot {}^{s^k} \dot{\boldsymbol{\mu}} - D_3^{s^{k+1}} \mathbf{g} \cdot \mathbf{1}}{\dot{\gamma}^{k+1}} D_1 \gamma^{k+1} + D_1^{s^{k+1}} \mathbf{g} \cdot \mathbf{1} \right) \mathbf{G}^{ks^{k-1}} \mathbf{z} \\
 &\quad + \left(\frac{{}^{s^{k+1}} \mathbf{f} - D_1^{s^{k+1}} \mathbf{g} \cdot {}^{s^k} \mathbf{f} - D_2^{s^{k+1}} \mathbf{g} \cdot {}^{s^k} \dot{\boldsymbol{\mu}} - D_3^{s^{k+1}} \mathbf{g} \cdot \mathbf{1}}{\dot{\gamma}^{k+1}} D_1 \gamma^{k+1} + D_1^{s^{k+1}} \mathbf{g} \cdot \mathbf{1} \right) \mathbf{J}^{ks^{k-1}} \mathbf{v} \\
 &\quad + \left(\frac{{}^{s^{k+1}} \mathbf{f} - D_1^{s^{k+1}} \mathbf{g} \cdot {}^{s^k} \mathbf{f} - D_2^{s^{k+1}} \mathbf{g} \cdot {}^{s^k} \dot{\boldsymbol{\mu}} - D_3^{s^{k+1}} \mathbf{g} \cdot \mathbf{1}}{\dot{\gamma}^{k+1}} D_2 \gamma^{k+1} + D_2^{s^{k+1}} \mathbf{g} \cdot \mathbf{1} \right) {}^{s^k} \mathbf{v}, \quad (\text{C.60})
 \end{aligned}$$

which is equal to

$${}^{s^{k+1}} \mathbf{z}(\tau) = \mathbf{G}^{k+1} \mathbf{G}^{ks^{k-1}} \mathbf{z} + \mathbf{G}^{k+1} \mathbf{J}^{ks^{k-1}} \mathbf{v} + \mathbf{J}^{k+1s^k} \mathbf{v}. \quad (\text{C.61})$$

Here we see that (C.61) is equal to (C.42). This proves that for any k , the first-order approximation of the post-impact state of two simultaneous jumps at τ can be found by evaluating the two jumps separately. Since k is a variable in this proof, using an induction-like proof, this holds for any amount of jumps as well. This is illustrated in Figure C.1.

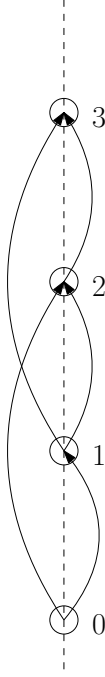


Figure C.1

When we take $k = 1$, we show that the jumps from 0 to 2 can be described by evaluating the jump from 0 to 1 and the jump 1 to 2 in succession. This also holds for $k = 2$. The jump from 0 to 3 can be described by evaluating the jump from 0 to 2 and the jump from 2 to 3 in succession. This way we proved that we can use (C.61) to find an expression for the first-order approximation of the post-impact state for l simultaneous jumps, with $l \in \mathbb{Z}$. Also, we show that multiple constant jump gains will result in a total jump which can also be described by a constant jump gain.

For l simultaneous jumps, we can find the first-order approximation of the post-impact state using

$${}^{l \leftarrow 0} \mathbf{z}(\tau) = {}^{l \leftarrow 0} \mathbf{L}(\mathbf{z}^0(\tau), \mathbf{v}(\tau), \tau) = {}^{l \leftarrow 0} \mathbf{G} \mathbf{z}^0(\tau) + \sum_{i=0}^{l-1} \left({}^{l \leftarrow i+1} \mathbf{G} {}^{i+1 \leftarrow i} \mathbf{J} \mathbf{v}^i(\tau) \right), \quad (\text{C.62})$$

where the superscript

$$b \leftarrow a = b \leftarrow (b-1) \leftarrow \dots \leftarrow (a+1) \leftarrow a, \quad (\text{C.63})$$

and

$${}^{b \leftarrow a} \mathbf{G} = {}^{b \leftarrow (b-1)} \mathbf{G} \dots {}^{(a+2) \leftarrow (a+1)} \mathbf{G} {}^{(a+1) \leftarrow a} \mathbf{G}, \quad (\text{C.64})$$

$${}^{b \leftarrow a} \mathbf{J} = {}^{b \leftarrow (b-1)} \mathbf{J} \dots {}^{(a+2) \leftarrow (a+1)} \mathbf{J} {}^{(a+1) \leftarrow a} \mathbf{J}. \quad (\text{C.65})$$

C.3 Stability analysis of LTHS

DEFINITION 1 AND 5 OF [55]

Appendix D

Positive Homogenization for Input-Dependent Guards

D.1 Conewise constant jump gain

This section is written under the assumption that in one macro event, only two modes are possible per contact point. The general form of a jump map for simultaneous impacts with is

$${}^{s^l \leftarrow s^0} \mathbf{z}(\tau) = {}^{s^l \leftarrow s^0} \mathbf{H}(\mathbf{z}^0(\tau), \mathbf{v}(\tau), \tau) = \begin{cases} \mathbf{G}^1(\mathbf{z}^0, \mathbf{v}^0, \tau), & \text{if condition 1 is true,} \\ \mathbf{G}^2(\mathbf{z}^0, \mathbf{v}^0, \tau), & \text{if condition 1 is true,} \\ \vdots & \vdots \\ \mathbf{G}^{p^{c_i}}(\mathbf{z}^0, \mathbf{v}^0, \tau), & \text{if condition } p^{c_i} \text{ is true,} \end{cases} \quad (\text{D.1})$$

where \mathbf{G} is in the form of (C.62). We will now derive the jump maps and associated conditions in (D.1) to make the expression explicit.

During a macro event for a certain perturbation, only a single order of micro events is feasible. This order can be found by determining the perturbed jump time of all possible micro events, and selecting the micro event with the earliest impact time as the next event. Mathematically, this is written as

$$s^{k+1} = \underset{s^{k+1}}{\operatorname{argmin}} \left({}^{s^{k+1} \leftarrow S^k} t_\epsilon \right). \quad (\text{D.2})$$

The impact time of the next micro event ${}^{s^{k+1} \leftarrow S^k} t_\epsilon$ can be approximated using the first order approximation

$${}^{s^{k+1} \leftarrow S^k} t_\epsilon = \tau + \epsilon \Delta^{k+1}. \quad (\text{D.3})$$

Now, since τ and ϵ are equal for each impact time, we can rewrite (D.2) to

$$s^{k+1} = \underset{s^{k+1}}{\operatorname{argmin}} \left(\Delta^{k+1} \right), \quad (\text{D.4})$$

which can be written as

$$s^{k+1} = s^k + \underset{\eta^* \in \chi}{\operatorname{argmin}} \left(- \frac{D_1 \gamma^{\eta^*} \left({}^{s^k} \alpha, {}^{s^k} \mu, \tau \right) {}^{S^k} \bar{\mathbf{z}} + D_2 \gamma^{\eta^*} \left({}^{s^k} \alpha, {}^{s^k} \mu, \tau \right) {}^{S^k} \bar{\mathbf{v}}}{\dot{\gamma}^{\eta^*}} \right), \quad (\text{D.5})$$

with χ the set of guard identifiers that are still open. Then

$$\eta^{k+1} = \operatorname{argmin}_{\eta^* \in \chi} \left(-\frac{D_1 \gamma^{\eta^*} \left(s^k \alpha, s^k \mu, \tau \right) S^k \bar{z} + D_2 \gamma^{\eta^*} \left(s^k \alpha, s^k \mu, \tau \right) S^k \bar{v}}{\dot{\gamma}^{\eta^*}} \right), \quad (\text{D.6})$$

with $s^{k+1} = s^k + \eta^{k+1}$ and η^{k+1} a guard function identifier. Finally, with

$$S^k \mathbf{a} = -\frac{D_1 \gamma^\eta \left(S^k \alpha, s^k \mu, \tau \right)}{\dot{\gamma}^\eta}, \quad S^k \mathbf{b} = -\frac{D_2 \gamma^\eta \left(S^k \alpha, s^k \mu, \tau \right)}{\dot{\gamma}^\eta}, \quad (\text{D.7})$$

(D.6) can be rewritten as

$$\eta^{k+1} = \operatorname{argmin}_{\eta^* \in \chi} \left(S^k \mathbf{a}^T S^k \bar{z} + S^k \mathbf{b}^T S^k \bar{v} \right). \quad (\text{D.8})$$

Now, by checking (D.6) for every micro event, we know which jump gains we should take to substitute into (C.62). For example a system with $c_i = 2$ and $p = 3$, with a macro event starting in $s_0 = 00$ and ending in $s_l = 22$, this gives

$$S^{2 \leftarrow 0} \mathbf{H} \left(s^0 \mathbf{z}(\tau), S^2 \mathbf{v}(\tau), \tau \right) = \begin{cases} {}^{(12)} S^{2 \leftarrow 0} \mathbf{G} s^0 \mathbf{z} + {}^{(12)} S^{2 \leftarrow 0} \mathbf{J} s^0 \mathbf{v}, & \text{if (I),} \\ {}^{12} S^{2 \leftarrow 1} \mathbf{G} {}^{1S^1 \leftarrow 0} \mathbf{G} s^0 \mathbf{z} + {}^{12} S^{2 \leftarrow 1} \mathbf{G} {}^{1S^1 \leftarrow 0} \mathbf{J} s^0 \mathbf{v} + {}^{12} S^{2 \leftarrow 1} \mathbf{J} {}^{1S^1} \mathbf{v}, & \text{if (II),} \\ {}^{21} S^{2 \leftarrow 1} \mathbf{G} {}^{2S^1 \leftarrow 0} \mathbf{G} s^0 \mathbf{z} + {}^{21} S^{2 \leftarrow 1} \mathbf{G} {}^{2S^1 \leftarrow 0} \mathbf{J} s^0 \mathbf{v} + {}^{21} S^{2 \leftarrow 1} \mathbf{J} {}^{2S^1} \mathbf{v}, & \text{if (III),} \end{cases} \quad (\text{D.9})$$

with

$$\text{(I)} : {}^{2S^1} \mathbf{a}^T {}^{2S^1} \mathbf{z} + {}^{2S^1} \mathbf{b}^T {}^{2S^1} \mathbf{v} = {}^{1S^1} \mathbf{a}^T {}^{1S^1} \mathbf{z} + {}^{1S^1} \mathbf{b}^T {}^{1S^1} \mathbf{v}, \quad (\text{D.10})$$

$$\text{(II)} : {}^{2S^1} \mathbf{a}^T {}^{2S^1} \mathbf{z} + {}^{2S^1} \mathbf{b}^T {}^{2S^1} \mathbf{v} > {}^{1S^1} \mathbf{a}^T {}^{1S^1} \mathbf{z} + {}^{1S^1} \mathbf{b}^T {}^{1S^1} \mathbf{v}, \quad (\text{D.11})$$

$$\text{(III)} : {}^{2S^1} \mathbf{a}^T {}^{2S^1} \mathbf{z} + {}^{2S^1} \mathbf{b}^T {}^{2S^1} \mathbf{v} < {}^{1S^1} \mathbf{a}^T {}^{1S^1} \mathbf{z} + {}^{1S^1} \mathbf{b}^T {}^{1S^1} \mathbf{v}. \quad (\text{D.12})$$

These conditions are illustrated in Figure D.1. Since the conditions are linear in \mathbf{z} and \mathbf{v} , they appear as lines in the state space of \mathbf{z} and \mathbf{v} . When we introduce more conditions, we will find several cones that relate a certain jump gain to \mathbf{z}, \mathbf{v} pair. When we look at the vector $r(\mathbf{z}, \mathbf{v})$ in Figure D.1, we notice that when r is multiplied with a constant α we will always stay in the same cone, i.e. use the same jump gain. Hence the name, conewise constant jump gain.

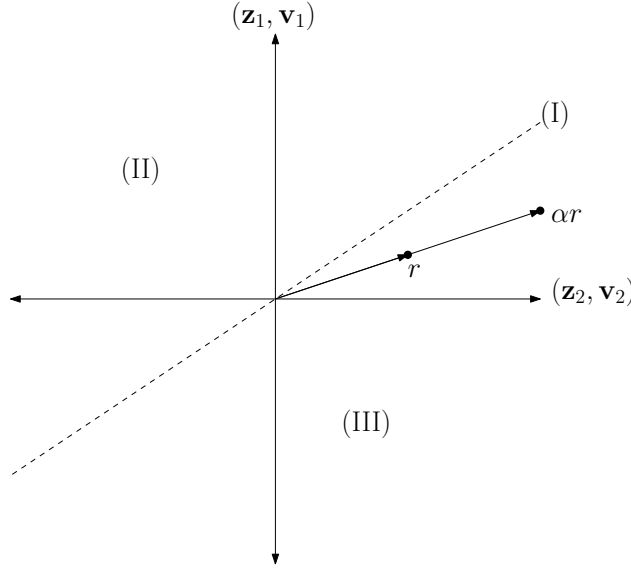


Figure D.1

D.2 Positive homogeneity

The first order approximation of the perturbed trajectory \mathbf{x}_ϵ can be found using $\alpha + \epsilon \mathbf{z}$, with

$$\begin{aligned} {}^{s^{k-1}}\dot{\mathbf{z}} &= {}^{s^{k-1}}\mathbf{A}(t) {}^{s^{k-1}}\mathbf{z} + {}^{s^{k-1}}\mathbf{B}(t) {}^{s^{k-1}}\mathbf{v}, \\ {}^{s^k}\mathbf{z} &= {}^{s^k \leftarrow s^{k-1}}\mathbf{H} \left({}^{s^{k-1}}\mathbf{z}, t \right), \\ {}^{s^k}\dot{\mathbf{z}} &= {}^{s^k}\mathbf{A}(t) {}^{s^k}\mathbf{z} + {}^{s^k}\mathbf{B}(t) {}^{s^{k-1}}\mathbf{v}, \end{aligned} \quad (\text{D.13})$$

where

$${}^{s^k}\mathbf{A}(t) = D_1 {}^{s^k}\mathbf{f} \left({}^{s^k}\alpha(t), {}^{s^k}\mu(t) \right), \quad (\text{D.14})$$

$${}^{s^k}\mathbf{B}(t) = D_2 {}^{s^k}\mathbf{f} \left({}^{s^k}\alpha(t), {}^{s^k}\mu(t) \right). \quad (\text{D.15})$$

When we look at (D.13), the continuous dynamics of the system are linear. Because of the conewise constant jump gain however, this linearity property is lost. We can see this by looking at the general solution of (D.13). A system $f(x, u)$ with state x and input u is linear if $f(x_1, v_1) + f(x_2, v_2) = f(x_1 + x_2, v_1 + v_2)$. Two solutions of (D.13) before jump are

$${}^{s^{k-1}}\mathbf{z}_1(\tau) = {}^{s^{k-1}}\phi(t, t_0) {}^{s^{k-1}}\mathbf{z}_1(t_0) + \int_{t_0}^{\tau} \left[{}^{s^{k-1}}\phi(t, s) {}^{s^{k-1}}\mathbf{B}(s) \mathbf{v}_1(s) \right] ds, \quad (\text{D.16})$$

$${}^{s^{k-1}}\mathbf{z}_2(\tau) = {}^{s^{k-1}}\phi(t, t_0) {}^{s^{k-1}}\mathbf{z}_2(t_0) + \int_{t_0}^{\tau} \left[{}^{s^{k-1}}\phi(t, s) {}^{s^{k-1}}\mathbf{B}(s) \mathbf{v}_2(s) \right] ds, \quad (\text{D.17})$$

with t_0 the initial time and τ the jump time. When we add these solutions together we find

$$\begin{aligned} {}^{s^{k-1}}\mathbf{z}_1(\tau) + {}^{s^{k-1}}\mathbf{z}_2(\tau) &= {}^{s^{k-1}}\phi(t, t_0) \left({}^{s^{k-1}}\mathbf{z}_1(t_0) + {}^{s^{k-1}}\mathbf{z}_2(t_0) \right) \\ &\quad + \int_{t_0}^{\tau} \left[{}^{s^{k-1}}\phi(t, s) {}^{s^{k-1}}\mathbf{B}(s) (\mathbf{v}_1(s) + \mathbf{v}_2(s)) \right] ds, \end{aligned} \quad (\text{D.18})$$

which is equal to the solution of ${}^{s^{k-1}}\mathbf{z}_3(t_0) = {}^{s^{k-1}}\mathbf{z}_1(t_0) + {}^{s^{k-1}}\mathbf{z}_2(t_0)$ with $\mathbf{v}_3(t) = \mathbf{v}_1(t) + \mathbf{v}_2(t)$. When ${}^{s^{k-1}}\mathbf{z}_1$ jumps with $\mathbf{G}^1(\mathbf{z}, \tau)$ and ${}^{s^{k-1}}\mathbf{z}_1(\tau)$ jumps with $\mathbf{G}^2(\mathbf{z}, \tau)$ we find the solutions post jump to be

$${}^{s^k}\mathbf{z}_1(\tau) = {}^{s^k}\phi(t, t_0) \mathbf{G}^1({}^{s^{k-1}}\mathbf{z}_1(t_0), \tau) + \int_{t_0}^{\tau} \left[{}^{s^k}\phi(t, s) {}^{s^k}\mathbf{B}(s)\mathbf{v}_1(s) \right] ds, \quad (\text{D.19})$$

$${}^{s^k}\mathbf{z}_2(\tau) = {}^{s^k}\phi(t, t_0) \mathbf{G}^2({}^{s^{k-1}}\mathbf{z}_2(t_0), \tau) + \int_{t_0}^{\tau} \left[{}^{s^k}\phi(t, s) {}^{s^k}\mathbf{B}(s)\mathbf{v}_2(s) \right] ds, \quad (\text{D.20})$$

which when added together results in

$$\begin{aligned} {}^{s^k}\mathbf{z}_1(\tau) + {}^{s^k}\mathbf{z}_2(\tau) &= {}^{s^k}\phi(t, t_0) \left(\mathbf{G}^1({}^{s^{k-1}}\mathbf{z}_1) + \mathbf{J}^1({}^{s^{k-1}}\mathbf{v}_1) + \mathbf{G}^2({}^{s^{k-1}}\mathbf{z}_2) + \mathbf{J}^2({}^{s^{k-1}}\mathbf{v}_2) \right) \\ &\quad + \int_{t_0}^{\tau} \left[{}^{s^k}\phi(t, s) {}^{s^k}\mathbf{B}(s) (\mathbf{v}_1(s) + \mathbf{v}_2(s)) \right] ds. \end{aligned} \quad (\text{D.21})$$

Here we see that the solution of ${}^{s^{k-1}}\mathbf{z}_3(t_0) = {}^{s^{k-1}}\mathbf{z}_1(t_0) + {}^{s^{k-1}}\mathbf{z}_2(t_0)$ with $\mathbf{v}_3(t) = \mathbf{v}_1(t) + \mathbf{v}_2(t)$, which jumps with $\mathbf{G}_3(\mathbf{z}, \tau)$, is only equal to (D.21) if $\mathbf{G}_1(\mathbf{z}, \tau) = \mathbf{G}_2(\mathbf{z}, \tau) = \mathbf{G}_3(\mathbf{z}, \tau)$. In other words, the system only maintains its linearity after jump if the jump maps are equal for each ante jump state. Because this is generally not true, we show that the system is positive homogeneous for any jump gains. A system $f(x, u)$ with state x and input u is called positive homogeneous, when $\alpha f(x, u) = f(\alpha x, \alpha u)$. If we multiply (D.19) with a constant α , we find

$${}^{s^k}\mathbf{z}_1(\tau) = \alpha {}^{s^k}\phi(t, t_0) \left(\mathbf{G}^1({}^{s^{k-1}}\mathbf{z}_1) + \mathbf{J}^1({}^{s^{k-1}}\mathbf{v}_1) \right) + \alpha \int_{t_0}^{\tau} \left[{}^{s^k}\phi(t, s) {}^{s^{k-1}}\mathbf{B}(s)\mathbf{v}_1(s) \right] ds. \quad (\text{D.22})$$

If we now look at the solution for $\mathbf{z}_4(t_0) = \alpha \mathbf{z}_1(t_0)$ with $\mathbf{v}_4(t) = \alpha \mathbf{v}_1(t)$ jumping with $\mathbf{G}^4(\tau)$, and using the fact that $\mathbf{G}^4(\tau) = \mathbf{G}^1(\tau)$ since the gains are conewise constant as illustrated in Figure D.1, we find the same solution as (D.22). This shows that (D.13) is positive homogeneous for any conewise constant jump gain ${}^{s^k \leftarrow s^{k-1}}\mathbf{H}({}^{s^{k-1}}\mathbf{z}, t)$. Hence the name, positive homogenization.

D.3 Stability analysis of PTTHS

Appendix E

Considered Trajectories

E.1 Associativity

E.2 Transversality

E.3 Superfluous Contacts

E.4 Nominal Guard-Activations

For impacts, the theory is valid for impacts away from a simultaneous impacts and for simultaneous impacts, but not for impacts very close to simultaneous impacts. In this case the nominal impact is not a simultaneous impact, but a perturbation can cause the order of impacts to change. I believe the jump gain is not conewise constant anymore in this case.

The same is true for impacts close to the border of stick and slip.

E.5 Non-impacting contact points can not switch modes

E.6 All closed contact points are in the same mode

If I do not assume this, then every combination of Γ_{i_C} has to be iterated until a feasible solution is found. If we do assume this, we can just check if all Γ_{i_C} go to stick. If not, then all Γ_{i_C} go to slip.

In this work only trajectories where all closed contacts are in the same mode are considered. This means that when (A.2) is smaller than zero, i.e. the reaction forces are infeasible for a stick post-impact mode, all contact points have a feasible slip post-impact mode. For trajectories where different contact points can be in slip and in stick at the same time, this conclusion can not be drawn. One should then iterate over all possible post-impact modes until a post-impact mode is found which has feasible reaction forces.

Appendix F

Simulation Design

F.1 Plank box dynamics

In Figure F.1 the plank-box model is illustrated. The block is fully actuated and the plank is attached to the solid environment with a spring and damper. The line contact is for now modeled using two contact-points C_L and C_R .

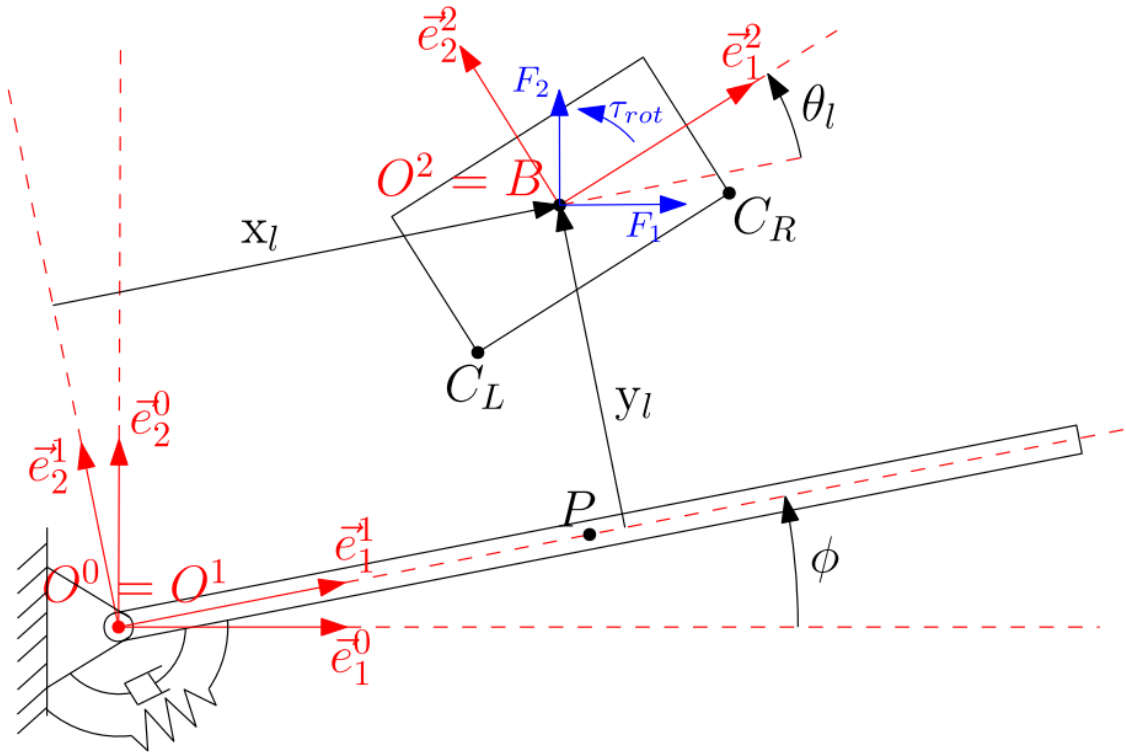


Figure F.1: *Block-plank model*

Global unconstrained dynamics

The global generalized coordinates are defined as

$$\mathbf{q}_g = [x_g \quad y_g \quad \theta_g \quad \varphi] , \quad (\text{F.1})$$

$$\mathbf{v}_g = [\dot{x}_g \quad \dot{y}_g \quad \dot{\theta}_g \quad \dot{\varphi}] . \quad (\text{F.2})$$

The equations of motion for the global unconstrained dynamics are then described by

$$\mathbf{M}_g(\mathbf{q}_g)\dot{\mathbf{v}}_g - \mathbf{H}_g(\mathbf{q}_g, \mathbf{v}_g) = \mathbf{S}_g(\mathbf{q}_g)\mathbf{u}, \quad (\text{F.3})$$

with

$$\mathbf{M}_g(\mathbf{q}_g) = \begin{bmatrix} m_B & 0 & 0 & 0 \\ 0 & m_B & 0 & 0 \\ 0 & 0 & J_B & 0 \\ 0 & 0 & 0 & \frac{m_P L_P^2}{4} + J_P \end{bmatrix} \quad (\text{F.4})$$

$$\mathbf{H}_g(\mathbf{q}_g, \mathbf{v}_g) = \begin{bmatrix} 0 \\ -gm_B \\ 0 \\ k_P \varphi - b_P \dot{\varphi} - \frac{L_P g m_P \cos(\varphi)}{2} \end{bmatrix} \quad (\text{F.5})$$

$$\mathbf{S}_g(\mathbf{q}_g) = \begin{bmatrix} 1 & 0 & 0 \\ 0 & 1 & 0 \\ 0 & 0 & 1 \\ 0 & 0 & 0 \end{bmatrix} . \quad (\text{F.6})$$

Local unconstrained dynamics

The global generalized coordinates \mathbf{q}_g can be rewritten to a set of local coordinates \mathbf{q}_l . In the plank box case they are related via

$$\mathbf{q}_g(\mathbf{q}_l) = \begin{bmatrix} \cos(\varphi)x_l - \sin(\varphi)y_l \\ \sin(\varphi)x_l + \cos(\varphi)y_l \\ \theta_l + \varphi \\ \varphi \end{bmatrix} . \quad (\text{F.7})$$

The local unconstrained equations of motion are then defined as

$$\mathbf{M}_l(\mathbf{q}_l)\dot{\mathbf{v}}_l - \mathbf{H}_l(\mathbf{q}_l, \mathbf{v}_l) = \mathbf{S}_l(\mathbf{q}_l)\mathbf{u}, \quad (\text{F.8})$$

with

$$\mathbf{M}_l(\mathbf{q}_l) = \begin{bmatrix} m_B & 0 & 0 & -m_B y_l \\ 0 & m_B & 0 & m_B x_l \\ 0 & 0 & J_B & J_B \\ -m_B y_l & m_B x_l & J_B & \frac{m_P L_P^2}{4} + m_B x_l^2 + m_B y_l^2 + J_B + J_P \end{bmatrix} \quad (\text{F.9})$$

$$\mathbf{H}_l(\mathbf{q}_l, \mathbf{v}_l) = \begin{bmatrix} m_B (x_l \dot{\varphi}^2 + 2\dot{y}_l \dot{\varphi} - g \sin(\varphi)) \\ -m_B (-y_l \dot{\varphi}^2 + 2\dot{x}_l \dot{\varphi} + g \cos(\varphi)) \\ 0 \\ k_P \varphi - b_P \dot{\varphi} - 2m_B \dot{\varphi} x_l \dot{x}_l - 2m_B \dot{\varphi} y_l \dot{y}_l - \frac{L_P g m_P \cos(\varphi)}{2} - g m_B x_l \cos(\varphi) + g m_B y_l \sin(\varphi) \end{bmatrix} \quad (\text{F.10})$$

$$\mathbf{S}_l(\mathbf{q}_l) = \begin{bmatrix} \cos(\varphi) & \sin(\varphi) & 0 \\ -\sin(\varphi) & \cos(\varphi) & 0 \\ 0 & 0 & 1 \\ -y_l \cos(\varphi) - x_l \sin(\varphi) & x_l \cos(\varphi) - y_l \sin(\varphi) & 1 \end{bmatrix}. \quad (\text{F.11})$$

Local constrained dynamics

First we have to determine the position vectors of the points C_L and C_R using Figure F.2. First we define the position vector of C_R ,

$$r_{C_R} = r_B + r_{BC_R} \text{ with,} \quad (\text{F.12})$$

$$r_B = [x_l \quad y_l \quad 0] \vec{e}^1, \quad (\text{F.13})$$

$$r_{BC_R} = [BH \quad HC_R \quad 0] \vec{e}^1, \quad (\text{F.14})$$

using the axis systems defined in the report of Hao. From Figure F.2 and that $\triangle BFG \cong \triangle C_R HG$ we can say

$$HC_R = \cos(\theta_l) C_R G, \quad (\text{F.15})$$

$$C_R G = FG - FC_R, \quad (\text{F.16})$$

$$FG = \tan(\theta_l) BF, \quad (\text{F.17})$$

and with $FC_R = \frac{l_B}{2}$ and $BF = \frac{L_B}{2}$ we find

$$HC_R = \sin(\theta_l) \frac{L_B}{2} - \cos(\theta_l) \frac{l_B}{2}. \quad (\text{F.18})$$

For BH we say

$$BH = BG - HG, \quad (\text{F.19})$$

$$BG = \frac{1}{\sin(\theta_l)} FG, \quad (\text{F.20})$$

$$HG = \sin(\theta_l) C_R G, \quad (\text{F.21})$$

which gives us

$$BH = \cos(\theta_l) \frac{L_B}{2} - \sin(\theta_l) \frac{l_B}{2}. \quad (\text{F.22})$$

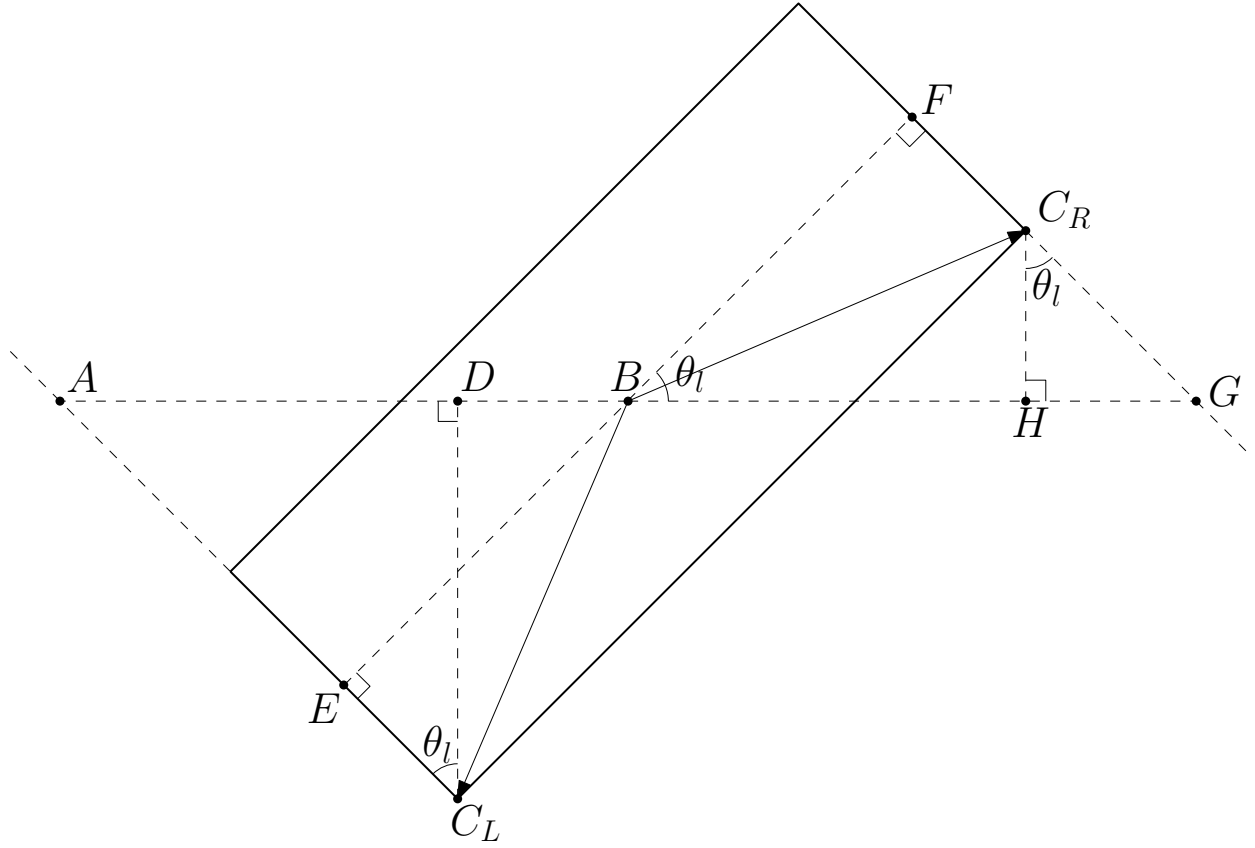


Figure F.2: *Geometry of the box, used to determine the position vectors of contactpoints C_L and C_R .*

With HC_R and BH known, the position vector of C_R is

$$r_{C_R} = \begin{bmatrix} x_l + \cos(\theta_l) \frac{L_B}{2} - \sin(\theta_l) \frac{l_B}{2} \\ y_l + \sin(\theta_l) \frac{L_B}{2} - \cos(\theta_l) \frac{l_B}{2} \\ 0 \end{bmatrix}^T \vec{e}^1. \quad (\text{F.23})$$

Using a similar approach for C_L we find

$$r_{C_L} = \begin{bmatrix} x_l + \cos(\theta_l) \frac{L_B}{2} + \sin(\theta_l) \frac{l_B}{2} \\ y_l - \sin(\theta_l) \frac{L_B}{2} - \cos(\theta_l) \frac{l_B}{2} \\ 0 \end{bmatrix}^T \vec{e}^1. \quad (\text{F.24})$$

The guard functions g_{N1} and g_{N2} are defined as

$$g_{N1} = \vec{r}_{C_L}^1 \vec{e}_2^1 - l_p = y_l - \frac{l_P}{2} - \sin(\theta_l) \frac{L_B}{2} - \cos(\theta_l) \frac{l_B}{2} = 0, \quad (\text{F.25})$$

$$g_{N2} = \vec{r}_{C_R}^1 \vec{e}_2^1 - l_p = y_l - \frac{l_P}{2} + \sin(\theta_l) \frac{L_B}{2} - \cos(\theta_l) \frac{l_B}{2} = 0, \quad (\text{F.26})$$

Since we are in a 2D-environment, the tangential reaction forces have the same dimensions as the normal reaction-forces. Therefore Equations (??), (??) and (??) can now be considered as, respectively,

$$\mathbf{g}_T = [g_{Ti_1}; g_{Ti_2}; \dots; g_{Ti_c}] \in \mathbb{R}^c \quad (\text{F.27})$$

$$\mathbf{\Lambda}_T = [\Lambda_{Ti_1}; \Lambda_{Ti_2}; \dots; \Lambda_{Ti_c}] \in \mathbb{R}^c \quad (\text{F.28})$$

$$\mathbf{W}_T = [\mathbf{w}_{Ti_1}; \mathbf{w}_{Ti_2}; \dots; \mathbf{w}_{Ti_c}] \in \mathbb{R}^{n \times c} \quad (\text{F.29})$$

The velocity vectors \dot{r}_{C_L} and \dot{r}_{C_R} are found by taking the time-derivative of r_{C_L} and r_{C_R} , and can be written as

$$\dot{r}_{C_L} = \begin{bmatrix} \dot{x}_l - \dot{\theta}_l \sin(\theta_l) \frac{L_B}{2} + \dot{\theta}_l \cos(\theta_l) \frac{l_B}{2} \\ \dot{y}_l - \dot{\theta}_l \cos(\theta_l) \frac{L_B}{2} + \dot{\theta}_l \sin(\theta_l) \frac{l_B}{2} \\ 0 \end{bmatrix} =: \begin{bmatrix} \dot{g}_{T1} \\ \dot{g}_{N1} \\ 0 \end{bmatrix}, \quad (\text{F.30})$$

$$\dot{r}_{C_R} = \begin{bmatrix} \dot{x}_l - \dot{\theta}_l \sin(\theta_l) \frac{L_B}{2} - \dot{\theta}_l \cos(\theta_l) \frac{l_B}{2} \\ \dot{y}_l + \dot{\theta}_l \cos(\theta_l) \frac{L_B}{2} + \dot{\theta}_l \sin(\theta_l) \frac{l_B}{2} \\ 0 \end{bmatrix} =: \begin{bmatrix} \dot{g}_{T2} \\ \dot{g}_{N2} \\ 0 \end{bmatrix}, \quad (\text{F.31})$$

with \dot{g}_{Ni} and \dot{g}_{Ti} the normal and tangential relative velocities. From (??) and (??) we can write

$$\dot{\mathbf{g}}_N = \mathbf{W}_N^T \mathbf{v} = \begin{bmatrix} \dot{y}_l - \dot{\theta}_l \cos(\theta_l) \frac{L_B}{2} + \dot{\theta}_l \sin(\theta_l) \frac{l_B}{2} \\ \dot{y}_l + \dot{\theta}_l \cos(\theta_l) \frac{L_B}{2} + \dot{\theta}_l \sin(\theta_l) \frac{l_B}{2} \end{bmatrix}, \quad (\text{F.32})$$

$$\dot{\mathbf{g}}_T = \mathbf{W}_T^T \mathbf{v} = \begin{bmatrix} \dot{x}_l - \dot{\theta}_l \sin(\theta_l) \frac{L_B}{2} + \dot{\theta}_l \cos(\theta_l) \frac{l_B}{2} \\ \dot{x}_l - \dot{\theta}_l \sin(\theta_l) \frac{L_B}{2} - \dot{\theta}_l \cos(\theta_l) \frac{l_B}{2} \end{bmatrix}, \quad (\text{F.33})$$

from which we can deduce

$$\mathbf{W}_N^T = \begin{bmatrix} 0 & 1 & -\cos(\theta_l) \frac{L_B}{2} + \sin(\theta_l) \frac{l_B}{2} & 0 \\ 0 & 1 & \cos(\theta_l) \frac{L_B}{2} + \sin(\theta_l) \frac{l_B}{2} & 0 \end{bmatrix}, \quad (\text{F.34})$$

$$\mathbf{W}_T^T = \begin{bmatrix} 0 & 1 & -\sin(\theta_l) \frac{L_B}{2} + \cos(\theta_l) \frac{l_B}{2} & 0 \\ 0 & 1 & -\sin(\theta_l) \frac{L_B}{2} - \cos(\theta_l) \frac{l_B}{2} & 0 \end{bmatrix}. \quad (\text{F.35})$$

Now we have all the information to write down the local constrained dynamics

$$\mathbf{M}_l(\mathbf{q}_l) \dot{\mathbf{v}}_l - \mathbf{H}_l(\mathbf{q}_l, \mathbf{v}_l) = \mathbf{S}_l(\mathbf{q}_l) \mathbf{u} + \mathbf{W}(\mathbf{q}_l) \mathbf{\Lambda}, \quad (\text{F.36})$$

with

$$\mathbf{W}(\mathbf{q}_l) := [\mathbf{W}_N \quad \mathbf{W}_T] \quad \text{and} \quad \mathbf{\Lambda} := \begin{bmatrix} \mathbf{\Lambda}_N \\ \mathbf{\Lambda}_T \end{bmatrix}. \quad (\text{F.37})$$

F.2 Reference Trajectory Design